In situ determination of carbaryl in complex biological matrices using a potentiometric chemical sensor, and study of superionic $BaSnF_4$ as a potential transducer material

Jamil Hantash

A Thesis

in

The Department

Of

Chemistry and Biochemistry

Presented in Partial Fulfillment of the Requirements

for the Degree of Master of Science (Chemistry) at

Concordia University

Montreal, Quebec, Canada

September 2006

Your file Votre référence
ISBN: 978-0-494-20727-7
Our file Notre référence
ISBN: 978-0-494-20727-7

Abstract

In situ determination of carbaryl in complex biological matrices using a potentiometric chemical sensor, and study of superionic $BaSnF_4$ as a potential transducer material

Jamil Hantash

Carbamate insecticides such as carbaryl (1-naphthyl N-methylcarbamate) are broad-spectrum insecticides that comprise the major portion of agricultural pesticides used in today's agricultural industry. Therefore, the synthesis of molecularly imprinted polymeric beads that can be used for isolating carbaryl from complex matrices would be a great asset. Conventional molecular imprinting technology allows the synthesis in organic solvents of molecularly imprinted polymers (MIPs) that have considerable molecular recognition ability, and can be used as a separation media. The results obtained showed that the use of an imprinted polymer cartridge as a pre-column in high performance liquid chromatography (HPLC), using ultra-violet detection and a "dilute and shoot" approach for the rapid, inexpensive and accurate determination of carbaryl in complex biological matrices (rat plasma and apple homogenate) with a detection limit of 1.00 ng/mL and a response that is linear ($r^2 > 0.98$) over the concentration range of 1.00 to 10.0 ng/mL, was successful. In the past decade, numerous biosensing methods for the detection of pesticides have been developed using enzyme-based and affinity-based sensors as well as several types of transducers and this has been the subject of several recent reviews. We report that the use of an imprinted carbaryl polymer column in a non-enzymatic flow injection potentiometric chemical sensor system for the determination of carbaryl in complex biological matrices (rat plasma) was successful. The potentiometric chemical sensor system efficiency in the determination of carbaryl in rat plasma was

validated in terms of selectivity, carry-over, calibration range and precision and accuracy in accordance with the Guidance for Industry Bioanalytical Method Validation, U.S. Department of Health and Human Services, Food and Drug Administration. However, the results showed that the use of $BaSnF_4$ as a solid state conductivity electrode as a part of a conductivity chemical sensor system for the determination of carbaryl in solution was not successful due to limitations in preparing a $BaSnF_4$ sheet resistant to the capillary pressure applied by the micro-fluid passing through the conductivity cell.

Acknowledgements

This thesis is dedicated to my late son (Sami Nasuh Hantash) who was born in July 16, 2003 and passed to heaven nine months later.

First I would like to thank my mother (Sabiha Salem) who inspired me throughout my life. I would not have accomplished any thing in my life without her prayers and love.

I would like to thank Dr George Dénès, Dr Raymond Le Van Mao, Dr Philippe G. Merle, Alan Bartlett, Dr Philip Raymond Oldfield and all my colleagues for all the support and the guidance throughout my thesis project. Also I thank Charles River Laboratories Montreal Inc. for the financial support.

Finally, I would like to thank my wife (Rima Salem) and my two daughters (Tia Tasmin and Mia Serene) for their never ending patients, support and love.

Table of Contents

List of Figures

List of Tables

Chapter 1
Introduction

1.1 Pesticides

A pesticide is any substance or mixture of substances intended for preventing, destroying, repelling, or mitigating any pest. Though often misunderstood to refer only to insecticides, the term pesticide also applies to herbicides, fungicides, and various other substances used to control pests. Pests are living organisms that occur where they are not wanted or that cause damage to crops, humans or other animals. Examples include insects, mice and other animals, unwanted plants (weeds), fungi, microorganisms such as bacteria and viruses, and prions. Pesticides are often referred to according to the type of pest they control. Another way to think about pesticides is to consider those that are chemical pesticides or are derived from a common source or production method. Other categories include biopesticides, antimicrobials, and pest control devices[1].

1.1.1 Chemical Pesticides

1.1.1.1 Organophosphate Pesticides

These pesticides affect the nervous system by disrupting the enzyme that regulates acetylcholine, a neurotransmitter. Most organophosphates are insecticides. They were developed during the early 19th century, but their effects on insects, which are similar to their effects on humans, were discovered in 1932. Some are very poisonous (they were used in World War II as nerve agents). However, they are not usually persistent in the environment[1].

1.1.1.2 Carbamate Pesticides

These pesticides affect the nervous system by disrupting an enzyme that regulates acetylcholine, a neurotransmitter. The enzyme effects are usually reversible. There are several subgroups within the carbamates[1].

1.1.1.3 Organochlorine Insecticides

These pesticides were commonly used in the past, but many have been removed from the market due to their health and environmental effects and their persistence (e.g. DDT and chlordane)[1].

1.1.1.4 Pyrethroid Pesticides

These pesticides were developed as a synthetic version of the naturally occurring pesticide pyrethrin, which is found in chrysanthemums. They have been modified to increase their stability in the environment. Some synthetic pyrethroids are toxic to the nervous system[1].

1.1.1.5 Biopesticides

Biopesticides are certain types of pesticides derived from such natural materials as animals, plants, bacteria, and certain minerals. For example, canola oil and baking soda have pesticidal applications and are considered biopesticides. At the end of 2001, there were approximately 195 registered biopesticide active ingredients and 780 products. Biopesticides fall into three major classes: microbial pesticides, plant incorporatants and biochemical pesticides.

1.1.1.5.1 Microbial pesticides

These pesticides consist of a microorganism (e.g., a bacterium, fungus, virus or protozoan) as the active ingredient. Microbial pesticides can control many different kinds of pests, although each separate active ingredient is relatively specific for its target pests. For example, there are fungi that control certain weeds, and other fungi that kill specific insects. The most widely used microbial pesticides are subspecies and strains of Bacillus thuringiensis, (Bt). Each strain of this bacterium produces a different mix of proteins, and specifically kills one or a few related species of insect larvae. While some Bt's control moth larvae found on plants, other Bt's are specific for larvae of flies and mosquitoes. The target insect species are determined by whether the particular Bt produces a protein that can bind to a larval gut receptor, thereby causing the insect larvae to starve[1].

1.1.1.5.2 Plant Incorporated Protectants (PIPs)

These are pesticidal substances that plants produce from genetic material that has been added to the plant. For example, scientists can take the gene for the Bt pesticidal protein, and introduce the gene into the plant's own genetic material. Then the plant, instead of the Bt bacterium, manufactures the substance that destroys the pest. The protein and its genetic material, but not the plant itself, are regulated by Environmental Protection Agency (EPA)[1].

1.1.1.5.3 Biochemical pesticides

These are naturally occurring substances that control pests by non-toxic mechanisms. Conventional pesticides, by contrast, are generally synthetic materials that directly kill or

inactivate the pest. Biochemical pesticides include substances, such as insect sex pheromones, that interfere with mating, as well as various scented plant extracts that attract insect pests to traps. Because it is sometimes difficult to determine whether a substance meets the criteria for classification as a biochemical pesticide, EPA has established a special committee to make such decisions[1].

1.2 Carbamates

The carbamates discussed in this thesis are those mainly used in agriculture, as insecticides, fungicides, herbicides, nematocides, or sprout inhibitors. In addition, they are used as biocides for industrial or other applications and in household products. A potential use is in public health vector control. Thus, these chemicals are part of the large group of synthetic pesticides that have been developed, produced, and used on a large scale in the last 40 years. The general formula of the carbamates is: $R_1NH - C\,O - OR_2$

Where R_1 and R_2 are alkyl or aryl groups.

More than 50 carbamates are known, and it is clear that it is not within the scope of this introduction to include all the information about each compound[1].

1.2.1 Carbaryl

Carbaryl is a wide-spectrum carbamate insecticide which controls over 100 species of insects on citrus, fruit, cotton, forests, lawns, nuts, ornamentals, shade trees, and other crops, as well as on poultry, livestock and pets. It is also used as a molluscicide and an acaricide. Carbaryl works whether it is ingested into the stomach of the pest or absorbed through direct contact. The chemical name for carbaryl is 1- naphthol N-

methylcarbamate. Carbaryl is formulated as a solid which varies from colorless to white to gray, depending on the purity of the compound. The crystals are odorless. This chemical is stable to heat, light and acids under storage conditions. It is non-corrosive to metals, packaging materials, or application equipment. It is found in all types of formulations including baits, dusts, wettable powder, granules, oil, molassas, aqueous dispersions and suspensions[2]. Carbaryl is a general use pesticide[1].

1.2.1.1 Toxicological effects

1.2.1.1.1 Acute toxicity

Carbaryl is moderately to very toxic, and can produce adverse effects in humans by skin contact, inhalation or ingestion. The symptoms of acute toxicity are typical of the other carbamates. Direct contact of the skin or eyes with moderate levels of this pesticide can cause burns. Inhalation or ingestion of very large amounts can be toxic to the nervous and respiratory systems resulting in nausea, stomach cramps, diarrhea and excessive salivation. Other symptoms at high doses include sweating, blurring of vision, incoordination, and convulsions. About fifty cases of occupational or accidental illnesses due to exposure to carbaryl have been reported, but no fatalities have been documented. The only documented fatality from carbaryl was through intentional ingestion. The oral lethal dose where 50% of the tested animals died (LD_{50}) of carbaryl ranges from 250 mg/kg to 850 mg/kg for rats, and from 100 mg/kg to 650 mg/kg for mice[1, 3]. The inhalation lethal concentration of carbaryl where 50% of the tested animals died (LC_{50}) for rats is 0,005 to 0.023 mg/kg [1]. Low doses can cause minor skin and eye irritation in rabbits, for which the dermal LD_{50} has been measured at greater than 2,000 mg/kg [2]. Carbaryl has little potential for skin or eye irritation. Occupational workers have the

greatest potential for exposure through inhalation or through the skin. The general public's highest risk of exposure is through ingestion of contaminated food[4].

1.2.1.1.2 Chronic toxicity

Athough it may cause minor skin and eye irritation, carbaryl does not appear to be a significant chronic health risk at or below occupational levels. Male volunteers who consumed low doses of carbaryl for six weeks did not show symptoms, but tests indicated slight changes in their body chemistry[2].

1.2.1.1.3 Reproductive and Teratogenic Effects

No reproductive or fetal effects were observed during a long-term study of rats, which were fed high doses of carbaryl[2]. The evidence for teratogenic effects due to chronic exposure is minimal in test animals. Birth defects in rabbit and guinea pig offspring occurred only at dosage levels which were highly toxic to the mother. A 1980 New Jersey epidemiological study found no evidence of excess birth defects in a town sprayed with carbaryl for gypsy moth control. There is only limited evidence that carbaryl causes birth defects in humans. The EPA has concluded that carbaryl does not pose a teratogenic risk to humans if used properly[5].

1.2.1.1.4 Mutagenic Effects

Numerous studies indicate that carbaryl poses only a slight mutagenic risk [2,6]. However, carbaryl can react with nitrite under certain conditions to give rise to N-nitrosocarbaryl. Nitrosocarbaryl has been shown to be highly mutagenic at low levels in laboratory test systems. This may be a concern to humans because there is a possibility that carbaryl, a pesticide, and nitrite, a substance found in food additives and in human saliva, may react

in the human stomach to form nitrosocarbaryl [5, 7]. Carbaryl has been shown to affect cell mitosis (cell division) and chromosomes in rats[2].

1.2.1.1.5 Carcinogenic Effects

Carbaryl has not caused tumors in ten long-term and lifetime studies of mice and rats. Rats were administered high daily doses of the pesticide for two years, and mice for eighteen months, with no signs of carcinogenicity[8]. However, N-nitrosocarbaryl, formed by the reaction of carbaryl and nitrite, has been shown to be carcinogenic in rats at high doses[9]. Also, mice exposed to carbaryl in the product, tricaprylin, for four weeks each, developed lung tumors[2].

1.2.1.1.6 Organ Toxicity

Ingestion of carbaryl affects the lungs, kidneys and liver. Inhalation will also affect the lungs [3,10]. Nerve damage can occur after administration of high doses for 50 days in rats and pigs[2]. Several studies indicate that carbaryl can affect the immune system in animals and insects. These effects however have not been documented in humans.

1.2.1.2 Fate in Humans and Animals

Most animals, including humans, readily break down carbaryl and rapidly excrete it in the urine and feces. Workers occupationally exposed by inhalation to carbaryl dust excreted 74% of the inhaled dose in the urine in the form of a breakdown product[1]. This is consistent with information on other species, which excreted nearly three quarters of a dose in their urine within 24 hours of administration[3]. The metabolism of up to 85% of carbaryl occurs within 24 hours after administration[1].

1.2.1.3 Ecological effects

Carbaryl is lethal to many nontarget insects. The pesticide is more active in insects than in mammals. The destruction of honeybee populations in sprayed areas is sometimes a problem. Carbaryl is moderately toxic to aquatic organisms, such as rainbow and lake trout, bluegill, and cutthroat. It is also moderately toxic to wild birds, with low toxicity to Canada geese[2]. Accumulation of carbaryl can occur in catfish, crawfish, and snails, as well as in algae and duckweed. Residue levels in fish were 140 fold greater than the concentration of carbaryl in water. In general, due to its rapid metabolism and rapid degradation, carbaryl should not pose a significant bioaccumulation risk in alkaline waters. However, under acidic conditions it may be significant[3].

1.2.1.4 Environmental fate

Carbaryl has a short residual life on treated crops. The insecticide remains at the application site, where it is slowly taken into the plant and metabolized. Insecticidal properties are retained for 3-10 days. Loss of carbaryl is due to sublimation and uptake into plants. Breakdown by sun light does not appear to be significant. Degradation of carbaryl in the soil is mostly due to sun light and bacterial action. It is bound by organic matter and can be transported in soil runoff. Carbaryl has a half-life of 7 days in aerobic soil and 28 days in anaerobic soil [11]. Degradation of carbaryl in crops occurs by hydrolysis inside the plants. It has a short residual life of less than two weeks. The metabolites of carbaryl have lower toxicity to humans than carbaryl itself. The breakdown of this substance is strongly dependant on acidity and temperature.

In pond water, carbaryl is broken down by bacteria through chemical processes. Evaporation does not occur. Carbaryl has a half-life of from 1 to 32 days in pond water.

In a stream, carbaryl that had washed in from forest spraying, decayed to 50% within a 24 hour period. It has been shown to degrade more slowly in the presence of mud in aquatic habitats. Carbaryl has been detected in groundwater in three separate cases in California[10]. Carbaryl has a half-life in the air of one to four months[10].

1.2.1.5 Metabolism

Metabolic reactions include: hydroxylation, hydrolysis, and conjugation. Hydrolysis results in the formation of 1-naphtol, carbon dioxide, and methylamine. Metabolites of carbaryl were identified in the urine of human volunteers after the ingestion of a 2 mg/kg dose[12]. Entero hepatic cycling of carbaryl metabolites is also considerable, especially after oral administration.

Only traces of the unchanged carbaryl could be detected in the urine indicating rapid metabolism. The only detectable metabolites in urine samples taken from workers exposed to carbaryl dust were 1-naphthylglucoronide and sulfate[13]. Carbaryl is metabolized by hepatic microsomal enzymes.

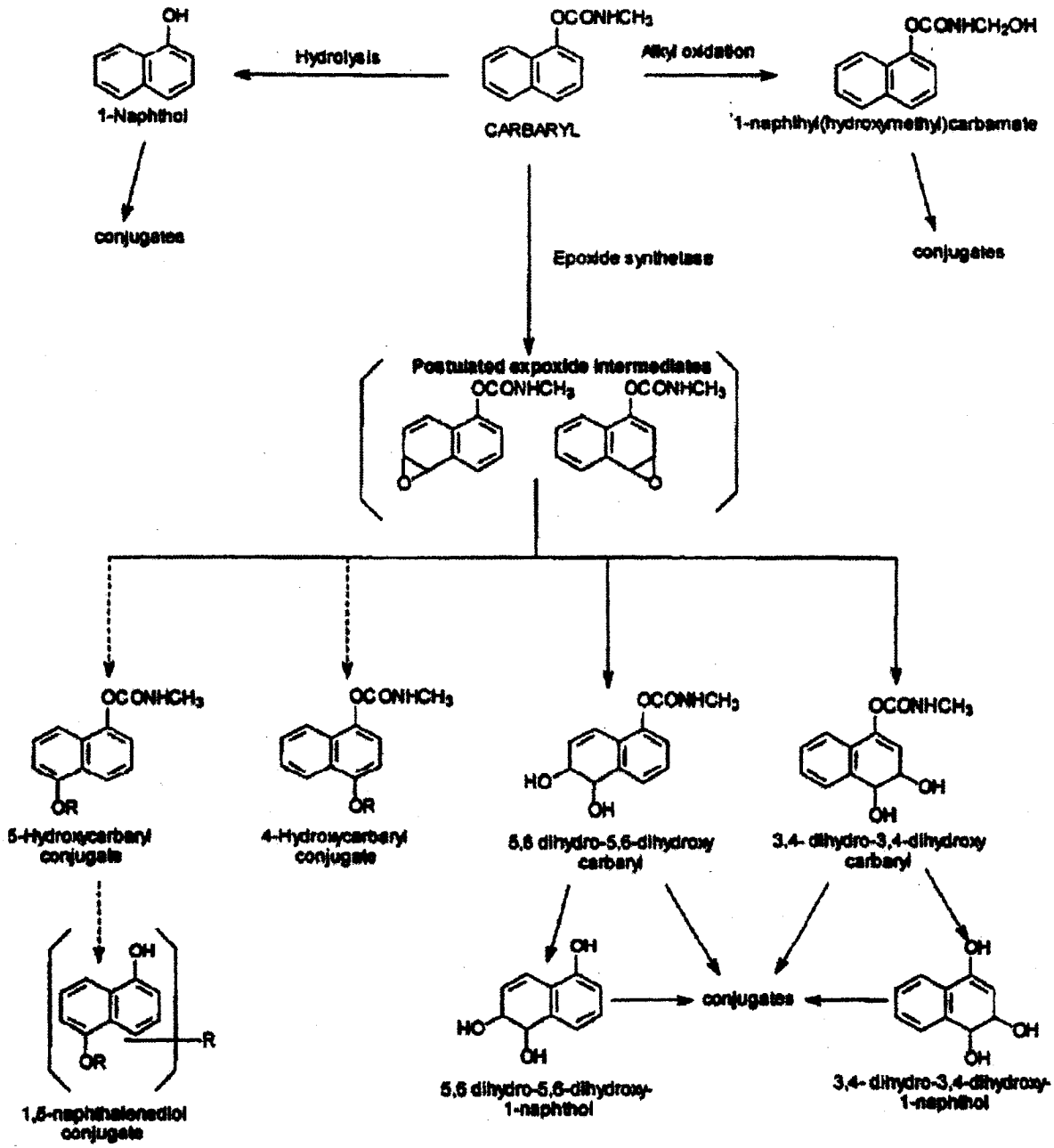

Figure 1: Carbaryl metabolic pathways[13]

1.2.1.6 Mode of Action

Carbaryl is an inhibitor of cholinesterase enzymes. In normal nervous system function, a burst of the neurotransmitter acetylcholine is released from a nerve cell terminal, diffuses across the synaptic cleft and transmits a nerve impulse to a specific cholinergic receptor. To end stimulation and restore the sensitivity of the receptor to new transmitter, acetylcholine at the receptor must continually be eliminated; this function is fulfilled by the enzyme acetylcholinesterase, which hydrolyzes acetylcholine to choline and acetic acid.

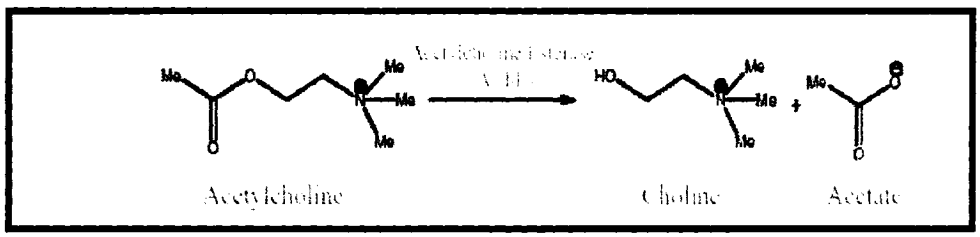

Equation 1

By inhibiting acetylcholinesterase, anticholinesterase carbamates allow acetylcholine to accumulate at cholinergic junctions[14]. This effect is dose-related and reversible. Chronic exposure may cause a cumulative effect. All identified metabolites of carbaryl are less active cholinesterase inhibitors than carbaryl itself.

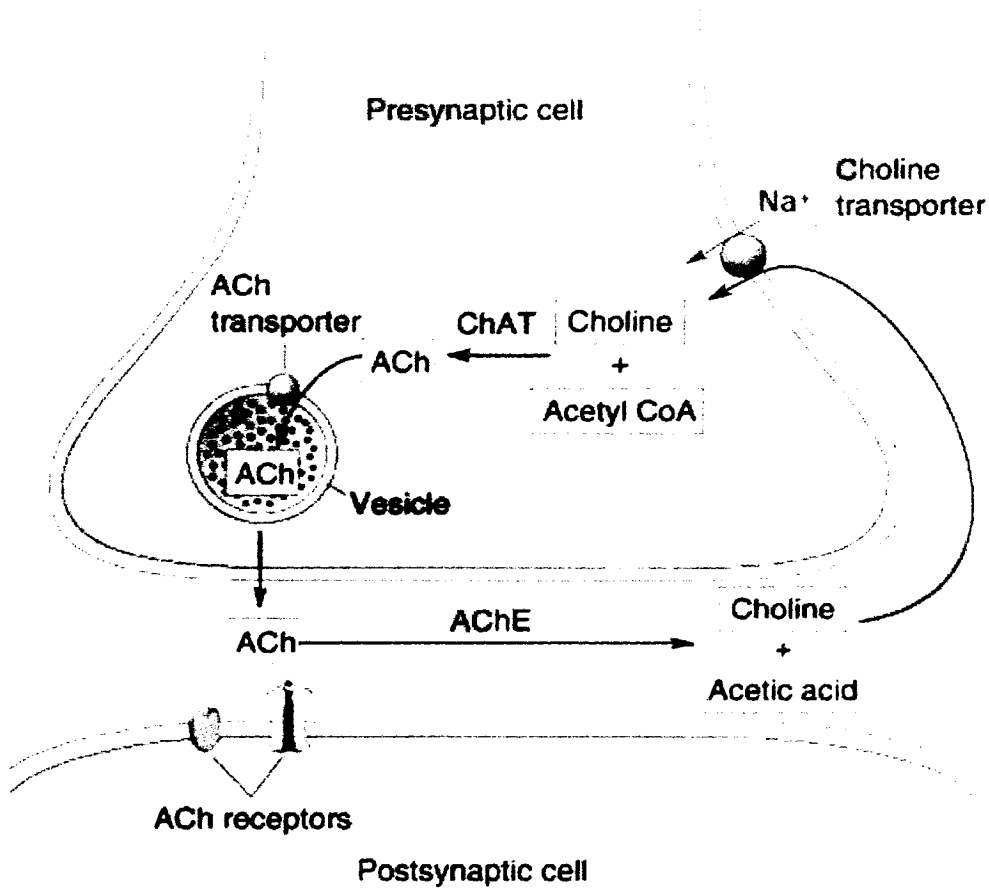

Figure 2: **Acetocholine system**[14]

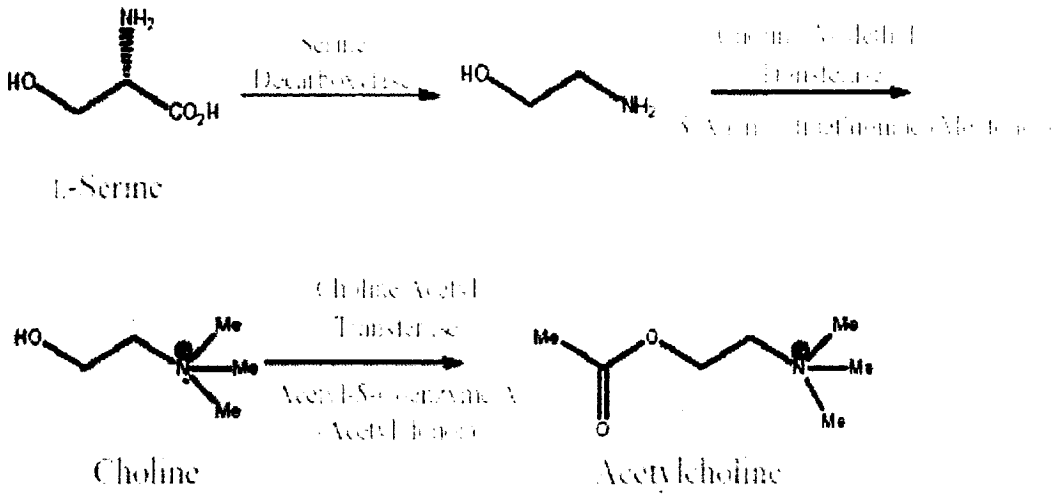

Figure 3 Biosynthesis of acetylcholine[14]

1.3 Polymer Synthesis

The study of polymer science begins with understanding the methods in which these materials are synthesized. Polymer synthesis is a complex procedure and can take place in a variety of ways. Addition polymerization describes the method where monomers are added one by one to an active site on the growing chain. The use of polymerization technique to produce pesticides molecular imprinted beads to be used in chromatographic methods is a great asset[15].

1.3.1 Addition Polymerization

The most common type of addition polymerization is free radical polymerization. A free radical is simply a molecule with an unpaired electron. The tendency for this free radical

to gain an additional electron in order to form a pair makes it highly reactive so that it breaks the bond on another molecule by stealing an electron, leaving that molecule with an unpaired election (which is another free radical). Free radicals are often created by the division of a molecule (known as an initiator) into two fragments along a single bond. The following equation shows the formation of a radical from its initiator, in this case benzoyl peroxide[15].

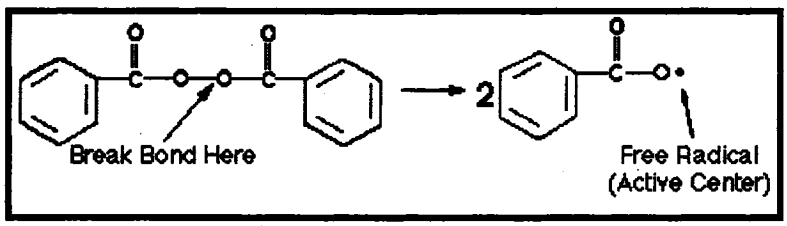

Equation 2

The stability of a radical refers to the molecule's tendency to react with other compounds. An unstable radical will readily combine with many different molecules. However a stable radical will not easily interact with other chemical substances. The stability of free radicals can vary widely depending on the properties of the molecule. The active center is the location of the unpaired electron on the radical because this is where the reaction takes place. In free radical polymerization, the radical attacks one monomer, and the electron migrates to another part of the molecule. This newly formed radical attacks another monomer and the process is repeated. Thus the active center moves down the chain as the polymerization occurs[15].

There are three significant reactions that take place in addition polymerization: initiation (birth), propagation (growth), and termination (death). These separate steps are explained below.

1.3.1.1 Initiation Reaction

The first step in producing polymers by free radical polymerization is initiation. This step begins when an initiator decomposes into free radicals in the presence of monomers. The instability of carbon-carbon double bonds in the monomer makes them susceptible to reaction with the unpaired electrons in the radical. In this reaction, the active center of the radical "grabs" one of the electrons from the double bond of the monomer, leaving an unpaired electron to appear as a new active center at the end of the chain. Addition can occur at either end of the monomer. In a typical synthesis, between 60% and 100% of the free radicals undergo an initiation reaction with a monomer. The remaining radicals may join with each other or with an impurity instead of with a monomer. "Self destruction" of free radicals is a major hindrance to the initiation reaction. By controlling the monomer to radical ratio, this problem can be reduced[15].

1.3.1.2 Propagation Reaction

After a synthesis reaction has been initiated, the propagation reaction takes over. In the propagation stage, the process of electron transfer and consequent motion of the active center down the chain proceeds. In the equation below, (chain) refers to a chain of connected monomers, and X refers to a substituent group (a molecular fragment) specific to the monomer. For example, if X were a methyl group, the monomer would be propylene and the polymer, polypropylene.

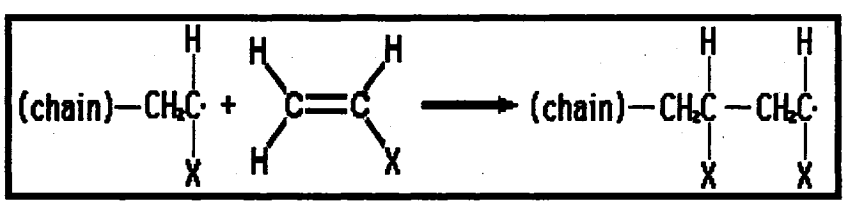

Equation 3

In free radical polymerization, the entire propagation reaction usually takes place within a fraction of a second. Thousands of monomers are added to the chain within this time. The entire process stops when the termination reaction occurs[15].

1.3.1.3 Termination Reaction

In theory, the propagation reaction could continue until the supply of monomers is exhausted. However, this outcome is very unlikely. More often the growth of a polymer chain is halted by the termination reaction. Termination typically occurs in two ways: combination and disproportionation. Combination occurs when free electrons from two growing chains join and form a single chain stop the polymer's growth. The following equation depicts combination, with the symbol (R) representing the rest of the chain.

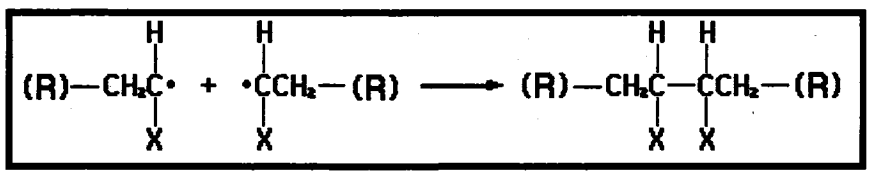

Equation 4

Disproportionation halts the propagation reaction when a free radical strips a hydrogen atom from an active chain. A carbon-carbon double bond takes the place of the missing hydrogen. Termination by disproportionation is shown in the equation beow.

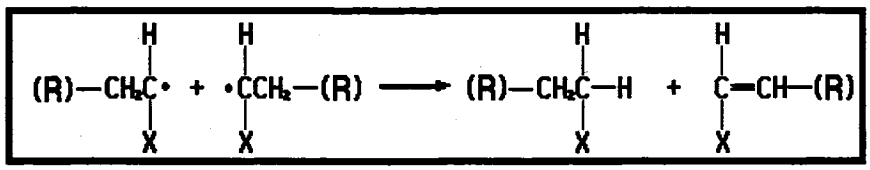

Equation 5

Disproportionation can also occur when the radical reacts with an impurity. This is why it is so important that polymerization be carried out under very clean conditions[15].

1.3.2 Living Polymerization

There exists a type of addition polymerization that does not undergo a termination reaction. This so-called "living polymerization" continues until the monomer supply has been exhausted. When this happens, the free radicals become less active due to interactions with solvent molecules. If more monomers are added to the solution, the polymerization will resume. Uniform molecular weights (low polydispersity) are characteristic of living polymerization. Because the supply of monomers is controlled, the chain length can be manipulated to serve the needs of a specific application. This assumes that the initiator is 100% efficient[15].

1.3.3 Suspension polymerization

Hoffman and Delbruch first developed suspension polymerization in 1909. In suspension polymerization the initiator is soluble in the monomer phase, which is dispersed by comminuting into the dispersion medium (usually water) to form droplets. The solubility of the dispersed monomer (droplet) phase and also the resultant polymer in the dispersion medium are usually low. The volume fraction of the monomer phase is usually within the range 0.1-0.5. Polymerization reactions may be performed at lower monomer volume fractions, but are not usually economically viable. At higher volume fractions, the concentration of continuous phase may be insufficient to fill the space between droplets. Polymerization proceeds in the droplet phase, and in most cases occurs by a free radical mechanism. Suspension polymerization usually requires the addition of small amounts of a stabilizer to hinder coalescence and break-up of droplets during polymerization. The size distribution of the initial emulsion droplets and, hence, also of the polymer beads that are formed, is dependent upon the balance between droplet break-up and droplet

coalescence. This is in turn controlled by the type and speed of agitator used, the volume fraction of the monomer phase, and the type and concentration of stabilizer used. If the polymer is soluble in the monomer, a gel is formed within the droplets at low conversion leading to harder spheres at high conversion. If the polymer is insoluble in the monomer solution, precipitation will occur within the droplets, which will result in the formation of opaque, often irregularly shaped particles. If the polymer is partially soluble in the monomer mixture, the composition of the final product can be difficult to predict. Polymer beads find applications in a number of technologies, such as molding plastics. However, their largest application is in chromatographic separation media (as ion exchange resin and as supports for enzyme immobilization). Such applications frequently require large particle surface areas, which necessitates the formation of pores (of the required dimensions) in the bead structure[16, 17, 18].

The polymer beads may be made porous by the inclusion of an inert diluent (or porogen) to the monomer phase, which may be extracted after polymerization. Other additions to the monomer phase can include UV stabilizers (aromatic ketones and esters), heat stabilizers (ethylene oxide derivatives and inorganic metal salts), molding lubricants and foaming agents (porogens).

1.3.4 Polymeric Stabilizers

Typical polymeric stabilizers used for oil-in-water suspension polymerization reactions are poly (vinyl alcohol) -co- (vinyl acetate) (formed from the partial hydrolysis (80-90%) of polyvinyl acetate), poly (vinyl-pyrrolidone), salts of acrylic acid polymers, cellulose ethers and natural gums. Polymeric stabilizers used in inverse suspension polymerization reactions include block copolymers poly (hydroxy-stearic acid) -co-poly) ethylene oxide).

Surfactants used for oil-in-water suspensions include spans and the anionic emulsifier (sodium 12-butinoyloxy-9-octadecenate)[15].

1.3.5 Polymerization Conditions and Kinetics

Extensive studies have shown that, in general, reaction kinetics in suspension polymerization is found to show good agreement with bulk phase kinetics (in absence of any monomer diluent). This observation suggests that in suspension polymerization, the emulsification conditions (agitation conditions, emulsion droplet size and concentration / type of stabilizer) appear to have little effect on reaction kinetics. Moreover, it can be concluded that any mass transfer between two phases in the emulsion does not affect the overall reaction rate. The major challenge in designing a suspension reaction is therefore the formation of a stable emulsion, preferably having a uniform size distribution. The monomer droplets are large enough to contain a large number of free radicals (may be as many as 10s) and this is why the polymerization in general proceeds with a similar mechanism to that of bulk polymerization, particularly when the polymer is soluble in the monomer [11, 12, 13].

1.3.6 Emulsion polymerization

This is a type of polymerization that takes place in an emulsion typically incorporating water, monomer, and surfactant. The most common type of emulsion polymerization is an oil-in-water emulsion, in which droplets of monomer (the oil) are emulsified (with surfactants) in a continuous phase of water. Water soluble polymers, such as certain polyvinyl alcohols or hydroxyethyl celluloses, can also be used to act as emulsfiers/stabilisers. Some of the popular emulsions available in the market include

polyvinyl acetate homopolymers and copolymers, styrene butadiene latex, and acrylic emulsions[15].

Figure 4 Micelle formation during emulsion polymerization

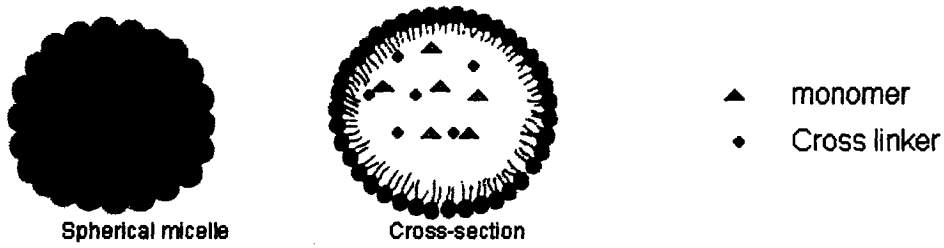

Source: http://zeus.plmsc.psu.edu/~manias/PlmSe406/chapter2-3.pdf

Advantages of emulsion polymerization include:

- The continuous water phase is an excellent conductor of heat and allows the heat to be removed from the system, allowing many reaction methods to increase their rate.
- Since polymer molecules are contained within the particles, viscosity remains close to that of water and is not dependent on molecular weight.
- The final product can be used as is and does not generally need to be altered or processed.

Most emulsion polymerizations use a radical polymerization method. Emulsion polymerization can be carried out as a batch reaction, but in many cases is performed as a starve-fed reaction to insure a good distribution of monomers into the polymer backbone chain. The leading theory for the mechanism of starve-fed, free-radical emulsion polymerization is summarized by the following:

- Surfactants emulsify the monomer in a water continuous phase.
- Excess surfactant creates micelles in the water.
- Small amounts of monomer diffuse through the water to the micelle.
- The initiator is water-soluble and introduced into the water phase where it reacts with the monomer in the micelles. This process differs from suspension polymerization where the initiator is soluble in the monomer and particle size gets larger. An example of an initiator is potassium persulfate. The persulfate ion breaks up in sulfate radical ions at about 50 °C.
- The micelles in total, comprise a much larger surface area in the system than the fewer, larger monomer droplets, which is why the initiator typically reacts with the micelle and not the monomer droplet.
- Monomer in the micelle quickly polymerizes and the growing chain terminates.
- More monomers from the droplets diffuses to the growing micelle/particle, where more initiators will eventually react.
- Monomer droplets and initiator are continuously and slowly added to maintain their levels in the system as the particles grow.
- When the monomer droplets have been completely consumed, the initiator is typically added in for a little while longer to consume any residual monomer.
- The final product is a dispersion of polymer particles in water, it can also be known as a polymer colloid, a latex, or commonly and inaccurately as an 'emulsion', inaccurate because the final form is no longer an oil-phase solubilised in a continuous phase, but rather finely dispersed discrete solid polymer particles[11, 12, 13, 14].

1.4 Molecular imprinting and Biosensors

Over the past two decades, enormous activity has taken place in the field of sensor technology. Biosensors, in particular, have attracted considerable attention because of their extraordinary sensitivities and specificities. However, such devices often lack storage and operational stability because they are based on a fragile biological recognition element: an enzyme or antibody. For this reason, biosensors have not become quite the commercial success expected in the early euphoric development phase.

An emerging technology called molecular imprinting, however, could provide an alternative. This technique leads to highly stable synthetic polymers that possess selective molecular recognition properties because of recognition sites within the polymer matrix that are complementary to the analyte in the shape and positioning of functional groups. Some of these polymers have high selectivities and affinity constants, comparable with naturally occurring recognition systems such as monoclonal antibodies or receptors, which make them especially suitable as constituents in chemical (biomimetic) sensors for analytical chemistry[19].

1.4.1 Molecular recognition

Molecular recognition between a molecular receptor (host) and a substrate (guest) in a matrix containing structurally related molecules requires discrimination and binding; this can happen only if the binding sites of the host and guest molecules complement each other in size, shape, and chemical functionality. Biological systems, such as enzyme-substrate, antibody-antigen, and hormone-receptor systems, demonstrate molecular recognition properties that have developed by natural selection. Chemical recognition systems, however, have been developed mainly by rational design in the laboratory,

although combinatorial approaches, which can generate recognition systems by selection from large libraries, will become increasingly important in the future. The principles of host-guest chemistry were set out by Cram, Lehn, and Pedersen in the 1960s and 1970s and have been developed for a multitude of synthetic or semi-synthetic systems such as crown ethers, cyclodextrins, and cyclophanes[20,21,22]. Such host-guest systems are potentially very useful as recognition elements in analytical applications and have been used in separation and isolation processes.

Molecular imprinting can be approached in two ways: the self-assembly approach[23] and the pre-organized approach[24] (Figure 5). These two approaches, which differ with respect to the interaction mechanism in pre-polymerization, follow common molecular recognition terminology [14,25].

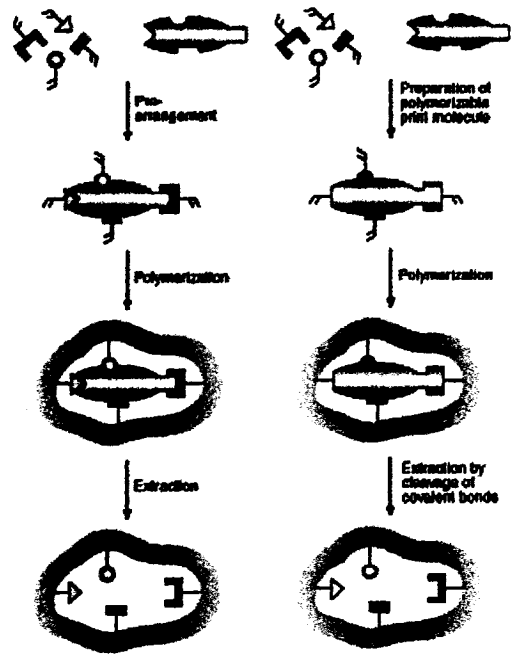

Figure 5 **Principles of molecular imprinting.(a) Self-assembly approach (right side diagram); (b) Pre-organized approach (left side diagram)[19].**

The self-assembly molecular imprinting approach involves host-guest complexes produced from weak intermolecular interactions (such as ionic or hydrophobic interactions, hydrogen bonding, and metal coordination) between the analyte and the monomer precursors. These self-assembled complexes are spontaneously established in the liquid phase and are then sterically fixed by polymerization with a high degree of cross-linking. After removal of the print molecules from the resulting macroporous matrix, vacant recognition sites that are specific to the print molecule are established. The shape of the sites, maintained by the polymer backbone and the arrangement of the functional groups in the recognition sites, results in affinity for the analyte[19].

The pre-organized molecular imprinting approach involves formation of strong, reversible, covalent arrangements (e.g., boronate esters, imines, and ketals) of the monomers with the print molecules before polymerization. Thus, the print molecules need to be "derivatized" with the monomers before the actual imprinting is performed. After cleaving the covalent bonds that hold the print molecules to the macroporous polymer matrix, recognition sites complementary to the analyte remain in the polymer[19].

So far, MIPs have been used primarily as stationary phases in HPLC. Recently, however, they have been used in TLC[26], CE[27], heterogeneous binding assays[28, 29], and in biomimetic affinity sensors.

1.4.2 Chemical sensors and molecular recognition

Chemical sensors provide an analytically powerful and inexpensive alternative to conventional technologies by enabling the identification of a target molecule in the

presence of numerous interfering species. A chemical sensor selectively recognizes a target molecule in a complex matrix and generates an output signal using a transducer that correlates to the concentration of the analyte (Figure 6). The recognition element is responsible for the selective binding (and in some cases, conversion) of the analyte in a matrix containing both related and unrelated compounds. Upon binding, the transducer translates the chemical event into a quantifiable output signal. When the analyte interacts with the recognition element, a change in one or more physicochemical parameters associated with the interaction occurs. This change may produce ions, electrons, gases, heat, mass changes, or light, and the transducer converts these parameters into an electrical output signal that can be amplified, processed, and displayed in a suitable form. The successful performance of a chemical sensor depends on the appropriate choice of recognition element and transducer[19].

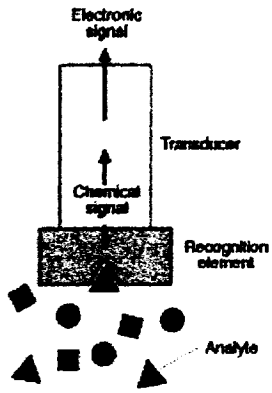

Figure 6 **Schematic of a chemical sensor, characterized by a recognition element and a transducer close to each other[19].**

Sensor performance is characterized by selectivity, sensitivity, stability, and reusability. Selectivity, a measure of how well a chemical sensor discriminates between the analyte and compounds of similar, or different, chemical structure, is principally determined by the recognition component within the sensor device. Sensitivity is determined by the recognition element and the transducer. Depending on the signal to noise (S/N), additional amplification steps can enhance sensitivity and lower the detection limit of the analyte. Maintaining long-term stability, withstanding harsh chemical environments, and operating at high temperatures and/or pressures are severe challenges for sensors, particularly when the recognition element is of biological origin. This, in part, restricts the application of biosensors[19].

Chapter 2

Use of an on-line imprinted polymer pre-column, for the liquid chromatographic-UV absorbance determination of carbaryl and its metabolite in complex matrices[1]

2.1 Introduction

Organophosphorous (e.g., parathion and malathion) and N-methylcarbamate (e.g, carbaryl, aldicarb) insecticides are believed to act by inhibiting cholinesterase, resulting in the accumulation of acetylcholine at the synapses in the nervous system, at neuromuscular junctions of the skeletal and smooth muscles, and secretory glands[30,31,32]. Signs and symptoms of overexposure may include miosis, blurred vision, lacrimation, excessive nasal discharge or salivation, sweating, abdominal cramps, nausea, vomiting, diarrhea, tremor, cyanosis and convulsions [15, 16, 33]. The LD^{50} for rats (oral) is 500 mg/kg [17, 34].

Carbaryl release in the environment is due to its uses as a molluscicide, an insecticide and acaricide on a variety of crops. Its release to soil will result in photolysis at the soil surface at a rate dependent upon the soil water content. Carbaryl will hydrolyze relatively rapidly in moist alkaline soil, but only slowly in acidic soil, and it may leach to groundwater based on its moderate soil absorption coefficient[35, 36]. Release of carbaryl to water will result in rapid hydrolysis at pH values of 7 and above. At higher pH values, carbaryl biodegradation may be significant. Its release to the atmosphere may result in

---

[1] J.amil Hantash, A. Bartlett, P. Oldfield, G. Dénès, R. O'Rielly, D. Roudiere, S. Menduni. Journal of Chromatography A, 1125 (2006) 104-111.

direct photolysis as carbaryl absorbs light at wavelengths above 290 nm[37]. Monitoring data indicate that carbaryl is a contaminant in food and a minor contaminant in drinking and surface water. Human exposure to carbaryl is expected to result mainly from ingestion of contaminated food, and occupational exposure in farm workers may be expected. Carbaryl persisted longer in soil water than in lake water [20, 21].

In addition, the wide use of carbaryl has increased the concern about possible pollution of water supplies and soil. The analysis of complex samples (eg. environmental and biological) generally involves a pretreatment step aimed at the isolation of the analytes of interest from as many interfering components as possible, dissolution of the analytes in a suitable solvent and pre-concentration [38]. In an analytical method, sample preparation is followed by a separation and detection procedure[39]. In spite of the fact that sample preparation, in most of the analytical procedures, takes 50-75% of the total time of the analysis, most technical innovations of the last decade are related to separation and detection[40]. The ideal approach to sample preparation is to exclude the step altogether or "dilute and shoot". This approach is sometimes possible when sample levels of targeted analytes are relatively high and the matrix components do not co-elute or otherwise interfere with ionization and/or detection of the analytes. In the field of residue analysis, sample preparation is considered to be of great importance. Compounds of interest must be released and recovered at low concentrations from a complex background of potentially interfering matrix co-extractives in a manner, which also preserves analyte integrity, prior to the application of highly sensitive analytical measurements [39, 40]. For the first time we report the use of molecular imprinted polymer *in situ* treatment for the determination of carbaryl and its metabolite in complex biological matrices (apple homogenate and rat plasma for environmental and toxicological purposes, respectively)

at a low detection limit of 1.00 ng/mL with a time saving, cost effective, dilute and shoot approach.

In the preparation of MIPs, suspension polymerization by free radical addition is used. The benefits of suspension polymerization over traditionally used bulk polymerization include ease of temperature (and hence, reaction) control and the formation of a directly usable product [41]. The particles formed can, in many cases, be used directly as beads for ion exchange or chromatography columns[42]. Disadvantages include a lower yield per reactor volume because of the additional inert aqueous phase. The suspension polymerization technique used in this paper is based on emulsions of noncovalent imprinting mixtures formed in liquid perfluorocarbons, which are highly immiscible with most organic compounds and therefore form an appropriate inert phase for suspension polymerization[43]. Polymers of methacrylic acid, highly cross-linked with ethylene dimethacrylate, provide such specific binding sites for the carbaryl molecule and its metabolite when using it as a template to be removed after polymerization. The cavity containing carboxyl groups of methacrylic acids should entrap the carbaryl molecule and its metabolite template to a greater extent than another antipode under the definite special orientation between their functions. The molecular imprinted polymer with a particle size of ~ 5 μm were isolated and packed into a pre-column (50 x 4.6 mm id) that is used to isolate carbaryl and its metabolite from complex matrices injected on HPLC without extensive sample preparation and clean up.

2.2 Experimental

2.2.1 Materials

Poly (ethylene glycol) 1000 monomethyl ether lot number 540656 and ethylene glycol dimethacrylate lot number 539511 from Polysciences Inc. Carbaryl lot number LB316-60B from Supleco. Polyfluoro-acrylate (PFAC-1) lot number 007207 from Oakwood products Inc. 1,1'-azobis (cyclohexanecarbonitrile) lot number 428253/1 52403135, 1-naphthol lot number 20505107, phosphate buffer lot number 440524/1 50403196 and trifluoromethyl undecafluorocyclohexane lot number 1055468 from Fluka. Methacrylic acid lot number 05406EC from Sigma-Aldrich.

2.2.2 Preparation of perfluoro polymeric surfactant (PFPS)

A mixture of 2-(N-ethylperfluorooctanesulfonamido) ethyl acrylate (8.01g) and acryloyl polyethylene 1000 monomethyl ether (1.52g) was dissolved in chloroform (20.0mL). To this solution, 1,1'-azobis (cyclohexanecarbonitrile) (48.0mg) was added. The mixture was heated for approximately 48 hours at approximately 60°C in a shaking water bath to complete polymerization. The mixture was left to cool at room temperature and then was heated in a water bath at approximately 30°C to remove chloroform and a thick yellow gel was obtained. The resultant PFPS was stored at 4°C[44].

Abbreviation used	Name	Empirical formula
$PEG_{1000}MME$	2-(N-ethylperfluorooctanesulfonamido) ethyl acrylate (hydrophilic side chain)	$C_nF_{(2n+1)}SO_2N(C_2H_5)CH_2CH_2OCOCH{=}CH_2$
PFA-1	acryloyl polyethylene 1000 monomethyl ether (hydrophopic side chain)	$CH_3O(CH_2CH_2)_{22}CH_2CH_2OCOCH{=}CH_2$
PFPS	perfluoro polymeric surfactant	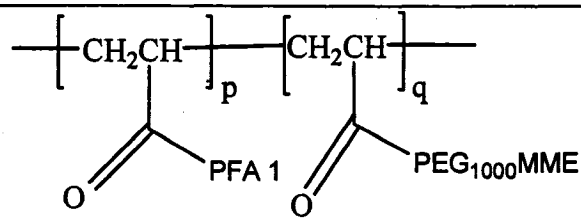

Figure 7: The structure of PFPS and its precursor monomers

2.2.3 Determination of the volume of porogenic solvent

The polymer beads were made porous by the inclusion of an inert diluent (or porogen) to the monomer phase, which was extracted after polymerization. The saturation volume of the porogenic solvent (chloroform) in perfluoro (methylcyclohexane) (PMC) was determined such that the amount of porogenic solvent used in the polymerization procedure was limited throughout the polymerization process in order to avoid fragmentation. The saturation volume was determined empirically by placing PMC (2.0 mL) in a clear glass vial and repeatedly adding porogenic solvent in small aliquots (15 μL) while mixing until a second distinct phase was visible. It was found that approximately 150 μL of chloroform was required for each 2.0 mL of PMC.

2.2.4 The imprinted mixture

Carbaryl is not soluble in chloroform, which is the porogenic solvent. The only other solvents that are candidates to be used in this type of polymerization are acetone and water. Acetone is known to produce large beads that cannot be used for chromatographic separation as well as having a dented bead surface that would effect the chromatography when used in a chromatographic column. Water is a strong competitive to form hydrogen bonds with the binding site of the imprinted polymer and therefore will reduce the probability and the number of imprinted sites for carbaryl. Therefore, the solution to this dilemma was to try to dissolve the carbaryl in the monomer methacrylic acid. To methacrylic acid (MAA) (207 mg), carbaryl (100 mg) and ethylene glycol dimethacrylate (EDMA) (2.51 g) were added and vortexed until a homogeneous solution was obtained, followed by the addition of 4.21 g of chloroform.

2.2.5 Preparation of carbaryl-imprinted polymer

Chloroform (1.5 mL) was placed in a 50 mL borosilicate pressure resistant round bottom flask in which PFPS (20 mg) and 1, 1' –azobis (cyclohexanecarbonitrile) (20 mg) were dissolved. To that mixture, perfluoro (methylcyclohexane) (20.0 mL) was added and the mixture was shaken to produce a uniform white opalescent emulsion to which the imprinted mixture was added and vortexed for 15 minutes. The mixture was exposed to ultraviolet light at a wavelength of 366 nm (intensity of 100 μW/cm2) at room temperature for approximately 3 hours while being vortexed. The resultant polymer was recovered by filtration through a glass fiber filter (Whatman type GFA). The polymer was washed with acetone (5.0 mL x 3) to remove the print molecule. The polymer then was washed twice with acetonitrile:phosphate buffer (0.5M; pH7.0) (3000 μL; 40:60,

v/v) and ultra pure water (5.0 mL x 3). The polymer was placed in an oven at approximately 35°C for approximately 4 hours. Spherical beads were obtained of various sizes [44].

2.2.6 Assessment of the polymer ability to reversibly bind carbaryl

Four SPE cartridges were prepared with approximately 50 mg of the polymer. Each SPE cartridge was conditioned with 0.5M phosphate buffer (2.0 mL; pH 7.0) followed by the addition of carbaryl standard (1000 µL, 50 ng/mL). The SPE was washed five times with acetonitrile:phosphate buffer (0.5M; pH7.0) (1000 µL; 40:60, v/v) and the carbaryl was eluted using acetonitrile:phosphate buffer (0.5M; pH 2.0) (500 µL; 40:60, v/v). Samples were collected after the addition of carbaryl to the SPE, after each wash step and after elution. The collected samples were injected on the HPLC using the method detailed in Table 1.

Table 1: **Method 1 - the isocratic high performance liquid chromatographic conditions used in the SPE assessment for the polymers reversible binding to carbaryl and 1-naphthol**

HPLC system	Agilent HP1100 series with 1050 pump
Analytical Column	Gemini C_{18} 5 µm (50 x 4.6 mm id)
Wavelength	280 nm
Mobile phase	Acetonitrile:water (50:50, v/v)
Column temperature	ambient
Autosampler temperature	Set at 4°C
Injection volume	100 µL

2.2.7 Packing the imprinted polymer into an analytical pr-column

The imprinted polymer was slurry-packed into a 50 X 4.60 mm id poly ether ether ketone (PEEK) column. The imprinted polymer was wetted with methanol, tightly packed, and subjected to a pressure of 114 bar, at a flow rate of 5.0 mL/min, for 30 minutes. The pre-column was checked for voids, re-packed, and subjected to a pressure of 114 bar again, at the same flow rate. This procedure was repeated until no voids were observed.

2.2.8 Preparation of biological samples

Apple homogenate was obtained by blending apple fruits with phosphate buffer, pH 7.0 (50:50, w/w). The homogenate was centrifuged (3000 rpm; 15 minutes) and the supernatant filtered through a 0.45 µm Teflon filter[45]. The filtrate was then spiked with carbaryl and 1-naphthol, vortexed, and transferred to injection vials for analysis by HPLC using the conditions outlined in Table 2.

In addition, rat plasma samples (100 μL) were spiked with carbaryl and 1-naphthol. Acetonitrile (300 μL) was added to each plasma sample and centrifuged (~ 14000 rpm; ~ 4°C; ~ 15 minutes) [45]. The supernatant was transferred to injection vials for analysis by HPLC using the conditions outlined in Table 2.

Table 2: Method 2 - the high performance liquid chromatographic conditions used to analyze the biological and environmental samples

HPLC system	Agilent HP1100 series with 1050 pump		
Pre-column	C3 (MIP1:MIP2, 50:50, w/w)		
Analytical Column	Gemini C_{18} 5 μm (50 x 4.6 mm id)		
Wavelength	280 nm		
Mobile phase A	Acetonitrile:phosphate buffer (0.5M; pH 7.0) (40:60, v/v)		
Mobile phase B	Acetonitrile:phosphate buffer (0.5M; pH 2.0) (40:60, v/v)		
Gradient	Time (minutes)	A (%)	B (%)
	0.0	100	0
	5.0	100	0
	5.1	0	100
	10.0	0	100
	10.1	100	0
	14.0	100	0
Autosamples temperature	Set at 4°C		
Injection volume	100 μL		

2.3 Results and Discussion

2.3.1 The polymeric surfactant and the polymerization

Creating a stable emulsion of an imprinted mixture in liquid perfluorocarbon proved to be a challenge due to the high density of the dispersant, which caused rapid creaming of the

emulsion, favoring the coalescence of dispersed droplets[46]. The perfluoro polymeric surfactant (PFPS) prepared from 2-(N-ethylperfluorooctanesulfonamido) ethyl acrylate and acryloyl polyethylene 1000 monomethyl ether produced a stable emulsion that could be used in the beads polymerization. The structure of PFPS and its precursor monomers are shown in Figure 7. The recovered PFPS (a sticky yellowish liquid) was stored at ~ 4°C.

Many attractive properties of MIPs, including their high stability and selectivity, depend on a high level of cross-linkage. The suspension polymerization utilizes PFPS as a dispersing agent in the polymerization mixture, producing spherical beads of a suitable size to be used in chromatographic separation media. The amount of surfactant used in the polymerization mixture influences the size of the beads recovered, and may result in a high degree of fragmentation [22]. The non-covalent imprinting technique used, relied on self-assembling functional monomers (methacrylic acid) around the template in the polymerization mixture, and since no covalent bonds form between the template and polymer, template removal involves simply washing the polymer repeatedly with a suitable solvent (acetone in our case). The rebinding of non-covalently imprinted polymers is an 'exact-fit' process since the interactions between the polymer and its target analyte is the same as those holding together the template monomer complexes. As a result, factors that tend to increase the stability of the initial complex will improve imprinting efficiency, while those that destabilize it will produce an inferior polymer. Binding to these polymers can be very rapid. In this case, the polymerization technique used, relies on hydrogen bonding to bind the analyte to the carboxylic arms of the imprinted polymeric cavity (see Figure 8). The polymeric beads recovered were

examined under a light microscope (see Figure 9). The beads were spherically shaped and free of aggregates and fragments.

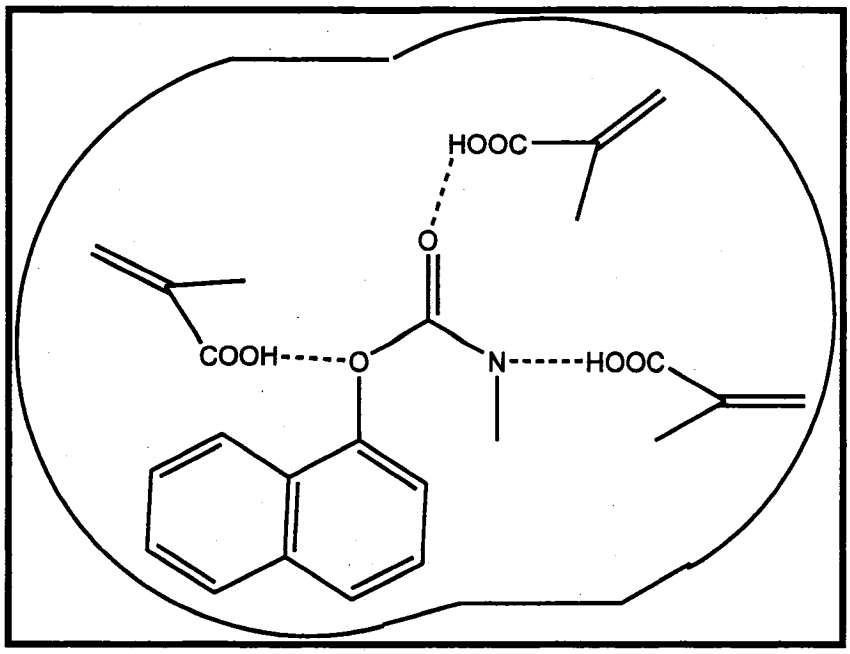

Figure 8: The binding cavity of the imprinted polymer featuring hydrogen bonding to bind the analyte to the carboxylic arms of the imprinted polymer

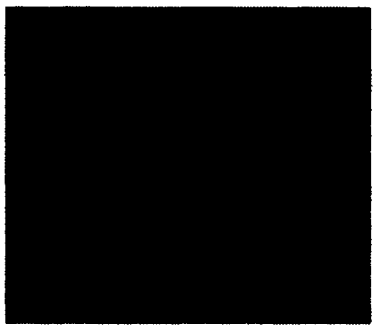

Figure 9: A light microscope image of the polymeric bead recovered using Olympus PX51 light microscope (40 x 60); MIP1 (carbaryl)

2.3.2 The polymers MIP1 and MIP2

Following the production of the carbaryl and 1-naphthol imprinted polymers MIP1 and MIP2, respectively, an assessment was performed using a solid phase extraction (SPE) cartridge (n = 4) packed with 100 mg of each polymer independently. Each cartridge was loaded with carbaryl standard (500 μL; 50 ng/mL) to assess the capacity of retaining carbaryl and the polymer selectivity. The SPE cartridge was washed with acetonitrile:phosphate buffer (0.5M; pH 7.0) (1000 μL; 40:60, v/v; 5 times) to assess any premature elution of carbaryl due to breakage of the hydrogen bonds between the functional monomer and the functional groups of the carbaryl molecule. The carbaryl was eluted using acetonitrile:phosphate buffer (0.5M; pH 2.0) (500 μL; 40:60, v/v, 10 times) to assess the elution profile of carbaryl from the polymer. Samples were collected after the addition of carbaryl to the SPE cartridge, after each wash step and after each elution step. The collected samples were analyzed by using the HPLC conditions detailed in Table 1. The solution recovered after the loading step showed that carbaryl was retained by MIP1 but was not retained by MIP2. The retained carbaryl by MIP1 did not elute after washing with acetonitrile:phosphate buffer (0.5M; pH 7.0) (40:60, v/v), however, elution did occur in the first elution step, demonstrating that the elution solution (acetonitrile: phosphate buffer (0.5M; pH 2.0) was sufficient to dissociate carbaryl from the binding sites on MIP1. This assessment was repeated again using a calibration standard of 1-naphthol (500 μL, 50 ng/mL) instead of carbaryl. During this phase of the experiment, the solutions recovered after the loading of 1-naphthol showed partial retention of 1-naphthol by MIP1 and complete retention by MIP2. Premature elution of 1-naphthol after retention by MIP2 did not occur after washing with acetonitrile:phosphate buffer (0.5M; pH 7.0) (40:60, v/v). Conversely, after retention

using MIP1, premature elution after the first wash step was observed, suggesting a weak retention due to the inability to form an 'exact fit' in the cavity of MIP1. Similar to carbaryl, 1-naphthol was eluted after the first elution step, which indicated that the elution solution strength was sufficient to dissociate it from the binding cavity of MIP2. Initially the elution solution that was tested was acetonitrile:sodium acetate buffer (0.1M; pH 4.0) (500 µL; 40:60, v/v, 10 times). The samples collected from each of the 10 elution steps showed a significant amount of carbaryl when analyzed by HPLC using ultraviolet detection. Therefore the procedure was repeated in replicates of ten using 1000 µL of the elution solution instead of 500 µL. The results showed that 6 mL of elution solution was necessary to completely elute carbaryl from MIP1. This suggests that the pH of the buffer component of the elution solution was not low enough to dissociate the carbaryl from the binding sites despite being less than the pKa of sodium acetate (pKa = 4.76). This also demonstrates that the pH of the buffer component of the elution solution plays a critical role in analyte elution.

2.3.3 Pre-column assessment

The MIP1 and MIP2 polymers were slurry-packed into three pre-columns. The first pre-column (C1) was packed with MIP1, the second pre-column (C2) was packed with MIP2 and the third pre-column (C3) was packed with a mixture of MIP1:MIP2 (50:50, w/w). Each pre-column was connected to an HPLC-UV system and a calibration standard of carbaryl (50 ng/mL; 100 µL) was injected followed by ultra pure water injections (n = 5) and a calibration standard of 1-naphtol followed by ultra pure water injections (n = 5). The HPLC method used is outlined in Table 2. The results showed that C1 and C3 retained carbaryl for 7.1 minutes, and the peak shape was symmetrical. As expected C2

did not retain carbaryl due to its inability to fit in the binding cavity of MIP2. On the other hand, 1-naphthol was retained by all pre-columns tested at a shorter retention time (6.5 minutes). Pre-column C3 showed that carbaryl and 1-naphthol can be separated due to their different retention times. There was no peak detected in any of the blanks injected after the calibration standards in all three pre-columns, showing that no carry-over between injections occurred.

2.3.4 The validation of the pre-column dilute and shoot method

Pre-column C3 was connected to an analytical column (Gemini C18 5 µm (50 x 4.6 mm id)) on an HPLC system equipped with a column-switching valve. The column switching valve configuration is illustrated in Figure 10.

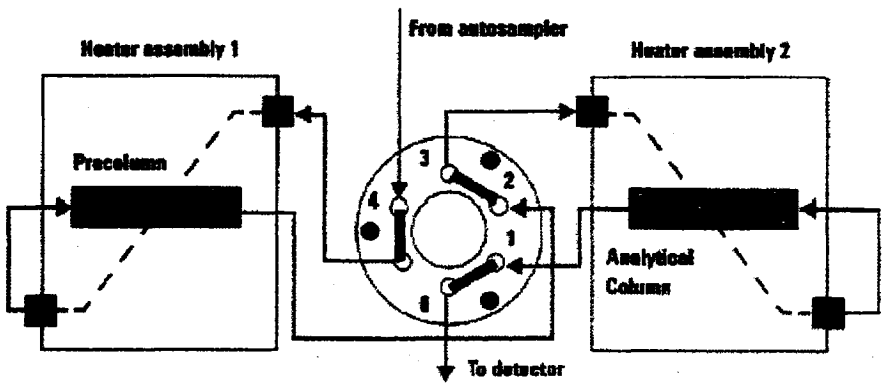

Figure 10: The column switching valve configuration

The previously prepared biological samples were injected onto the pre-column and connected to the detector outlet, bypassing the analytical column. After 5 minutes, the switching valve changed position and the solution passed from the pre-column to the analytical column for 9 minutes. When the sample was injected (time = 0 minutes),

mobile phase A (acetonitrile:phosphate buffer (0.5M; pH 7.0) (40:60, v/v)) was used to allow all interfering species and other components of the biological matrix tested to elute, eliminating contamination or retention on the analytical column. The switching valve was then switched to the analytical column at time = 5 minutes and mobile phase B (acetonitrile: phosphate buffer (0.5M; pH 2.0) (40:60, v/v)) was used, eluting the desired analytes from the pre-column into the analytical column. 1-naphthol and carbaryl retention times were 6.7 and 7.1 minutes, respectively. The signal-to-noise ratio was greater than 4 and the lower limit of detection for carbaryl and 1-naphthol was 1.0 ng/mL. Ten rat plasma and ten apple homogenate spiked standards at carbaryl concentrations of 1.00, 1.60, 2.00, 3.00, 4.00, 5.00, 6.00, 7.00, 8.00, and 10.0 ng/mL, and three levels of quality control rat plasma and apple homogenate spiked samples at carbaryl concentrations of 1.80, 5.00 and 8.00 ng/mL were prepared and analyzed in replicates of six on three different occasions. 1-Naphtol was spiked at a constant concentration of 10.0 ng/mL and used as an internal standard. The method was validated for the extraction efficiency of carbaryl and 1-naphthol from rat plasma and apple homogenate in accordance with the Guidance for Industry Bioanalytical Method Validation as outlined by the United States Food and Drug Administration (FDA)[47]. The method was validated in terms of selectivity, linearity, Lower Limit of Quantitation (LLOQ), carry-over, and intra and inter-assay precision. For selectivity, at least five of the six lots of blank matrix (rat plasma and apple homogenate) tested had no interfering peaks from the blank matrix at the retention times of the analytes. For linearity, the coefficient of determinations (r^2) for the three occasions were 0.996, 0.998, and 0.994 for the rat plasma samples, and 0.995, 1.00 and 0.998 for the apple homogenate samples, and

the individual back-calculated concentrations for all the standards were within 15% of their theoretical values.

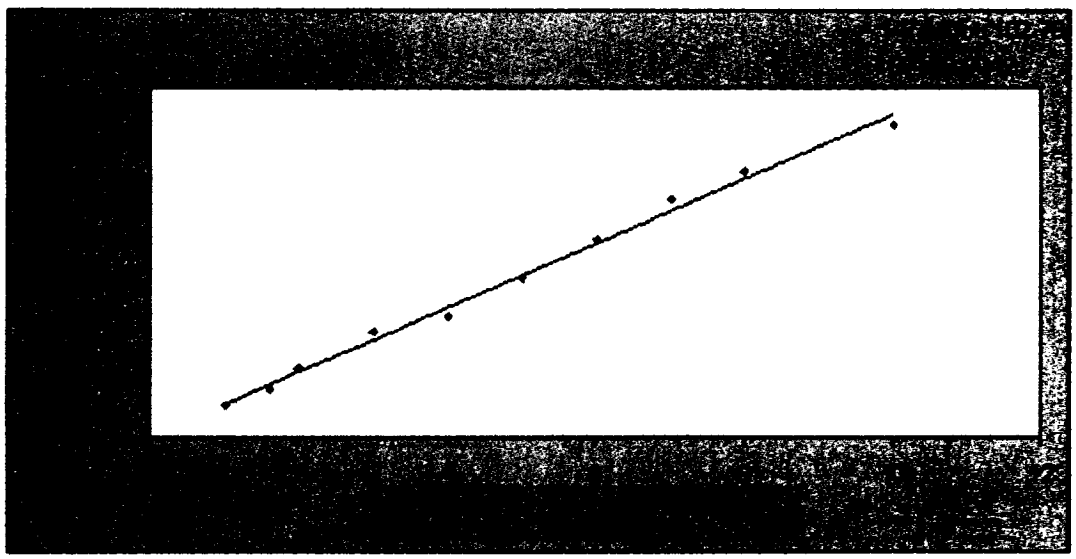

Figure 11 A representative calibration curve for carbaryl extracted rat plasma standards

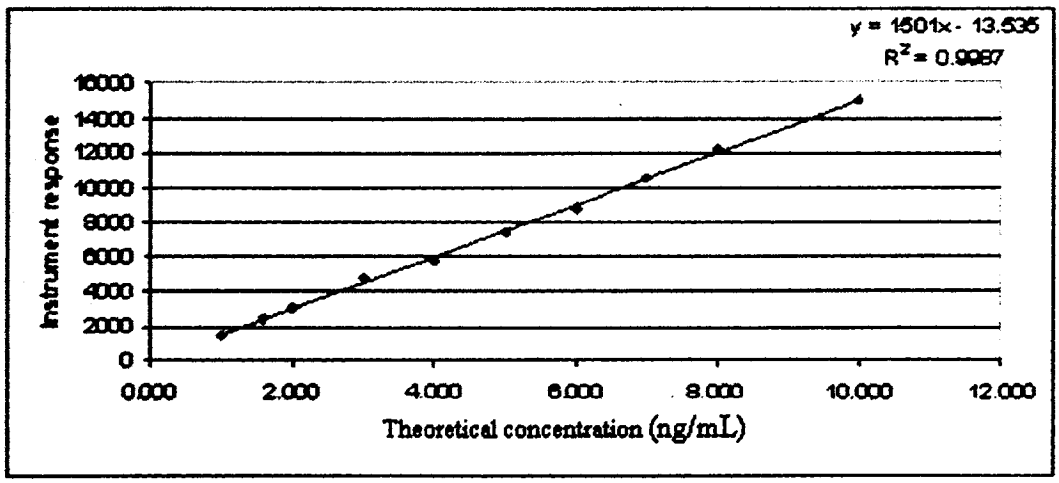

Figure 12 **A representative calibration curve for carbaryl extracted apple homogenate standards**

For the LLOQ, the mean relative error of all six rat LLOQ plasma samples was –2.3% with a CV of 3.2% and for the apple homogenate LLOQ samples, the mean relative error was 8.4% with a CV of 3.8%. For carry-over, there were no peaks at the retention time of the analyte or the internal standard in the blank injections after the highest calibration standard for both matrices. For intra-assay precision and accuracy, the mean relative error of a minimum of five out of six QC spiked samples, for the low, middle and high concentrations were within 15% of their theoretical concentrations for both matrices. For inter-assay precision and accuracy, for rat plasma samples, the global mean relative errors, for the low, middle and high QC spiked samples were 4.3, 4.8 and 1.1% with global CVs of 2.5, 0.7 and 4.1%, respectively and for apple homogenate samples, the global mean relative errors, for the low, middle and high QC spiked samples were 2.6,

2.3 and 1.4% with global CVs of 3.4, 1.4 and 1.7%, respectively. Results are presented in Appendix A. Representative chromatograms are presented in the Figures below.

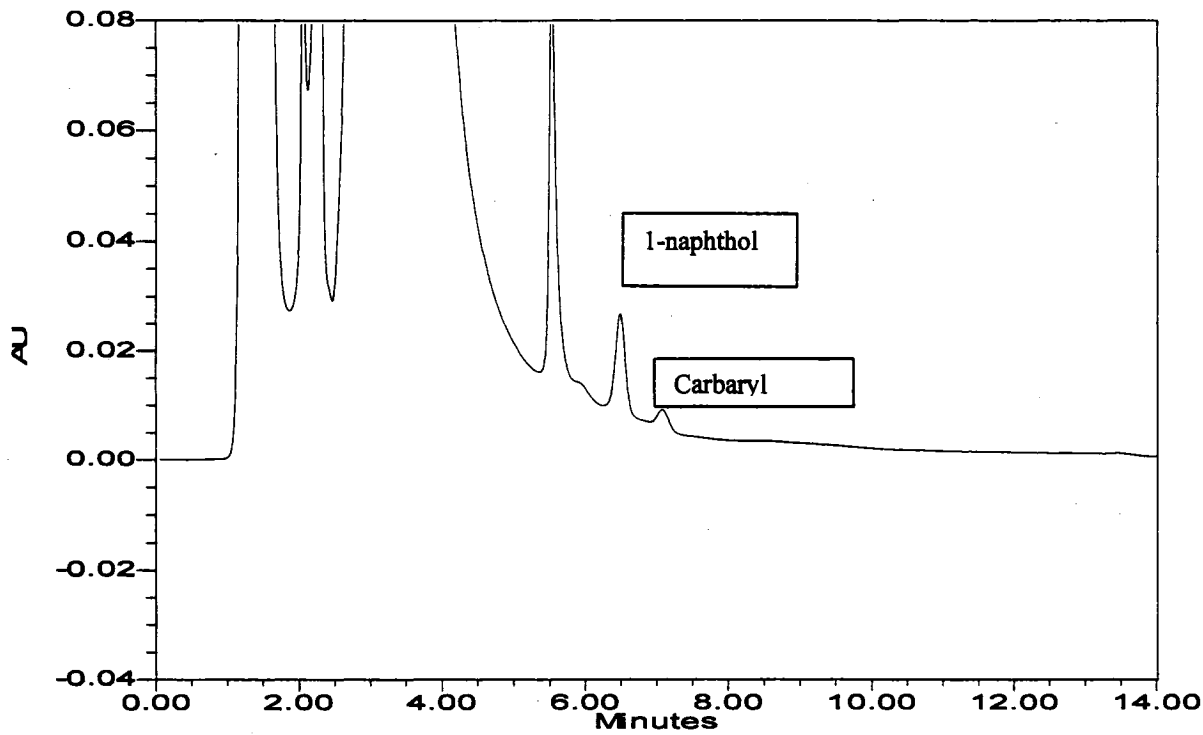

Figure 13: chromatogram of injected standard (carbaryl and 1-naphthol nominal concentration of 1.0 ng/mL) on C3 connected to Gemini C_{18} column using HPLC method

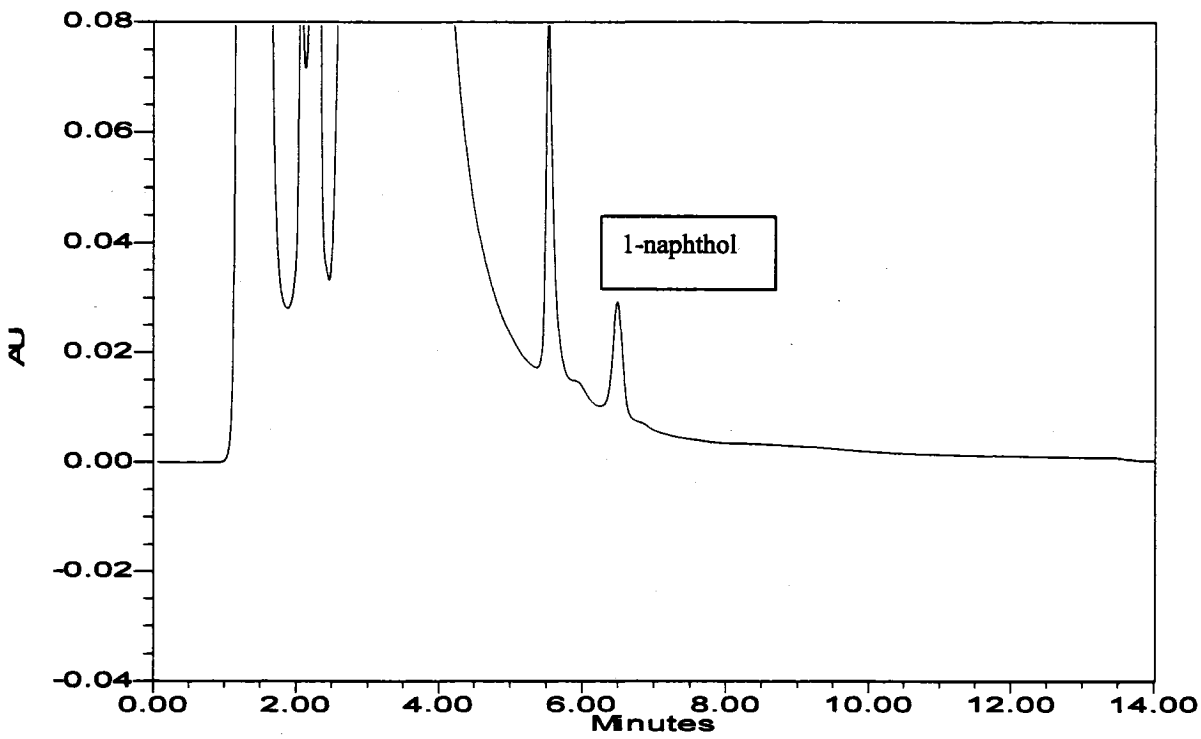

Figure 14: chromatogram of injected standard (1-naphthol concentration of 1 ng/mL) on C3 connected to Gemini C_{18} column using HPLC method

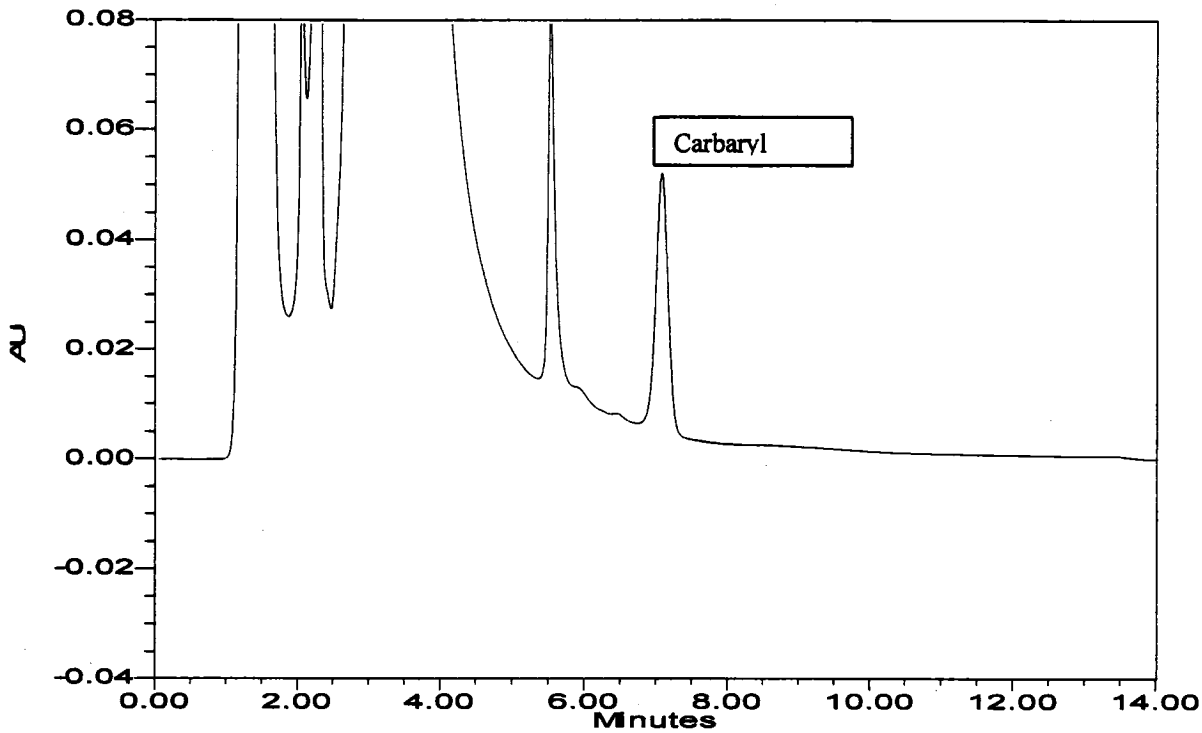

Figure 15: chromatogram of injected standard (carbaryl concentration of 10.0 ng/mL) on C3 connected to Gemini C_{18} column using HPLC method

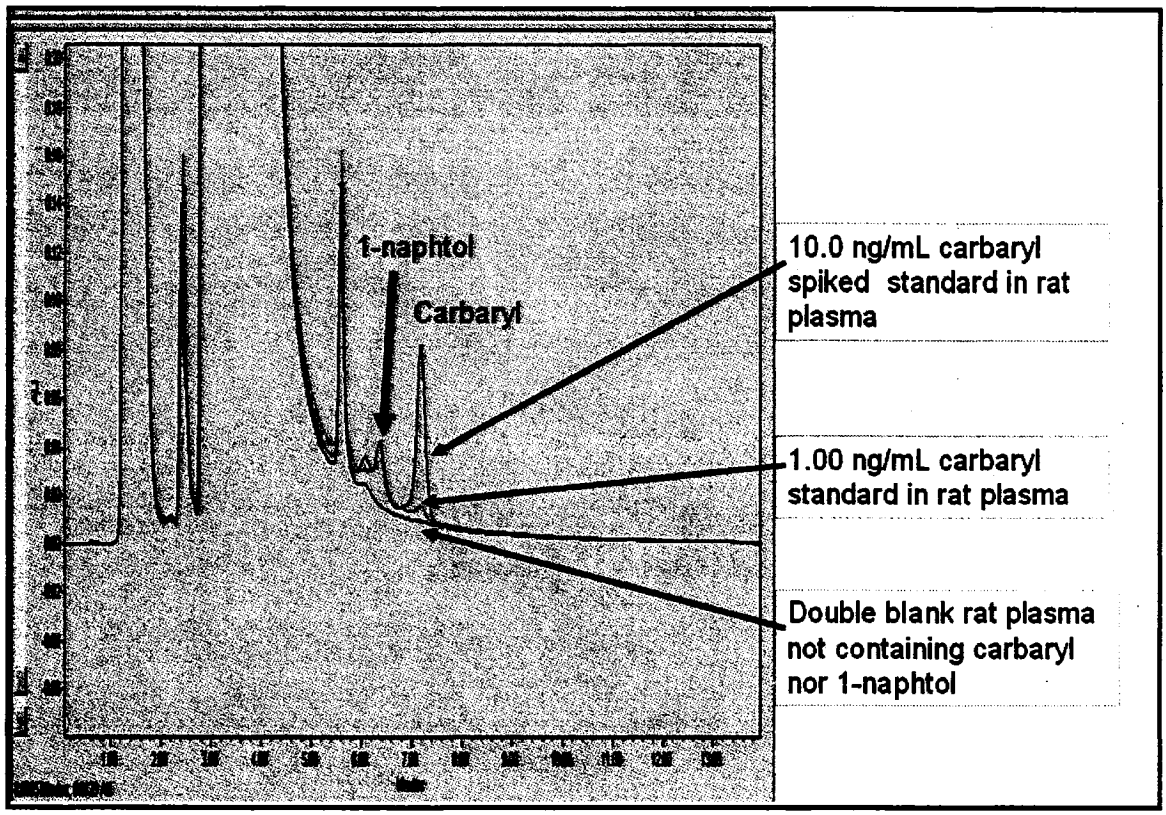

Figure 16 chromatogram of injected standard (carbaryl and 1-naphthol nominal concentration of 10.0 and 1.0 ng/mL) and a double blank

2.4 CONCLUSION

Two imprinted polymers MIP1 and MIP2 were developed and showed that each polymer exhibited a high retentive ability for its analyte (carabryl or 1-naphthol). The imprinted polymer demonstrated resistance to the disassociation of the polymer-carbaryl hydrogen bond linkage. Elution of carbaryl and 1-naphthol from the polymers was shown to be quantitative. The dilute and shoot approach for the rapid, inexpensive and accurate determination of carbaryl and its metabolite (1-naphthol) in complex biological matrices

(rat plasma and apple homogenate) with a detection limit of 1.00 ng/mL and a response that is linear ($r^2 > 0.98$) over the concentration range of 1.00 to 10.0 ng/mL was validated in accordance with the Guidance for Industry Bioanalytical Method Validation as outlined by the United States Food and Drug Administration (FDA).

Chapter 3

In-situ determination of carbaryl in biological matrices via a non-enzymatic chemical sensor

3.1 The Electrochemical Detector

The electrochemical detector responds to substances that are either oxidizable or reducible and the electrical output is an electron flow generated by a reaction that takes place at the surface of the electrodes. If the reaction proceeds to completion (exhausting all the reactant) the current becomes zero and the total charge generated will be proportional to the total mass of material that has been reacted. This process is called *coulometric* detection. If, however, the mobile phase is flowing past the electrodes, the reacting solute will be continuously replaced as the peak passes through the detector. As long as there is solute present between the electrodes, a current will be maintained, albeit varying in magnitude. Until relatively recently, this procedure was the most common employed in electrochemical detection and is called *amperometric* detection[19].

The electrochemical detector requires three electrodes, the working electrode (where the oxidation or reduction takes place), the auxiliary electrode and the reference electrode (which compensates for any changes in the background conductivity of the mobile phase). The processes taking place at the electrode surface can be very complex; nevertheless, the dominant reaction can be broadly described as follows:

At the actual electrode surface the reaction is extremely rapid and proceeds almost to completion. This results in the layer close to the electrode being virtually depleted of

reactant. As a consequence, a concentration gradient is established between the electrode surface and the bulk of the solution[19].

This concentration gradient causes solute to diffuse into the depleted zone at a rate proportional to the solute concentration in the bulk of the mobile phase. Thus, the current generated at the electrode surface will be determined by the rate at which the solute reaches the electrode and consequently, as the process is diffusion controlled, will depend on solute concentration and the magnitude of solute diffusivity[19].

3.1.1 Electrode Configurations

The electrodes can take a number of different geometric forms. Some examples of different electrode configurations are shown in the figure below. Examples (A) and (B) are two common forms of thin-layer cells. Configuration (A) has the working electrode sealed into the cell wall with the reference and auxiliary electrodes situated down-stream to the working electrode.

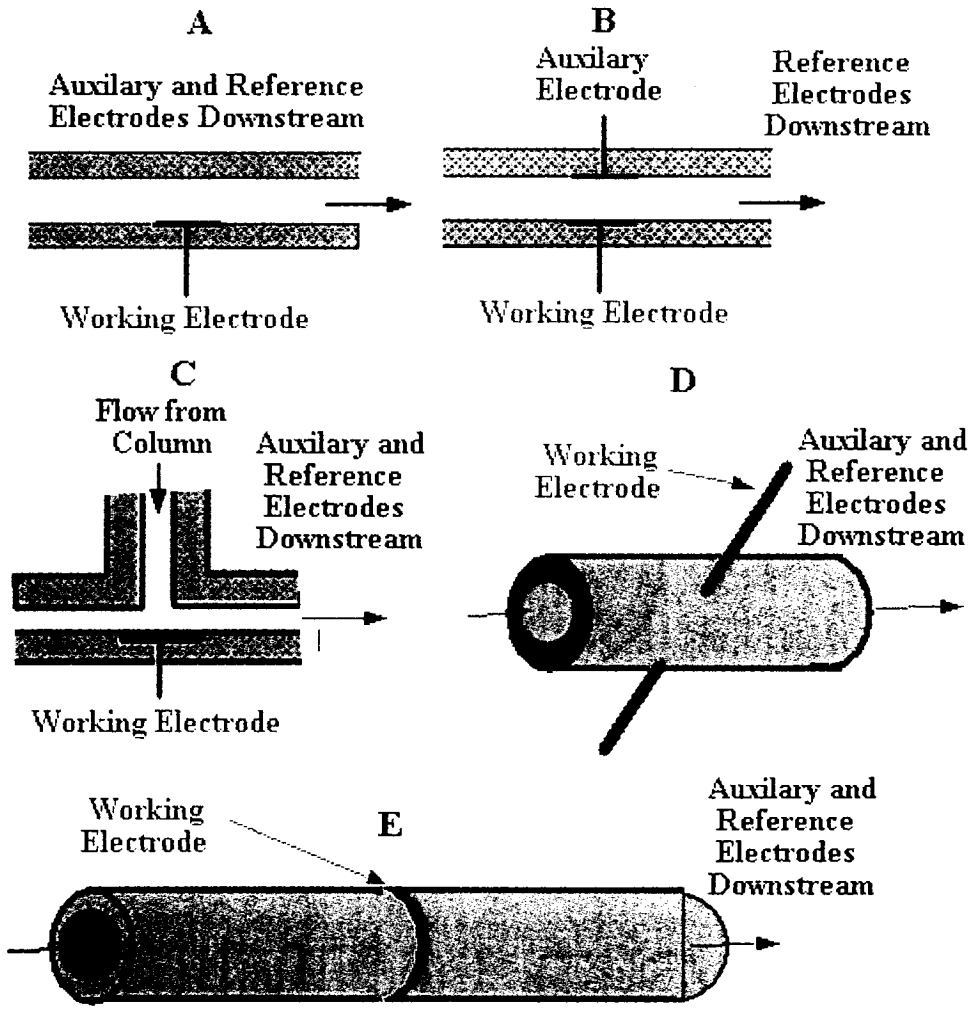

Source: http://www.ids-healthcare.com/hospital_management/global/esa_biosciences/electrochemical_detection/101_0/g_supplier.html

Figure 17 Different Electrode Configurations

Configuration (B) is similar to (A) but with the auxiliary electrode sealed in the wall of the tube opposite the working electrode and, again, the reference electrode down-stream. Configuration (C) is a wall-jet electrode where the eluent is allowed to impinge directly onto the working electrode, which is situated opposite the jet. This arrangement not only

increases the value of (v) (the velocity of the liquid passing over the electrode and thus the transfer coefficient (K_T)) but also scrubbs the surface of the working electrode helping to reduce the need for frequent cleaning. (D) and (E) are two examples of cylindrical electrodes; in (D) the working electrode is in the form of a rod stretching across the diameter of the sensor cell and in (E) the working electrode comprises an annular ring set in the cell wall. In both cases the auxiliary and the reference electrodes are situated down-stream to the working electrode[48] .

3.1.2 Electrode Construction

The choice of electrode construction material is restricted due to the need for mechanically ruggedness and long-term stability. The most common material is carbon paste made from a mixture of graphite and some suitable dielectric substance. This material has the disadvantage that it is soluble in some solvents, although, using special waxes or polymers as dielectric binders to contain the graphite, helps reduce the solubility problem. Vitreous or 'glassy' carbon is an excellent electrode material particularly if organic solvents are to be used and is probably the most popular contemporary electrode material. Glassy carbon is produced by slowly baking a suitable resin at elevated temperatures until it is carbonized and then heating it to a very high temperature. Vitreous carbon is relatively pure, mechanically strong, has good electrical properties and can be readily cleaned mechanically. It also performs particularly well when operated at a negative potential. Glassy carbon electrodes are preferable to carbon paste electrodes due to their inherent resistance to solvents[48].

Electrochemical detection imposes certain restrictions on the type of chromatography that is employed and the mobile phase that is used. The detecting system requires a

conducting mobile phase and thus must contain water. Thus, the majority of 'normal phase' systems are not usable. In addition, very high solvent concentrations may render it insufficiently conducting. Reversed phase chromatography, however, is ideally suited to electrochemical detection. Nevertheless, certain precautions must be taken for its effective use. The mobile phase must be completely oxygen free, which can be removed by bubbling helium through the solvent reservoir. It is also important to remove oxygen from the sample before making an injection. The solvents must also be free of metal ions or serious baseline instability will result. Non-aqueous solvents such as pure acetonitrile can be employed but certain salts like tetrabutyl-ammoniumhexafluorophosphate must be added to render the solvent conducting[48].

3.2 Introduction

The analysis of carbamate is usually carried out by gas and liquid chromatography, with selective- element detector [49, 50]. In an analytical method, sample preparation is followed by a separation and detection procedure. In spite of the fact that sample preparation, in most of the analytical procedures, takes 50-75% of the total time of the analysis, most technical innovations of the last decade are related to separation and detection. Nevertheless, these procedures frequently require lengthy extraction and clean up steps that increase the risk of sample lost, time consuming and constitute the primary source of errors and discrepancies between laboratories. On the other hand, the recent regulatory pressure to reduce the amount of organic solvent wastes generated in these procedures has forced the application of alternative methods for pesticides determination.

In recent decade numerous biosensing methods for detection of pesticides have been developed using enzyme based affinity based sensors as well as several types of

transducers and this has been the subject of several recent reviews[51, 52, 53, 54]. Enzymatic determination of pesticides is most often based on inhibition. The procedures involve the measurement of the uninhibited activity of the enzyme, followed by an incubation period for the reaction between enzyme and inhibitor and the measurement of the enzyme activity after the inhibition. Application of single use screen-printed biosensor in batch measurements and flow injection analysis with enzyme biosensors is the most developed procedures[39]. Flow-injection systems generally require another final step to reactivate enzyme after inhibition for reuse, which in general is only partial. This also makes the analysis time longer.

For the first time we report the development of a flow injection chemical sensor system using molecular imprinted polymer (MIP) in situ treatment for the determination of carbaryl in complex biological matrices (rat plasma for environmental and toxicological purposes) at a low detection limit of 10.0 μg/mL with a time saving, cost effective and non-enzymatic approach. A potentiometric detection principal was investigated, using a pH electrode, to detect the increase of hydrogen ions. The study was focused on carbaryl, the pesticide that has been used in large amount in Asia especially Thailand[55] and its residue was found in water and soil samples in Thailand[56].

The carbaryl molecular imprinted polymer was prepared as described in chapter 2 with a particle size of ~ 5 μm isolated and packed into a column (50 x 4.6 mm id) that is used to isolate carbaryl from complex matrices injected on the flow injection chemical sensor without extensive sample preparation and clean up or expensive enzyme and lengthy incubation times.

3.3 Experimental

3.3.1 Materials

Carbaryl lot number LB316-60B from Supleco. Phosphate buffer lot number 440524/1 50403196 from Fluka.

3.3.2 Packing the imprinted polymer into an analytical column

The imprinted polymer that was previously prepared as described in Chapter 2 was slurry-packed into a 50 X 4.60 mm id poly ether ether ketone (PEEK) column. The imprinted polymer was wet with methanol, tightly packed, and subjected to a pressure of 114 bar, at a flow rate of 5.0 mL/min, for 30 minutes. The column was checked for voids, re-packed, and subjected to a pressure of 114 bar again, at the same flow rate. This procedure was repeated until no voids were observed.

3.3.3 Preparation of biological samples

Rat plasma samples (100 µL) were spiked with carbaryl. Acetonitrile (300 µL) was added to each plasma sample and centrifuged (~ 14000 rpm; ~ 4°C; ~ 15 minutes). The supernatant was transferred to injection vials for analysis.

3.4 Results and Discussion

3.4.1 Column assessment

The MIP polymer were slurry-packed into a column. The column (C1) was packed with MIP. The column was connected to an HPLC-UV system and a calibration standard of carbaryl (50 ng/mL; 100 µL) was injected followed by ultra pure water injections (n = 5). The results showed that C1 retained carbaryl for 7.1 minutes, and the peak shape was

symmetrical. There was no peak detected in any of the blanks injected after the calibration standards, showing that no carry-over between injections occurred.

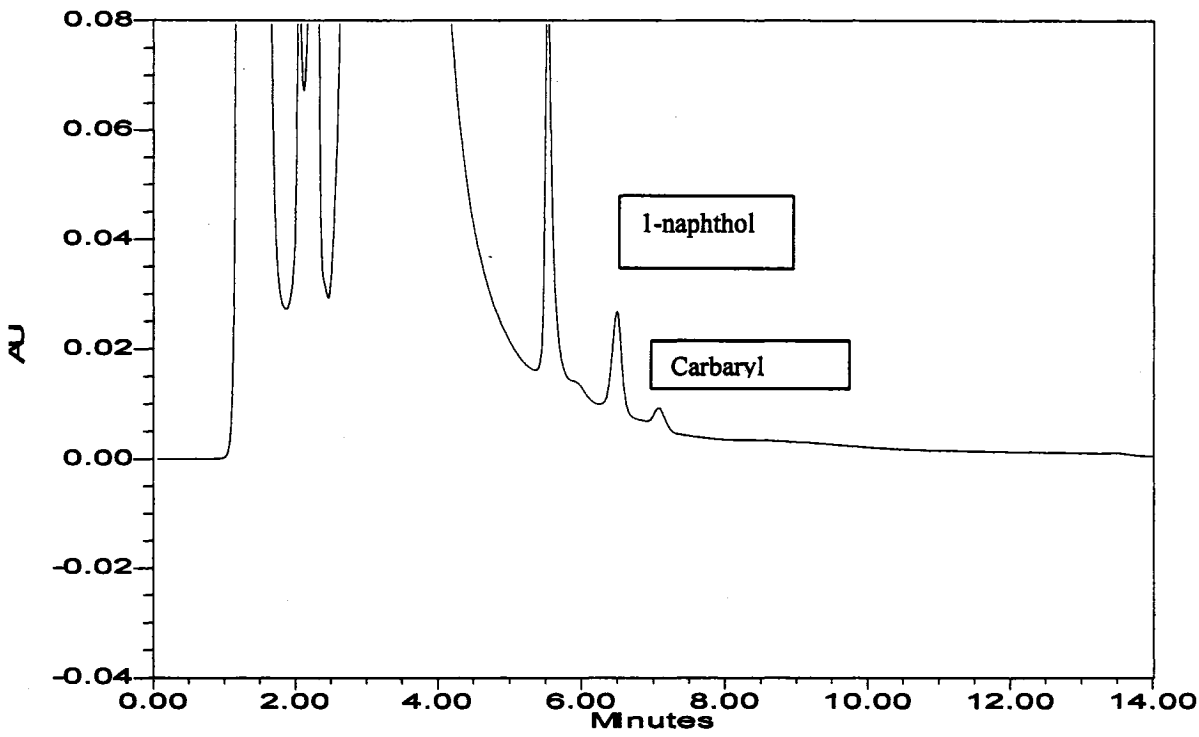

Figure 18 **chromatogram of injected standard (carbaryl and 1-naphthol nominal concentration of 1.0 ng/mL) on C3 connected to Gemini C_{18} column using HPLC method**

3.4.2 Potentiometric chemical sensor design and operation

A flow injection chemical sensor system, and a potentiometric (Ion analyzer, PHM 250, Radiometer) were developed and studied (see figure below).

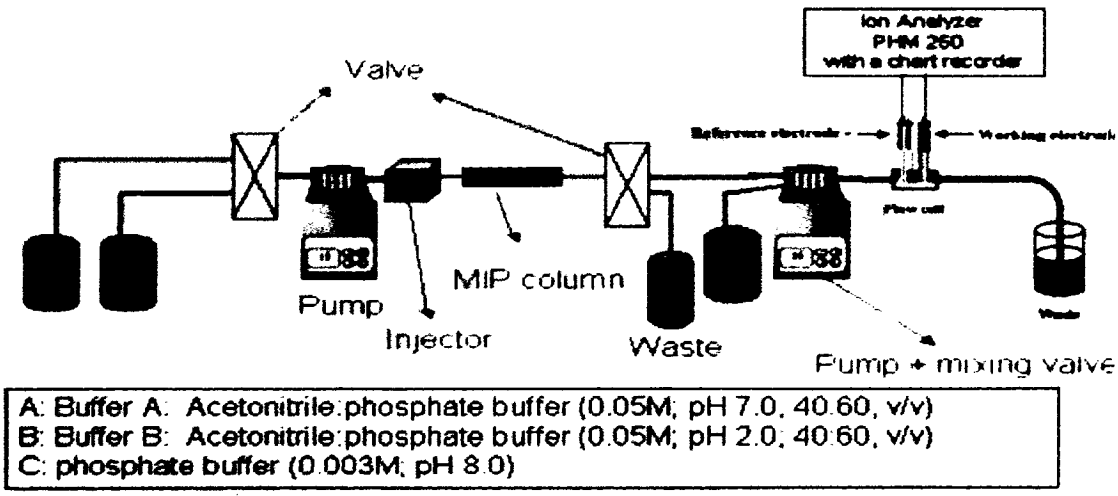

Figure 19 Schematic diagram showing the flow-injection chemical sensor system

The potentiometric system used pH electrode that is readily available. The responses of the system were measured using the peak heights. Parameters affecting the responses of the flow systems were optimized by changing a single variable while the others were kept constant, to obtain a high sensitivity in a short period of time. For analysis of a sample containing carbaryl, the sample (1000 μL) was injected into the carrier buffer A (acetonitrile:phosphate buffer , 0.050M; pH 7.0; 40:60, v/v) that was pumped through the column. Immobilized carbaryl in the binding sites of MIP in the column were washed by allowing buffer A to continue flowing while the valve was connected to waste position (ie no flow through the cells) for ~3 minutes after the injection was complete. The valves were then set to allow buffer B (acetonitrile:phosphate buffer , 0.050M; pH 2.0; 40:60, v/v) to flow and the micro-fluid to pass through the flow injection cell. Carbaryl bound to the carboxylic acid arms in the binding cavity of the MIP will be protonated and hence dissociate from the binding cavity to the buffer B. The optimum buffer capacity was

found to be phosphate buffer (0.005M). On the other hand, carbaryl required phosphate buffer of minium of 0.050 M to elute from the column. Therefore, the flow injection was diluted in situ by allowing 0.1 mL/min to flow from column to the second pump and a line of buffer C (phosphate buffer, 0.003M; pH 8.0) to flow into the pump at a rate of 0.9 mL/minute. This raise in the local pH of the flow cell by buffer C allow protonated carbaryl to lose a proton and become neutral.

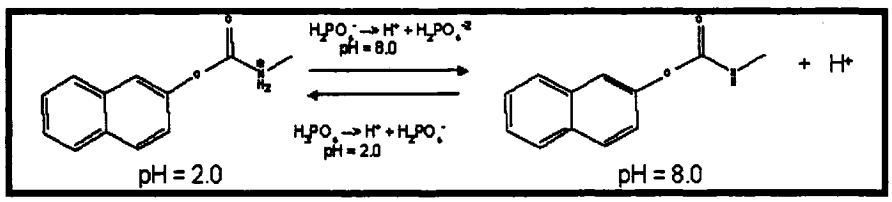

Equation 6

The pH change generated by de-protonation of carbaryl in alkaline medium was measured. The second pump equipped with a mixing valve to allow the homogeneous mixing of the fluid from the two lines before passing to the flow cell for detection without introducing any gas bubbles.

3.4.2.1 The effect of phosphate buffer concentration

In the potentiometric system the pH change generated by the release of proton when carbaryl undergoes deporotonation as shown in Equation 6 was measured. A high buffer capacity would lead to a low sensitivity. On the other hand, if the buffer with a lower capacity was used, sensitivity would increase but this may case the change of the local pH during the measurement. Phosphate buffer was used in this system because it is a widely used biochemical buffer. When the response of the system to different concentrations of buffer was investigated, higher concentration gave lower response. Although the maximum signal was obtained with the lowest buffer concentration (3.0

mM), its low buffering capacity caused the shift of the baseline with time due to pH change. The lowest buffer concentration that gave a steady baseline was 5.0 mM and this was selected for this work.

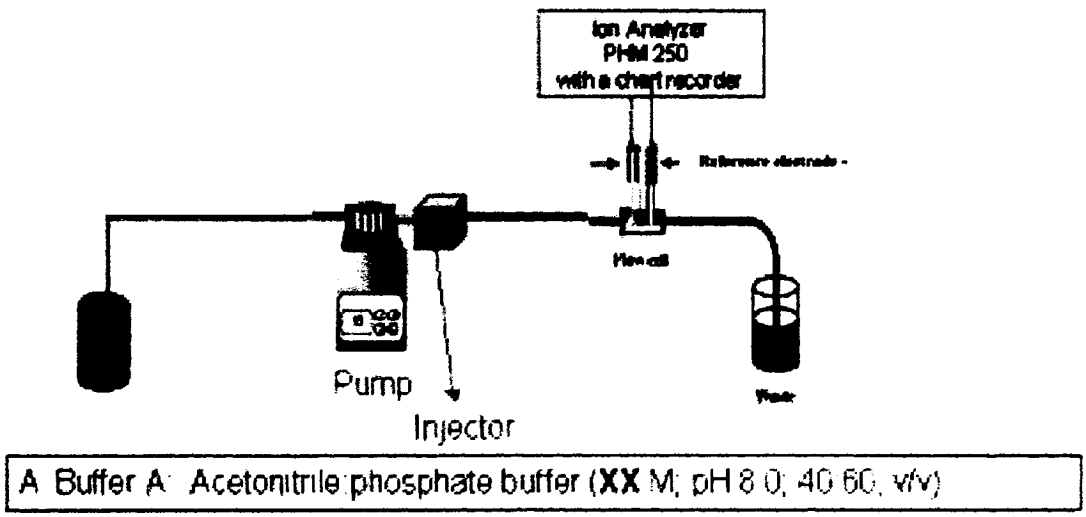

Figure 20 **Modified chemical sensor schematics for the determination of the effect of pH and concentration variation of the phosphate buffer used**

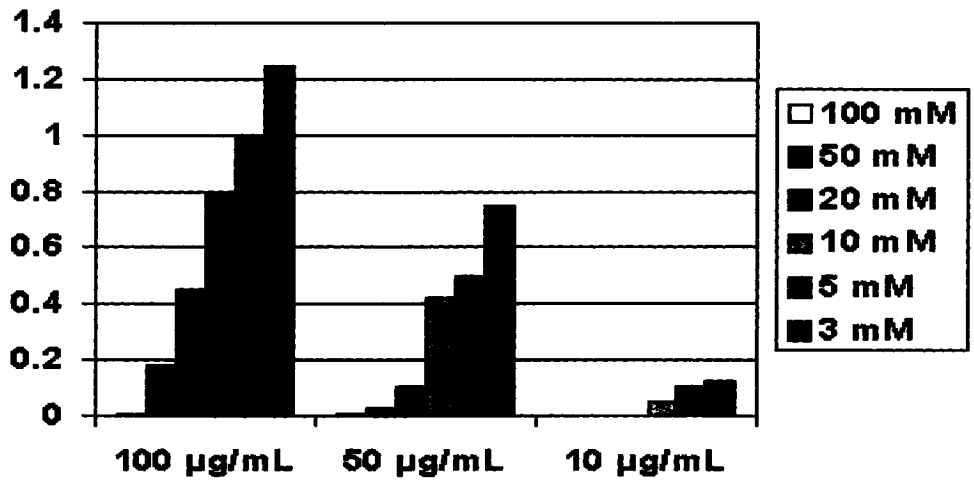

Figure 21 **The instrument response versus the phosphate buffer concentration**

3.4.3 The validation of the chemical sensor system

The signal-to-noise ratio was greater than 4 and the lowest limit of detection for carbaryl was 10.0 μg/mL, representative chromatograms are shown in the figure below.

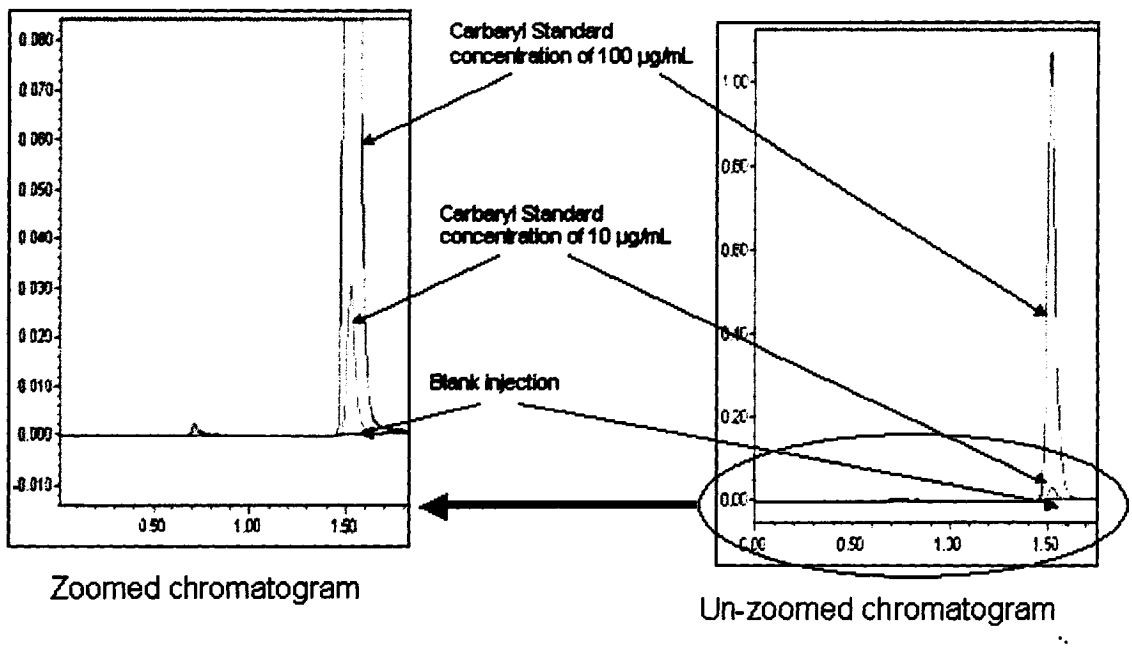

Figure 22 Representative chromatogram

Ten rat plasma spiked standards at carbaryl concentrations of 10.0, 16.0, 20.0, 30.0, 40.0, 50.0, 60.0, 70.0, 80.0 and 100.0μg/mL, and three levels of quality control rat plasma spiked samples at carbaryl concentrations of 18.0, 50.0 and 80.0 μg/mL were prepared and analyzed in replicates of six on three different occasions. The method was validated for the detection efficiency of carbaryl from rat plasma in accordance with the Guidance for Industry Bioanalytical Method Validation as outlined by the United States Food and Drug Administration (FDA) [47]. The method was validated in terms of selectivity,

linearity, lower limit of quantitation (LLOQ), carry-over, and intra and inter-assay precision and accuracy. For selectivity at least five of the six lots of blank matrix (rat plasma) tested had no interfering peaks from the blank matrix at the retention times of the analyte. For linearity, the coefficient of determinations (r^2) for the three occasions were 0.9983, 0.9978, and 0.9984 for the rat plasma samples, and the individual back-calculated concentrations for all the standards were within ±15% of their theoretical values, a representative linear curve is present in the figure below.

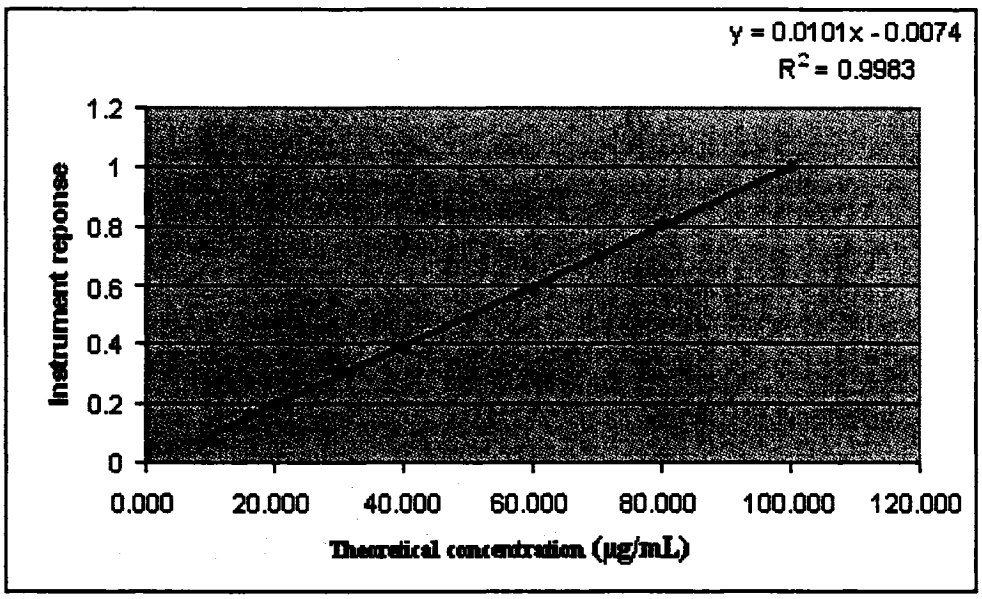

Figure 23 **A representative calibration curve of carbaryl covering the range of 10.0 to 100 µg/mL**

For Lower Limit of Quantitation (LLOQ), the mean relative error of all six rat LLOQ plasma samples was –2.3% with a CV of 3.2%. For carry-over, there were no peaks detected at the retention time of the analyte in the blank injection after the highest

calibration standard. For intra-assay precision and accuracy, the mean relative error of a minimum of five out of six QC spiked samples, for the low, middle and high concentrations, were within ±15% of their theoretical concentrations. For inter-assay precision and accuracy the global mean relative errors, for the low, middle and high QC spiked samples were 4.3, 4.8 and 1.1% with global CVs of 2.5, 0.7 and 4.1%, respectively.

3.5 Conductivity chemical sensor design and operation

The electrical conductivity detector can only detect substances that ionizes and consequently, is frequently used in the analysis of inorganic acids, bases and salts. It has also found particular use in the detection of organic acids and bases that are frequently required in environmental studies and in biotechnology applications. It measures the conductivity of the mobile phase. There is usually background conductivity which must be backed-off by suitable electronic adjustments. If the mobile phase contains buffers, the detector gives a base signal that completely overwhelms that from any solute usually making detection impossible. Thus, the electrical conductivity detector is a bulk property detector, which senses all ions whether they are from a solute or from the mobile phase. There are two ways of defining detector response, either as detector output (usually in mv) per unit change in solute concentration or as the detector output per unit change in the units of detector measurement (e.g. the sensitivity of a conductivity detector would be defined in terms of detector output per unit change in electrical conductivity). The sensor is the simplest of all the detectors consisting of only two electrodes situated in a suitable flow cell. The electrical conductivity-sensing cell used is shown in the Figure below.

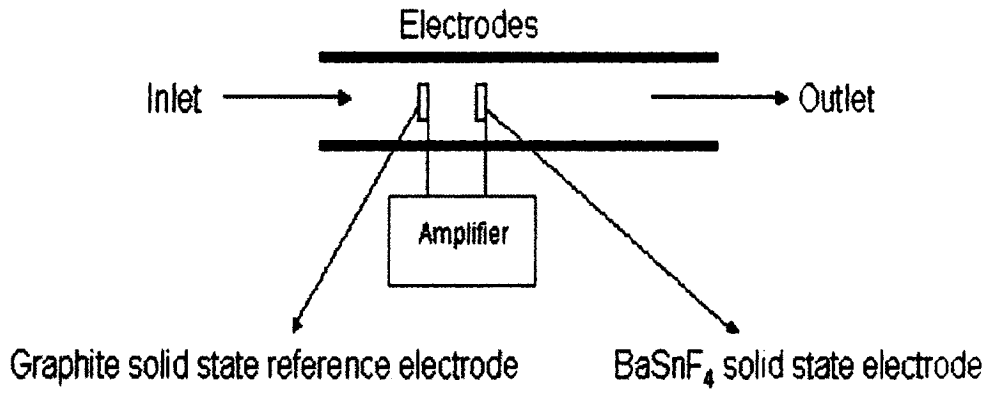

Figure 24 Schematic diagram showing the flow-injection conductivity cell

It consists of two electrodes situated in a suitable flow cell. The electrodes are arranged to constitute one arm of a Wheatstone bridge. When ions enter the detector cell, the electrical resistance changes and the out of balance signal is fed to a suitable amplifier. The output from the amplifier was passed directly to a potentiometric recorder. The detector actually measures the electrical resistance between the electrodes, which by suitable non-linear amplification, can be made to provide an output that is linearly related to solute concentration. It is essential that an AC voltage is used across the electrodes to measure the cell impedance to avoid electrode polarization. The frequency of the AC potential across the electrodes was around 10 kHz.

The choice of electrode construction material is restricted due to the need for mechanically ruggedness and long-term stability. Therefore, an attempt to try $BaSnF_4$ as a working electrode was undertaken. $BaSnF_4$ thin sheets were prepared by precipitation reaction as described in Chapter 4. The precipitated layers of $BaSnF_4$ on a gold plate were used as a solid-state electrode. The aim was to be able to measure the change in

conductivity of the layered $BaSnF_4$ as carbaryl concentration changes in the micro-fluid solution passing in the capillary. Unfortunately due to the fact that $BaSnF_4$ layers are extremely fragile, the capillary pressure applied by the micro-fluid passing through the capillary resulted in cracks in the surface of the layer within less than 30 seconds. The cracks cause faulty conductivity readings. All attempts to prepare a thicker and higher pressure resistance $BaSnF_4$ sheets failed.

3.6 CONCLUSION

The developed flow-injection chemical sensor system using carbaryl molecular imported polymer can be used to detect pesticides in biological samples with a good sensitivity and low detection limit. The dilute and shoot approach for the rapid, inexpensive and accurate determination of carbaryl in complex biological matrix (rat plasma) with a detection limit of 10.0 μg/mL and a response that is linear ($r^2 > 0.98$) over the concentration range of 10.0 to 100 μg/mL was validated in accordance with the Guidance for Industry Bioanalytical Method Validation as outlined by the United States Food and Drug Administration (FDA). The attempt to use $BaSnF_4$ as a solid-state electrode to be used in a conductivity cell for the determination of carbaryl was not successful. The obstacle in preparing $BaSnF_4$ sheets that can resist the capillary pressure in the flow cell was the main reason.

Chapter 4

Study of $BaSnF_4$ versus method of preparation

4.1 Introduction

Ionic conductivity in solids is due to ionic motion at temperatures well below their melting point, coupled with unusually low values of activation energy. In recent years there has been a great deal of experimental and theoretical work performed on the ionic mobility in materials which crystallize in the fluorite type structure, or closely related to it[57, 58]. Most of the tin(II) containing fluoride ion conductors cannot be obtained in the form of useable crystals because the crystallite shape is usually highly anisotropic (sheet or needle-shape crystals) due to the stereoactivity of tin(II) lone pair, which creates very effective cleavage planes[59-61]. Such materials have potentials for use for thermodynamic measurement devices, specific electrodes, gas sensors, and solid-state batteries. $PbSnF_4$, the highest performance fluoride ion conductor, has been used in the fabrication of an oxygen sensor[59, 62-64].

J. D. Donaldson and B. J. Senior in 1967 [60, 61, 65] reported the immediate precipitation of crystalline metal(II) tin(II) fluorides, $SrSn_2F_6$, $BaSn_2F_6$ and $PbSnF_4$ when the metal(II) nitrate is added to SnF_2 in aqueous medium. For the calcium nitrate/tin(II) fluoride system, Dénès et al. found that the precipitate has a variable composition; however, it is not amorphous[62, 63, 64, 66-70] in contrast with Donaldson and Senior's report[60, 65]. Depending on the conditions of preparation, crystalline $CaSn_2F_6$ or a nanocrystalline $Ca_{1-x}Sn_xF_2$ fluorite-type solid solution precipitates, or often, a mixture of both. Two new $MSnF_4$ compounds [M = Sr, and Ba] were prepared by direct reaction, at 550°C, and

furthermore, $PbSnF_4$ was prepared by direct reaction at 250°C[65, 66, 59-65]. The three $MSnF_4$ compounds were shown to be isotypic and to be a tetragonal distortion of the fluorite-type CaF_2, with M/Sn order along the $\vec{c}$ axis[59]. A similar distortion is found in the PbClF type, however in this case, it is due to Cl/F order parallel to $\vec{c}$ [71]. Among the MF_2 fluorides, those crystallizing in the fluorite type-structure have the highest fluoride ion conductivity[67, 72]. It is presumably the availability of a large number of potential interstitial sites in the middle of the empty F_8 cubes, i.e. those that do not contain a metal ion, which makes easy the formation of Frenkel defects[72]. However, in a recent study, Dénès has shown that this theory does not explain why the conductivity of β-PbF_2 is much higher than that of BaF_2, since it should be easier to move fluoride ions within the BaF_2 lattice, owing to the large size of Ba^{2+} compared to Pb^{2+}, which results in larger empty F8 cubes[68, 72]. Dénès hypothesized that the presence of the soft ion Pb^{2+} in the typically ionic fluorite structure seems to favor fluoride ion disorder[69, 73].

The crystal structure of $BaSnF_4$ and of isostructural α-$PbSnF_4$ was solved by using a combination of X-ray and neutron diffractions, EXAFS and ^{119}Sn Mössbauer spectroscopy [59-61, 62, 68, 70, 71, 72, 73, 74, 75, 76, 77, 78]. It is closely related to the fluorite-type with the following key differences as can be seen in Figure 25 and Figure 26:

- ...Ba Ba Sn Sn ... order parallel to $\vec{c}$, responsible for the doubling of the *c* parameter, and for the loss of both the cubic symmetry and the F Bravais lattice.
- The tin 5-coordination instead of being cubic like Ba in BaF_2. It is based on a sp^3d^2 hybridization of tin, and therefore an octahedral distribution of electron pairs, with four equal Sn-F equatorial bonds, equal to the sum of the ionic radii

(2.282Å), and one very short axial Sn-F bond (2.029Å), strongly covalent in trans-position relative to the stereoactive lone pair.

- The barium coordination is 12, whereby the BaF_8 cube of BaF_2 is distorted, and the fluorine axially bonding to the four tin atoms neighboring to a Ba form four additional bonds to barium, located in equatorial positions.
- The disappearance of the fluoride ion layer that should be between the adjacent tin layers, and its replacement by a sheet of stereoactive lone pairs, create a very efficient cleavage plane which make $BaSnF_4$ a two-dimensional structure that has very strong anisotropic behavior, in contrast with the three-dimensional structure of BaF_2, the latter having isotropic properties.

With the fluorine axially bonding tin occupying the F_8 cubes that are empty in BaF_2, the $BaSnF_4$ structure does not offer the same potential interstitial sites for the formation of Frenkel defects as BaF_2 does, and therefore, its ionic conductivity would be expected to be much lower. To the contrary, its fluoride ion mobility is about three orders of magnitude as high as that of BaF_2[79, 77]. This has been attributed to the fluoride disorder created by the Sn(II) soft atom which is covalently bonded in an ionic type structure[63, 73], similarly to the reason why β-PbF_2 has a higher conductivity than BaF_2. This hypothesis has been corroborated by neutron diffraction of isotypic $PbSnF_4$ versus temperature, which has shown that the two fluorine sites in bridging positions get underpopulated when temperature increases, and the missing fluoride ions partially populate the spacing between tin layers, i.e. in the sheets of lone pair[80, 75].

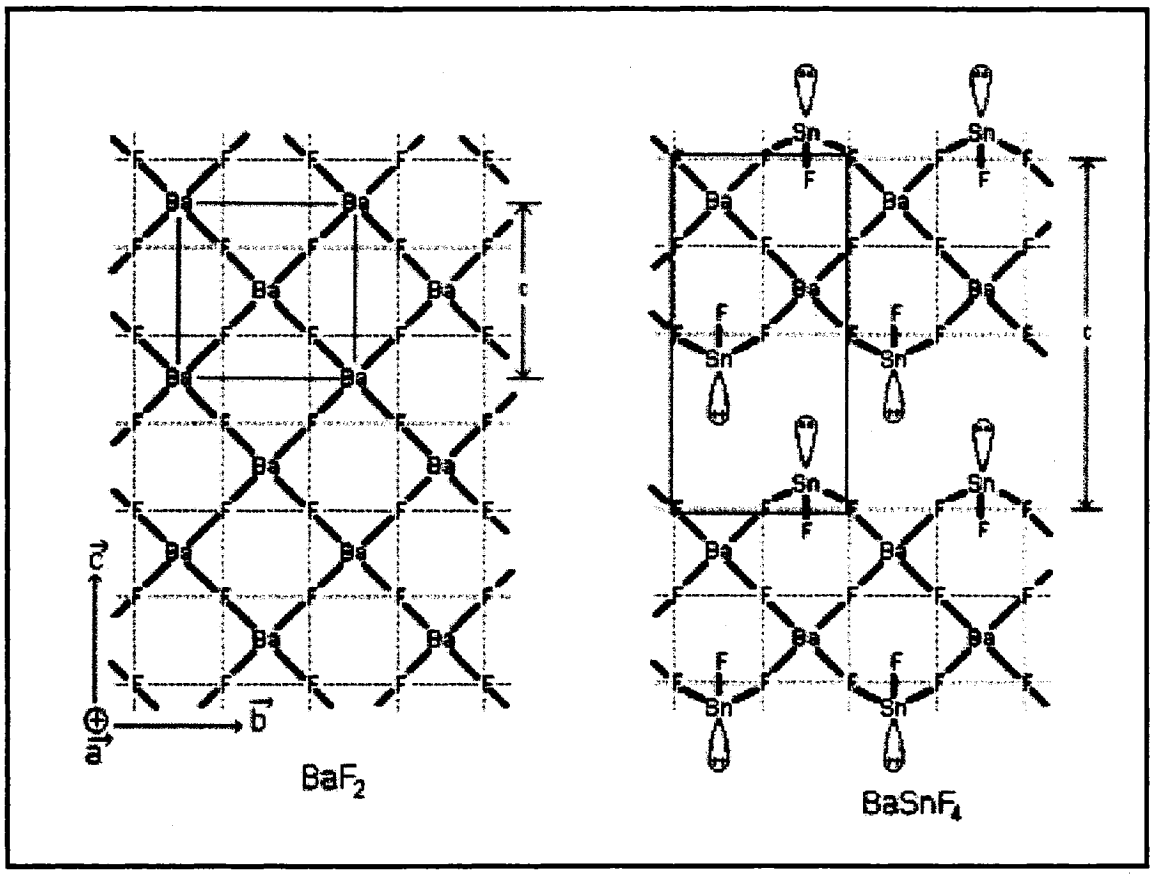

Figure 25 Projection of a slice of the structure of BaF_2 and $BaSnF_4$ on the ($\vec{a},\vec{b}$) plane in the BaF_2 axes [61, 68, 69]

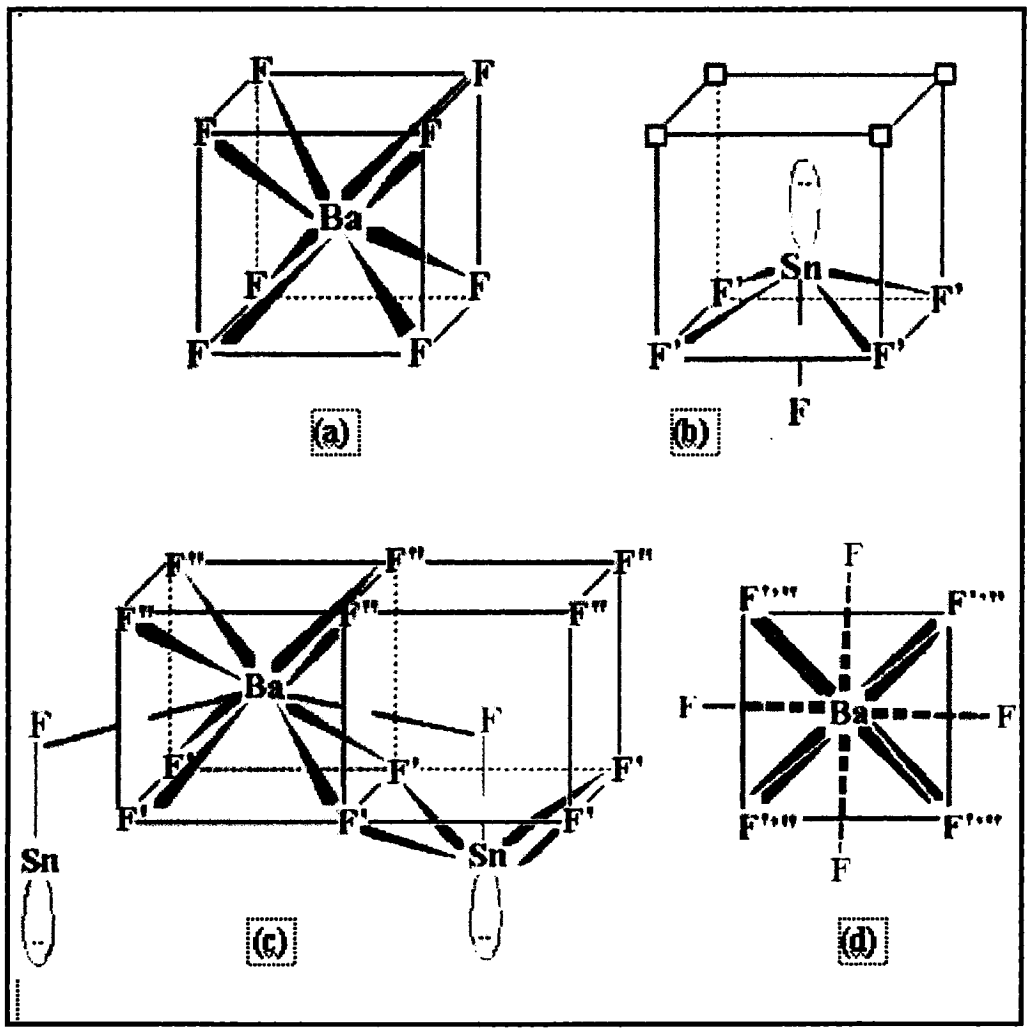

Figure 26 Barium and tin coordination in BaF_2 and in $BaSnF_4$:(a) BaF_8 cube in BaF_2, (b) $SnFF'_4E$ pseudo-octahedron in $BaSnF_4$, (c) $BaF''_4F'_4F_4$ unit in $BaSnF_4$ and (d) Top view of the barium coordination in $BaSnF_4$ (F' and F'') are superimposed [61, 68, 69, 78]

The multi-walled carbon nanotube, boron-doped diamond and glassy carbon electrodes, and most importantly, graphite electrodes are the most commonly used electrodes in conductivity flow cells [79, 81]. It was hoped that since $BaSnF_4$ is known to be a superionic

conductor, it could increase the sensitivity of the impedance measurement of the conductivity cell when a graphite electrode is used as a reference electrode. Therefore we tried to adapt $BaSnF_4$ in the design of the flow cell indicated in Figure 27. When ions enter the detector cell, the electrical resistance changes and the out of balance signal is fed to a suitable amplifier. The output from the amplifier is either digitized, and the binary number sent to a computer for storage, or the output is passed directly to a potentiometric recorder. The detector actually measures the electrical resistance between the electrodes which by suitable non-linear amplification, can be made to provide an output that is linearly related to solute concentration. It is essential that an AC voltage is used across the electrodes to measure the cell impedance to avoid electrode polarization. The frequency of the AC potential across the electrodes is usually around 10 kHz. The $BaSnF_4$ electrode was prepared by leaching $BaSnClF_3.0.8H_2O$ phase that was prepared by precipitation reaction at ambient temperature by the addition of $BaCl_2$ solution to SnF_2 solution or vise versa.

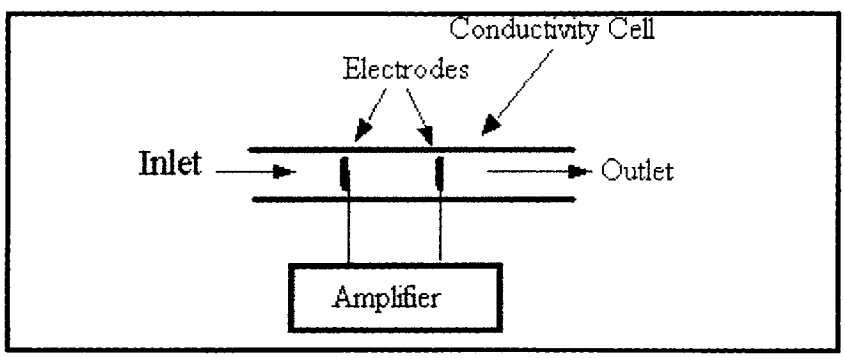

Figure 27 Conductivity flow cell where one electrode is a graphite electrode and the other electrode is a $BaSnF_4$ electrode

4.2 Experimental Methods

4.2.1 Materials

The following reactants were used for the syntheses: SnF_2 99%, $BaCl_2 \cdot 2H_2O$ analytical grade, BaF_2 99% from Sigma-Aldrich, and doubly distilled or deionized water.

4.2.2 Precipitation and Leaching Reactions

Earlier works have shown that the materials obtained by precipitation reaction are very highly dependent on the experimental conditions [79, 80, 82,] therefore the experimental parameters were carefully controlled. Some of these were kept constant: Reaction temperature (T) = room temperature (RT = 23°C), speed of addition = 1.0 mL/min, time between preparation of SnF_2 solution and using it ($t(SnF_2) = 0$).

Precipitation reactions were carried out according to procedure developed earlier in our laboratory, either by adding a 1.274M solution of $BaCl_2 \cdot 2H_2O$ to a saturated solution of SnF_2 (1.500M) (Ba → Sn) upon stirring, or vice versa (Sn → Ba), on stirring, which resulted in the immediate precipitation of a white solid. The solid was filtered, washed with cold distilled water, and allowed to dry in air at ambient temperature. The dried solid (1.500 g) was stirred in 60 mL of ultra pure water for a given period of time and then washed with cold distilled water, and allowed to dry in air at ambient temperature. All reaction containers used were made of PEEK (poly ether ether ketone) resistant to fluoride ions. Then they the precipitates were studied by X-ray diffraction.

4.2.3 Direct Reactions at High Temperatures:

The starting materials used in these reactions are BaF_2 and SnF_2. The reagents were used without further purification since no impurity was detected by X-ray diffraction. The mass of each reactant used was determined from the reaction stoichiometery and desired mass of product. The thoroughly ground mixture of reactants was placed in a copper tube under nitrogen, according to the procedure established by Dénès[75, 81] heated at 500°C for 4 hours and allowed to cool to ambient temperature, outside the oven, and then were studied by X-ray diffraction.

4.2.4 Characterization by X-ray diffraction:

In this work, the powder diffraction method was used for phase identification of the bulk materials, for unit-cell parameters determination, and for estimating the average crystallite dimensions. The products were obtained as powders.

A diffractometer Philips PW 1050-25, automated with the SIE122 system of Difftech was used. The source of X-ray was a copper anode tube and the monochromatic radiation ($Cu\ K_\alpha$, $\lambda = 1.54178\text{Å}$) was isolated by a back monochromater. The X-ray tube was powered at 800 W (40 KV and 20 mA). Mathematical search matching of unknown patterns by comparison to the JCPDS library of reference patterns was performed with the μPDSM software from Fein-Marquat. Visual comparison between the experimental X-ray diffraction and the previously discovered phases in our laboratory, not yet added to the JCPDS library of reference patterns, was performed.

4.2.5 Particle size and microcrystallinity:

The line width of the Bragg peaks, corrected from instrumental broadening, gives the average crystallite diameter in the crystal direction represented by its (hkl) indexation provided the materials is free of strain in that direction. The diameter is calculated using Scherrer's formula, after applying Warren's correction for instrumental broadening[82];

Scherrer's formula: $t\,(\text{Å}) = 0.9\,\lambda / B\cos\Phi$

Equation 7

where: $t(Å)$: Average crystallite diameter;

θ: Bragg angle;

λ: Radiation wavelength;

B: Line broadening due to small particle size, in radians, obtained from Warren's formula[82]:

$$B^2 = B_m^2 - B_s^2$$

Equation 8

where:

B_s: Linewidth at half height (in radians) of a peak at a similar position, for a well crystalline standard. *LiF* was used as standard because it is well crystalline, stable, and its peaks do not overlap with the peaks of our materials.

B_m: Measured linewidth at half height for the sample (in radians).

4.3 Results and Discussion

4.3.1 Precipitation Reaction

The source of barium was $BaCl_2.2H_2O$, and the mole fraction X of barium chloride in the reaction mixture was varied from 0.04 to 0.95 by adjusting the amount of $BaCl_2 \cdot 2H_2O$ solution used with a fixed amount of SnF_2 solution. All materials precipitated were studied by X-ray powder diffraction. The phase diagram obtained by precipitation versus the stoichiometry X of the reaction mixture, and versus the method of addition is shown on figures 28 to 33. The mole fraction X of $BaCl_2$ in the reaction mixture is given in equation 9.

X = [Ba]/([Ba] + [Sn]) **Equation 9**

where [Ba] = number of moles of $BaCl_2.2H_2O$

and [Sn] = number of moles of SnF_2

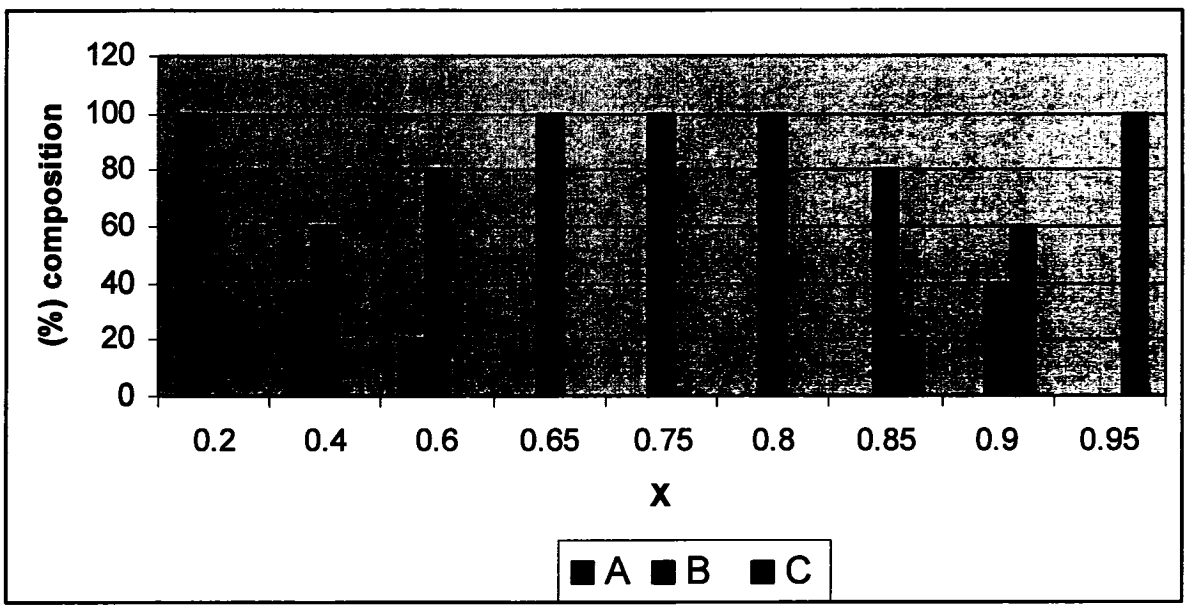

Figure 28 Estimated percentage of the phases obtained by precipitation reaction (Sn → Ba) versus X. Stirring was stopped at the end of the addition of the reactant, without additional water being added.

Where:

A = $BaSn_2Cl_2F_4$

B = $BaSnClF_3.0.8H_2O$

C = $Ba_{1-x}Sn_xCl_{1+y}F_{1-y}$

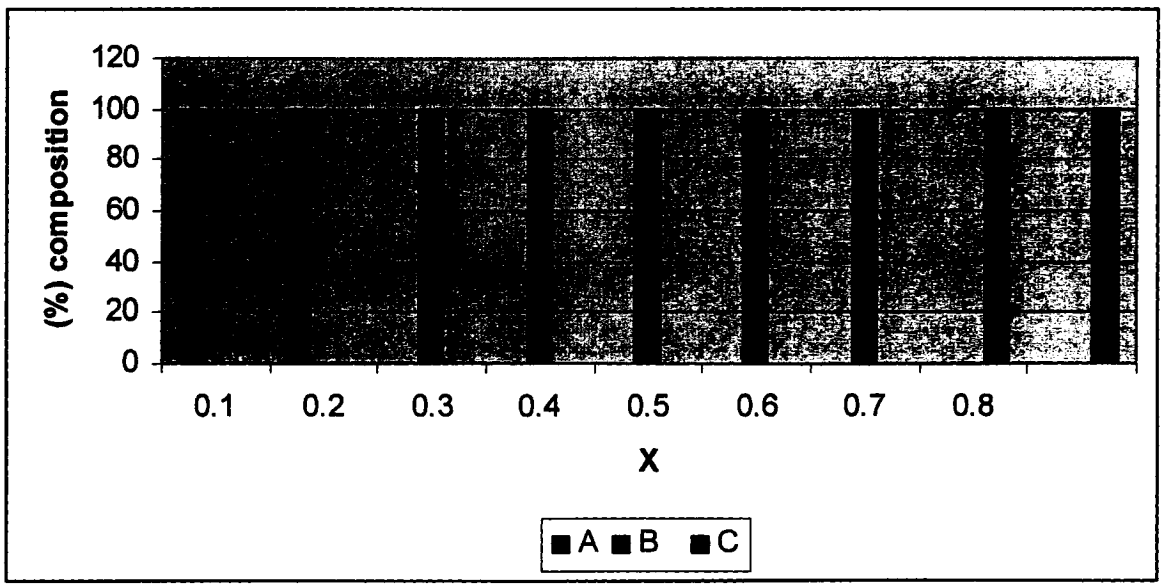

Figure 29 Estimated percentage of the phases obtained by precipitation reaction (Sn → Ba) versus X. Stirring was allowed for 24 hours after the end of the addition of the reactant, without additional water being added

Where:

A = $BaSn_2Cl_2F_4$

B = $BaSnClF_3.0.8H_2O$

C = $Ba_{1-x}Sn_xCl_{1+y}F_{1-y}$

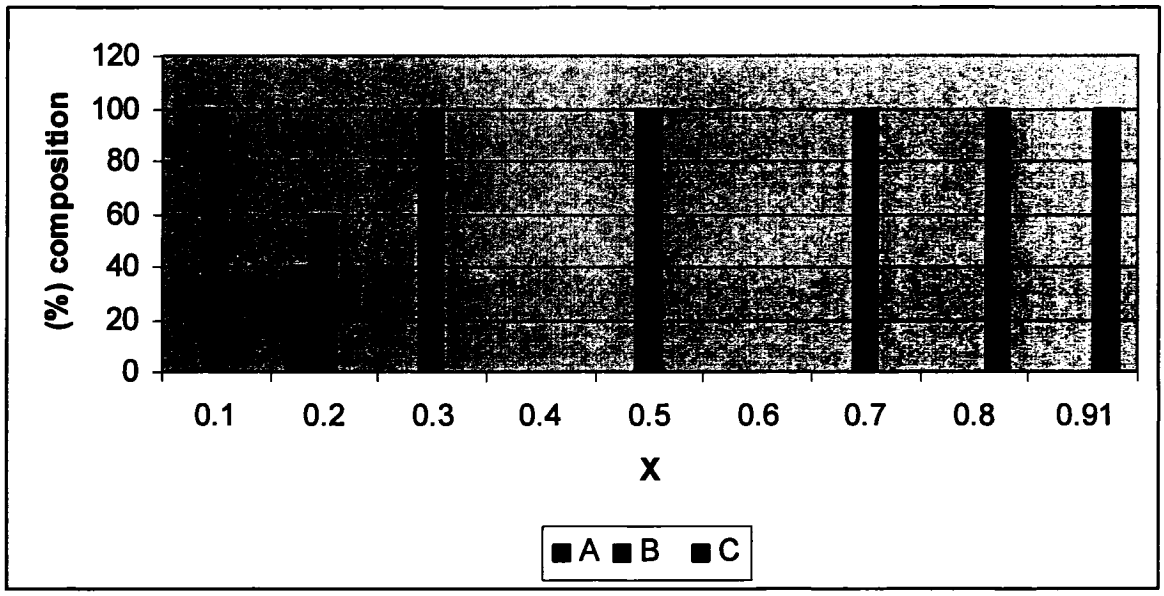

Figure 30 Estimated percentage of the phases obtained by precipitation reaction (Sn → Ba) versus X. Stirring was allowed for 48 hours after the end of the addition of the reactant, without additional water being added

Where:

A = $BaSn_2Cl_2F_4$

B = $BaSnClF_3.0.8H_2O$

C = $Ba_{1-x}Sn_xCl_{1+y}F_{1-y}$

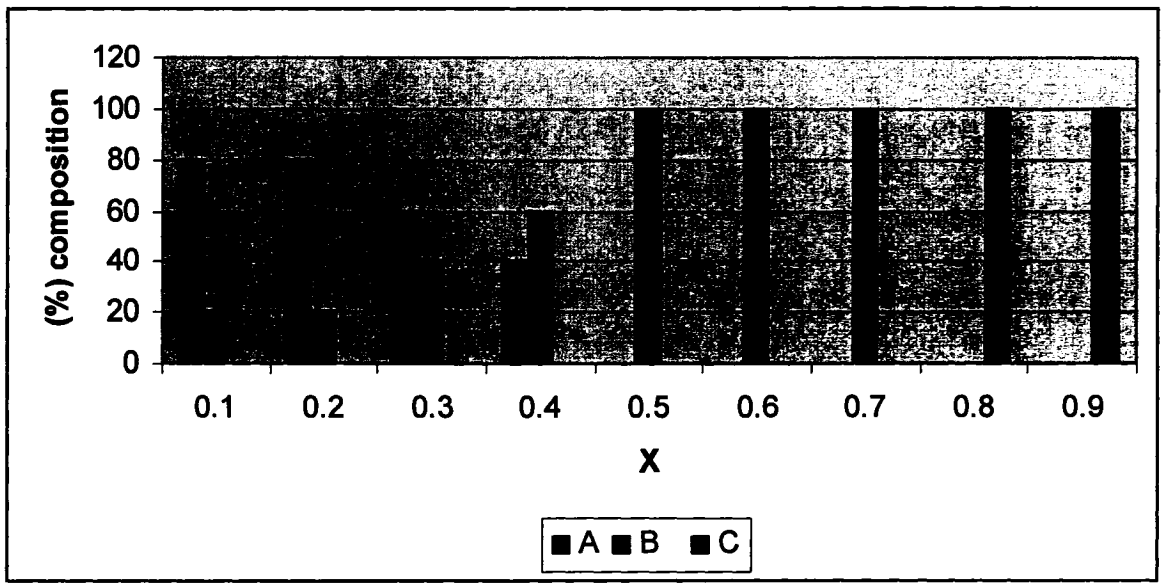

Figure 31 Estimated percentage of the phases obtained by precipitation reaction (Sn → Ba) versus X. Stirring was allowed for 24 hours after the addition of 100 mL of water at the end of the addition of the reactant

Where:

A = $BaSn_2Cl_2F_4$

B = $BaSnClF_3.0.8H_2O$

C = $Ba_{1-x}Sn_xCl_{1+y}F_{1-y}$

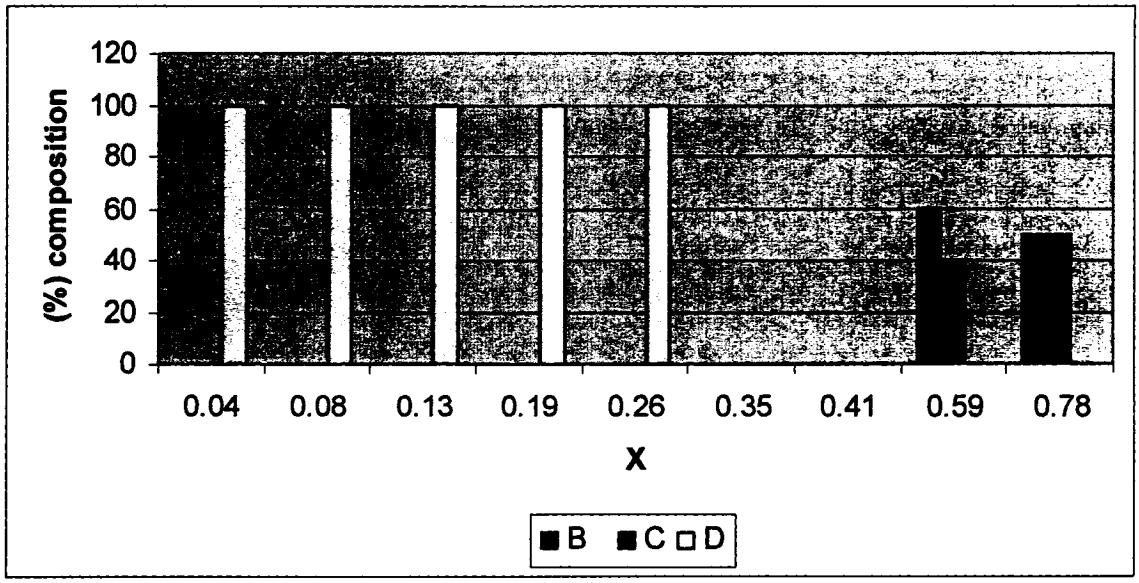

Figure 32 Estimated percentage of the phases obtained by precipitation reaction (Sn → Ba) versus X. Stirring was allowed for 74 hours after the addition of 100 mL of water at the end of the addition of the reactant

Where:

B = $BaSnClF_3.0.8H_2O$

C = $Ba_{1-x}Sn_xCl_{1+y}F_{1-y}$

D = $BaSn_2F_6$

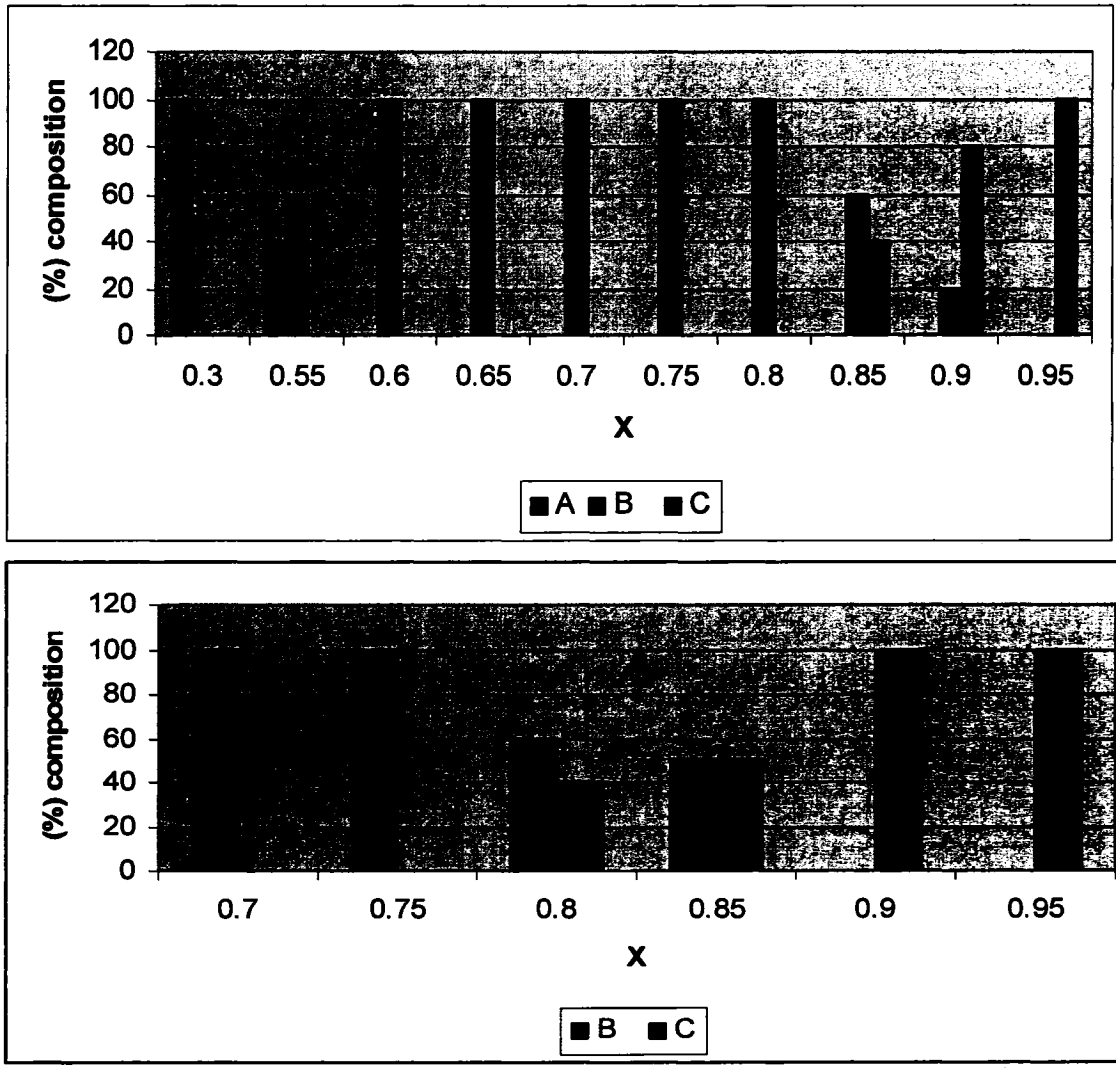

Figure 33 Estimated percentage of the phases obtained by precipitation reaction (Ba → Sn) versus X. Stirring was stopped at the end of the addition of the reactant, without additional water being added; the bottom chart is repetition of the same experimental conditions carried out to produce the phases in the top chart at X 0.70 to 0.95

Where:

B = $BaSnClF_3.0.8H_2O$

C = $Ba_{1-x}Sn_xCl_{1+y}F_{1-y}$

Figures 28 to 33 show a strong similarity with earlier preparations in our laboratory [78-80, 82], i.e. at low X (low amount of Ba and Cl in the reaction mixture), the precipitated phases are rich in Sn and F and as X increases, the Ba/Sn and Cl/F ratios of the phases precipitated increase. Figure 28 to 30 show the phase diagrams of the precipitate for Sn → Ba versus t(product), i.e. stirring time after the end of addition of SnF_2 to the solution of $BaCl_2$, without addition of water at the end of the addition of SnF_2. A clear trend is observed: As stirring time increase from 0 to 48 hours, the product precipitated at low X changes from $BaSnCl_2F_4$ (observed up to X = 0.60 for t(product) = 0) to just a minor amount observed at X = 0.20 for t(product) = 48 hours. Therefore, additional stirring of the reaction mixture after the end of addition of SnF_2 in $BaCl_2$ results in the precipitate loosing SnF2, according to equation 10.

$$BaSn_2Cl_2F_{4\,(s)} + 0.8\,H_2O_{(l)} \rightarrow BaSnClF_3.0.8H_2O_{(s)} + Sn^{2+}_{(aq)} + Cl^-_{(aq)} + F^-_{(aq)}$$

Equation 10

The opposite effect is observed also for Sn → Ba, when water is added to the reaction mixture at the end of precipitation under continued stirring (figs. 28-31), i.e. the amount of $BaSn_2Cl_2F_4$ increases at the expenses of $BaSnClF_3.0.8H_2O$ when the reacted mixture is stirred in water. This results from loss of barium, according to equation 11.

$$2\,BaSnClF_3.0.8H_2O_{(s)} \rightarrow BaSn_2Cl_2F_{4\,(s)} + 1.6H_2O_{(l)} + Ba^{2+}_{(aq)} + 2\,F^-_{(aq)}$$

Equation 11

This is somewhat similar to leaching that takes places when the isolated precipitate is stirred in pure water, except here that only Ba^{2+} leaches since the solid gets richer in Cl^-,

when in leaching experiments in pure water, both Ba^{2+} and Cl^- leach out and $BaSnF_4$ is obtained when starting from $BaSnClF_3.0.8H_2O$ (see section 4.3.2). The difference can be attributed to the species present in solution when t(product) > 0.

Figure 33 show, for Ba → Sn, that repetition of the precipitate for $0.80 < X < 0.90$, the reaction is not strictly reproducible. This phenomenon was observed in our laboratory earlier, and it can be attributed to a region of instability where the change from $BaSnClF_3.0.8H_2O$ to $Ba_{1-x}Sn_xCl_{1+y}F_{1-y}$ is taking place in a precipitate richer in one of the products or the other.

The same materials are not always produced by the two methods of addition (Ba → Sn or Sn → Ba) at the same given overall stoichiometry X of the reaction mixture. This can be accounted for by the fact that the local stoichiometry at the reaction site is usually not the same as the overall stoichiometry of the reaction mixture, and it is strongly dependent on the method of addition. The ions in excess at the reaction site can determine which product is formed at a given time in the precipitation reactions if stirring is unable to homogenize the reaction mixture before precipitation starts, regardless of the overall stoichiometry of the reactants, unless all the reactants in the receiving solution have been used up and no further reaction takes place, except in some cases, the reaction of the precipitate already formed with the dissolved species being added. Other reactions parameters also have a strong influence on the materials that precipitate. The rate of addition of one reactant to the other must be chosen to be slow enough in such a way that the reactants being added have enough time to be mixed with the reactants of the receiving solution to form a fairly homogeneous mixture at the reaction site before much of them have reacted. Build up of the reactants being added occurs if a fast addition rate

is used. A sufficiently slow rate of addition allows the reaction to take place smoothly with less chance to have multiphase products. In the present work, the rate of addition was set at approximately 1.0 mL/min. for all reactions.

Prior to the recent studies in our laboratory, using Ba/Sn/Cl/F compounds, the three $MSnF_4$ compounds (M = Sr, Ba, and Pb) had been prepared by direct reaction between MF_2 and SnF_2 under dry conditions at high temperature[59]. However, in recent years attempts by Dénès et al. to obtain $BaSnF_4$ by the aqueous route was successful, upon leaching of some Ba/Sn/Cl/F compounds in water[80 & 83]. For some precipitates obtained at high X values, the Search-Match® gives $BaSnF_4$ as one possible phase present in the solid. No other match was satisfactory, however, many other lines were present, which could be attributed to the tin(II) barium chloride fluorides discovered and characterized recently in our laboratory. When the new material discovered by Denes et al. previously, $BaSnClF_3 \cdot 0.8H_2O$ precipitates, no match was found to be reasonable except some $BaSnF_4$ and/or $BaSn_2F_6$ in some samples. It should be pointed out that, in all cases, $BaSnF_4$ was never obtained pure just by precipitation before stirring it in water (fig. 33).

Furthermore, stirring the product formed by addition of a $BaCl_2$ solution to a SnF_2 solution (Ba $\rightarrow$ Sn), or vice versa (Sn $\rightarrow$ Ba), in the mother liquid after the end of the addition (t(product) > 0) did not give pure $BaSnF_4$. This is probably due to the fact that the presence of extra-unused ions in the mother liquid, especially a large excess of chloride ions, favors the chloride-fluorides over chloride-free $BaSnF_4$.

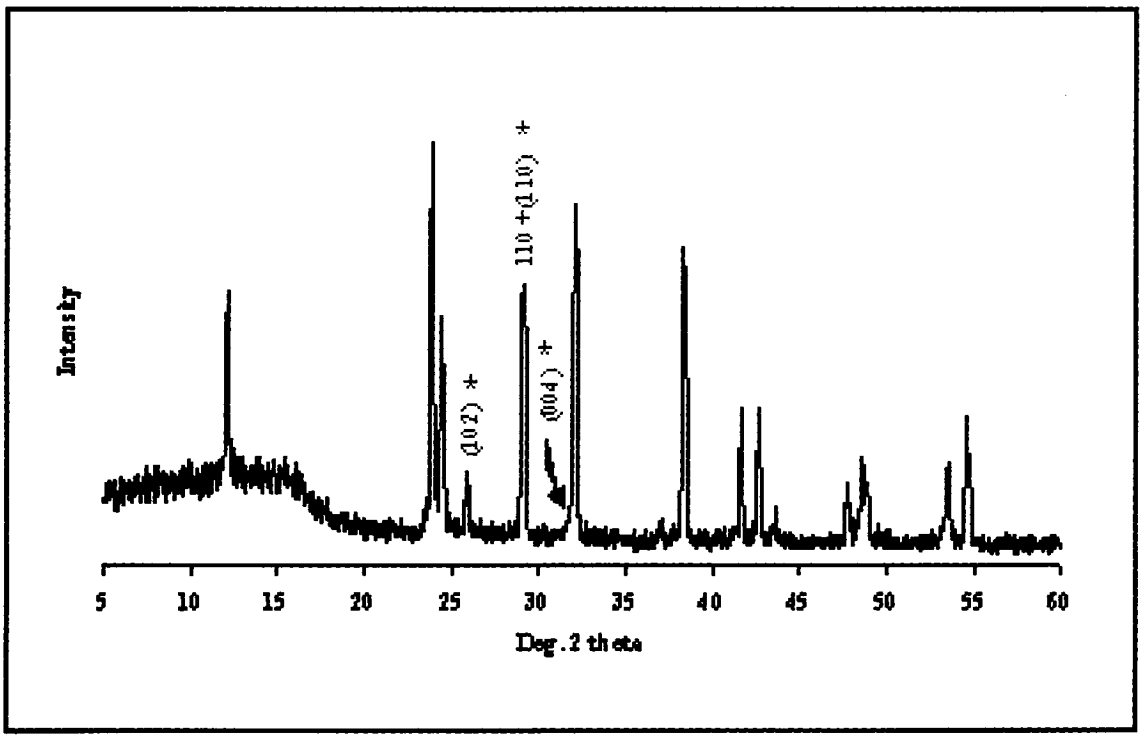

Figure 34 **X-ray diffraction pattern of a precipitated sample that contains two phases (X = 0.95, Ba → Sn). The starred peaks correspond to $BaSnF_4$ that is present in traces amount, and the remaining peaks correspond to $Ba_{1-x}Sn_xCl_{1+y}F_{1-y}$. The (110) peak of $BaSnF_4$ and the (110) peak of $Ba_{1-x}Sn_xCl_{1+y}F_{1-y}$ overlap near perfectly well.**

4.3.2 Leaching Reaction

In an attempt to prepare $BaSnF_4$ from the barium tin(II) chloride fluorides obtained by the precipitation reactions, and to study the $BaSnF_4$ obtained versus the conditions of preparation and of leaching, approximately 1.0 g of each precipitate was stirred in 60 mL water at room temperature for a given period of time, since $BaSnF_4$ is poorly soluble in water. After filtration, the solid residue was washed with cold water and allowed to dry in air at ambient conditions. The phase diagram obtained by leaching reaction versus the stoichiometry X of the reaction mixture of the precipitated phase, and versus the method of addition is shown in figures 35 to 39.

The phases obtained by leaching versus the starting precipitate are summarized in table 3.

Table 3 Solid obtained by leaching in water versus the starting precipitate

Solid before leaching	Solid after leaching
$BaSn_2F_6$	$BaSn_2F_6$
$BaSn_2Cl_2F_4$	$BaSn_2F_6$ + some $BaSnF_4$ (minor)
$BaSnClF_3.0.8H_2O$	$BaSnF_4$ + some $BaSn_2F_6$ (minor)
$Ba_{1-x}Sn_xCl_{1+y}F_{1-y}$	$Ba_{1-x}Sn_xCl_{1+y}F_{1-y}$

It can be seen from figures 35 to 39 and from table 3 that only the stoichiometric barium tin(II) chloride fluorides $BaSn_2Cl_2F_4$ and $BaSnClF_3.0.8H_2O$ undergo a chemical transformation upon leaching. In contrast, $BaSn_2F_6$ and $Ba_{1-x}Sn_xCl_{1+y}F_{1-y}$ were never found to yield any other compound. The two compounds that change on stirring in water do so mainly by minimal leaching, i.e. the Ba/Sn ratio does not change, as far as the major compound formed is concerned, as can be seen in table 4.

Table 4 Change of the chemical composition of the solid on leaching

Solid before leaching	Solid after leaching	Ba/Sn change	(%) change of anion
$BaSn_2Cl_2F_4$	$BaSn_2F_6$	0	33
$BaSnClF_3.0.8H_2O$	$BaSnF_4$	0	25

In both cases, the loss of chloride ion is the main change, and this is more major for the formation of $BaSn_2F_6$ and $BaSn_2Cl_2F_4$. In addition, the transformation of $BaSnClF_3.0.8H_2O$ to $BaSnF_4$ involves a loss of water, and in both cases, a structural change takes place upon leaching. The solid residual of pure $BaSnF_4$ recovered showed a significant mass loss had taken place on leaching. The starting $BaSnClF_3.0.8H_2O$ phase had completely disappeared.

Before leaching

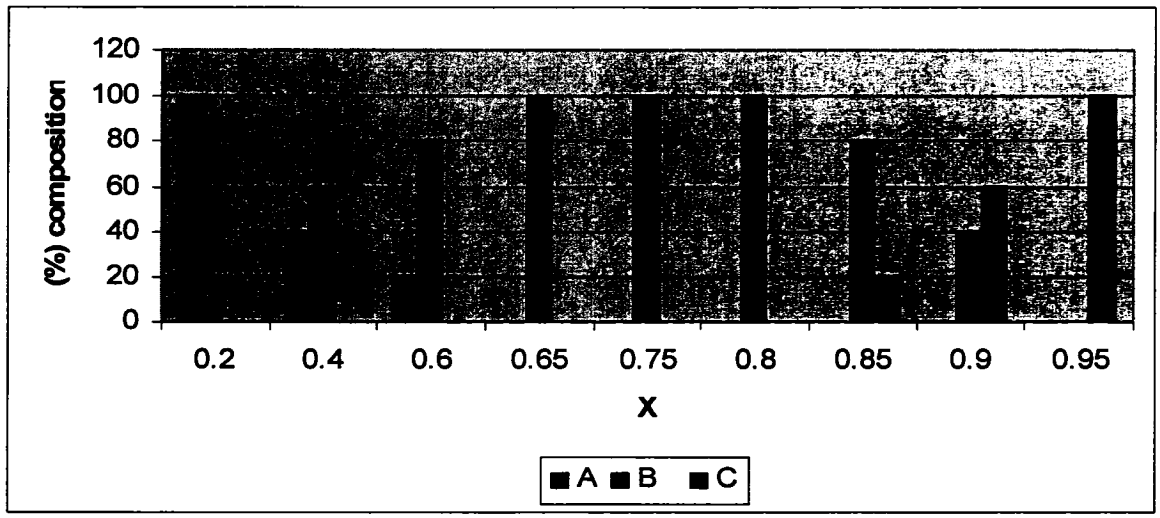

After Leaching

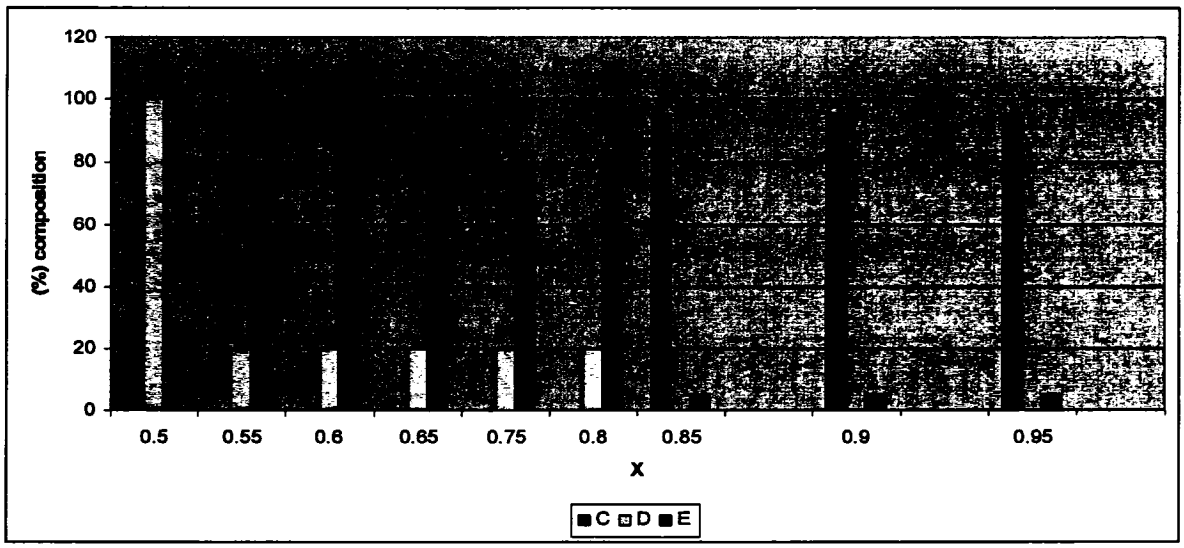

Figure 35 Leaching phases obtained by precipitation reaction (Sn → Ba), reaction stopped at the end of the addition of the reactant and without additional water added, leaching time was 46 hours

Where:

A = $BaSn_2Cl_2F_4$; B = $BaSnClF_3.0.8H_2O$; C = $Ba_{1-x}Sn_xCl_{1+y}F_{1-y}$; D = $BaSn_2F_6$; E = $BaSnF_4$

Before leaching

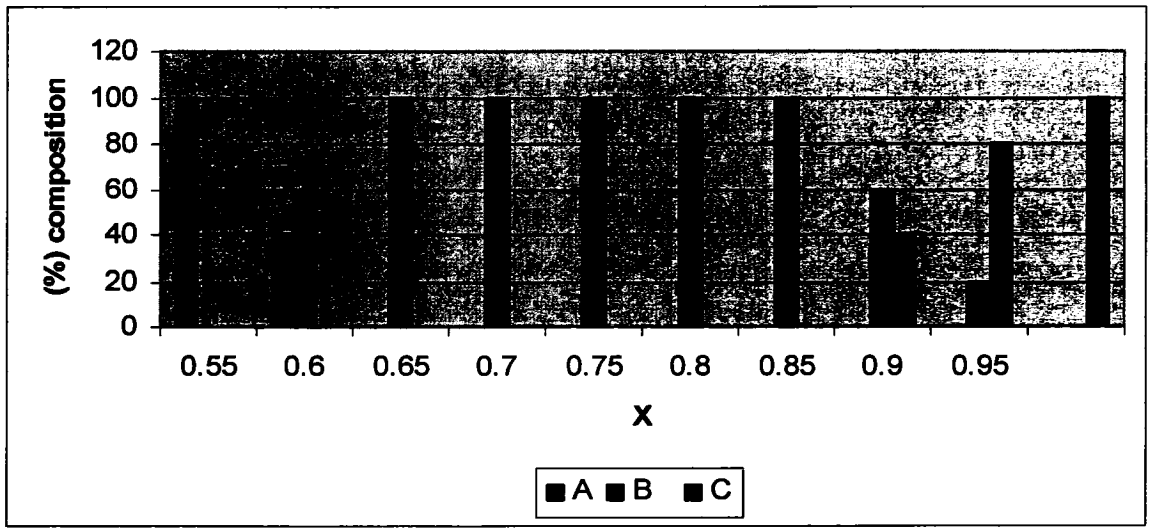

After Leaching

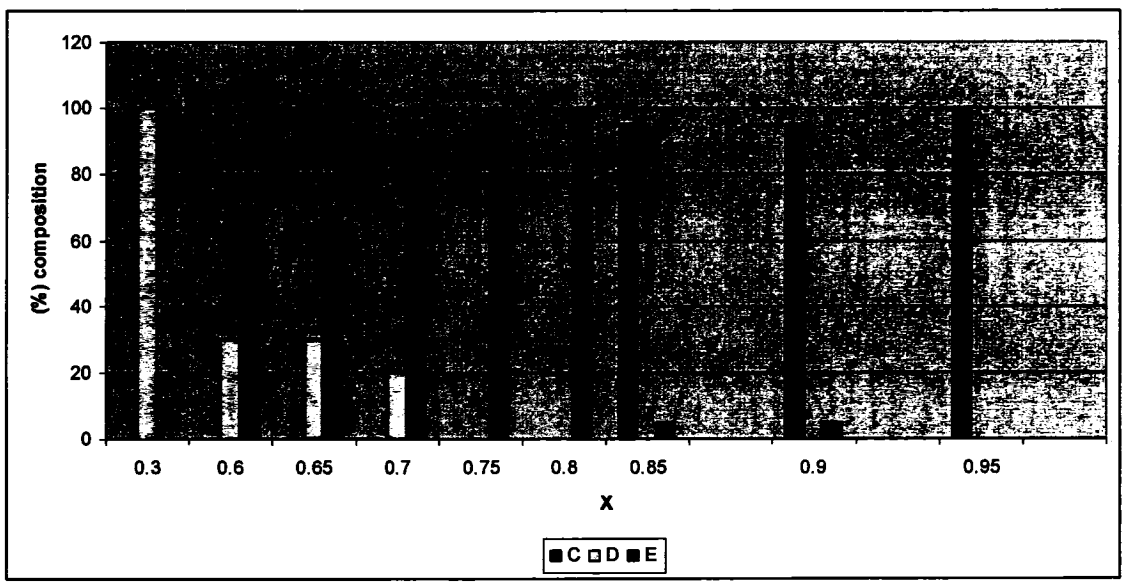

Figure 36 Leaching phases obtained by precipitation reaction (Ba → Sn), reaction stopped at the end of the addition of the reactant and without additional water added, leaching time was 72 hours

Where:

A = $BaSn_2Cl_2F_4$; B = $BaSnClF_3.0.8H_2O$; C = $Ba_{1-x}Sn_xCl_{1+y}F_{1-y}$; D = $BaSn_2F_6$; E = $BaSnF_4$

Before leaching

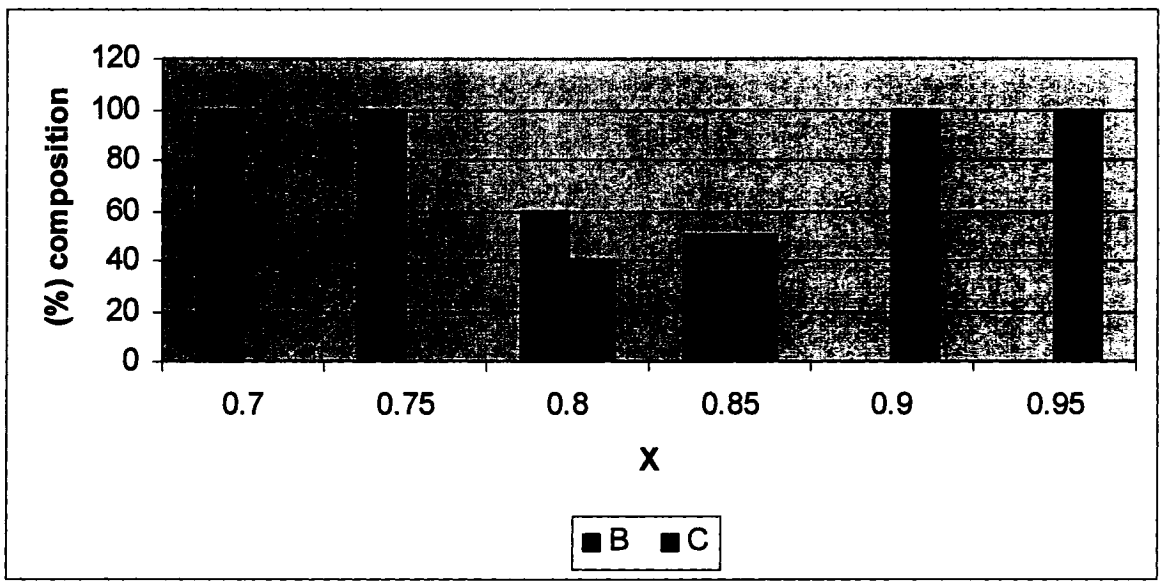

After Leaching

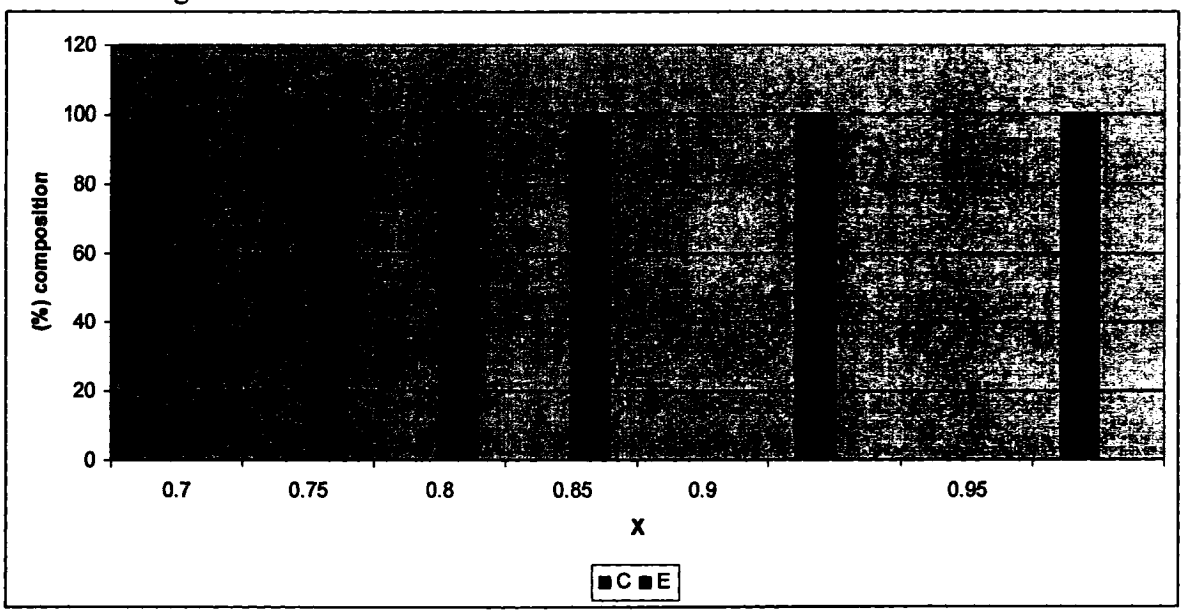

Figure 37 Leaching phases obtained by precipitation reaction (Ba → Sn), reaction stopped at the end of the addition of the reactant and without additional water added, leaching time was 84 hours

Where:

B = $BaSnClF_3.0.8H_2O$; C = $Ba_{1-x}Sn_xCl_{1+y}F_{1-y}$; E = $BaSnF_4$

Before leaching

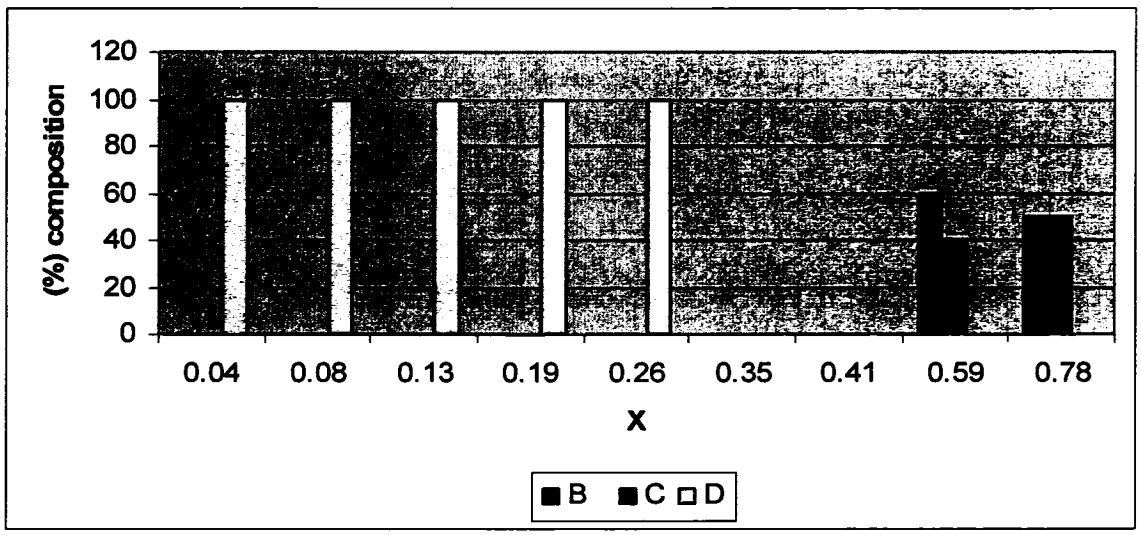

After Leaching

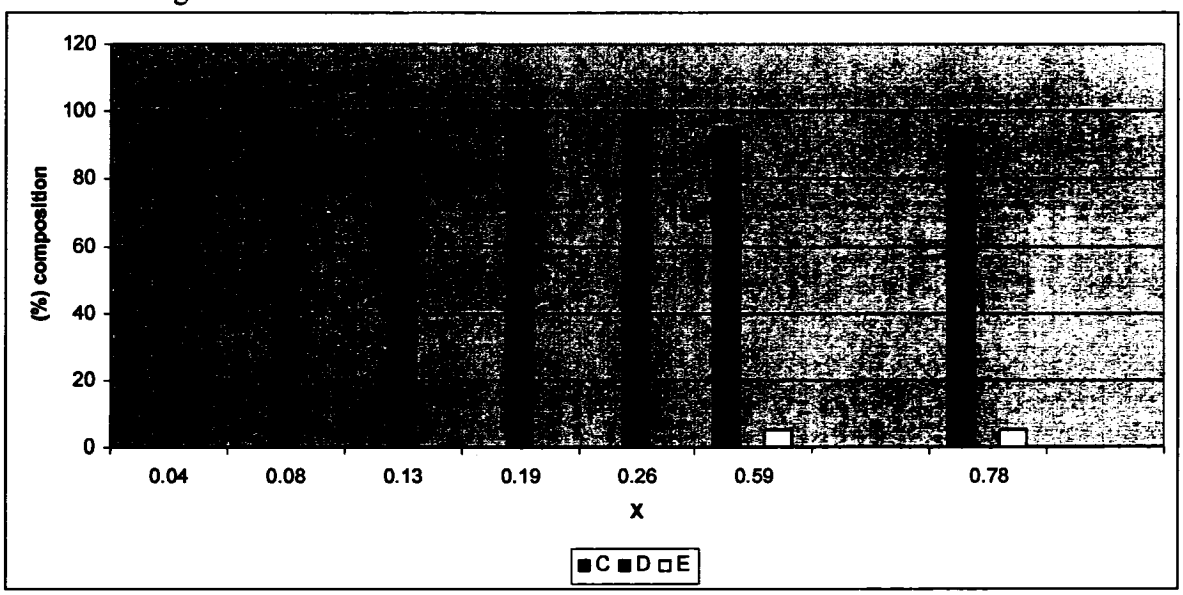

Figure 38 Leaching phases obtained by precipitation reaction (Sn → Ba), reaction allowed stirring for 74 hours after the addition of 100 mL of water at the end of the addition of the reactant, leaching time was 24 hours

Where:

B = $BaSnClF_3.0.8H_2O$; C = $Ba_{1-x}Sn_xCl_{1+y}F_{1-y}$; D = $BaSn_2F_6$; E = $BaSnF_4$

Before leaching

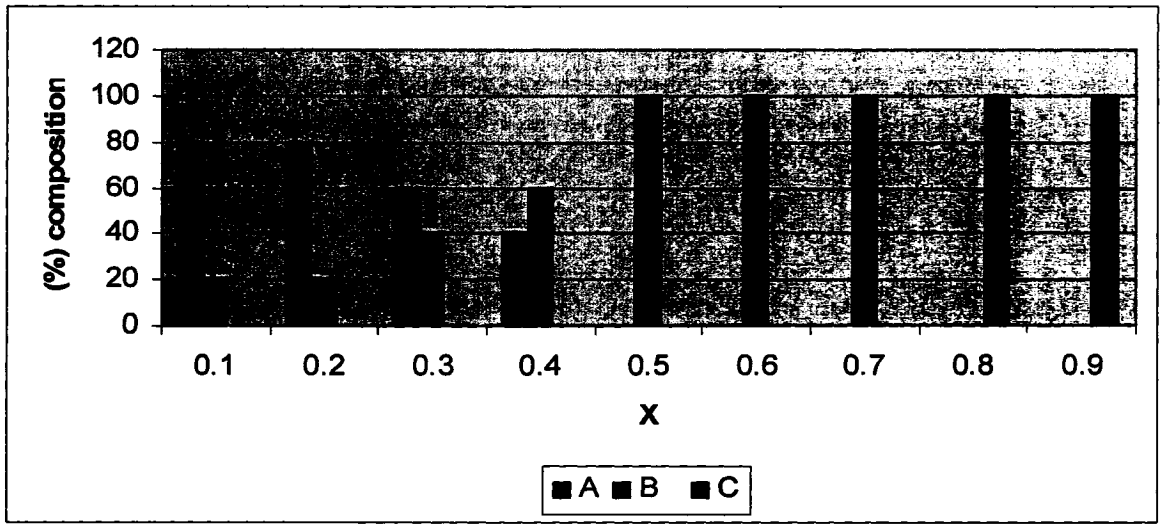

After Leaching

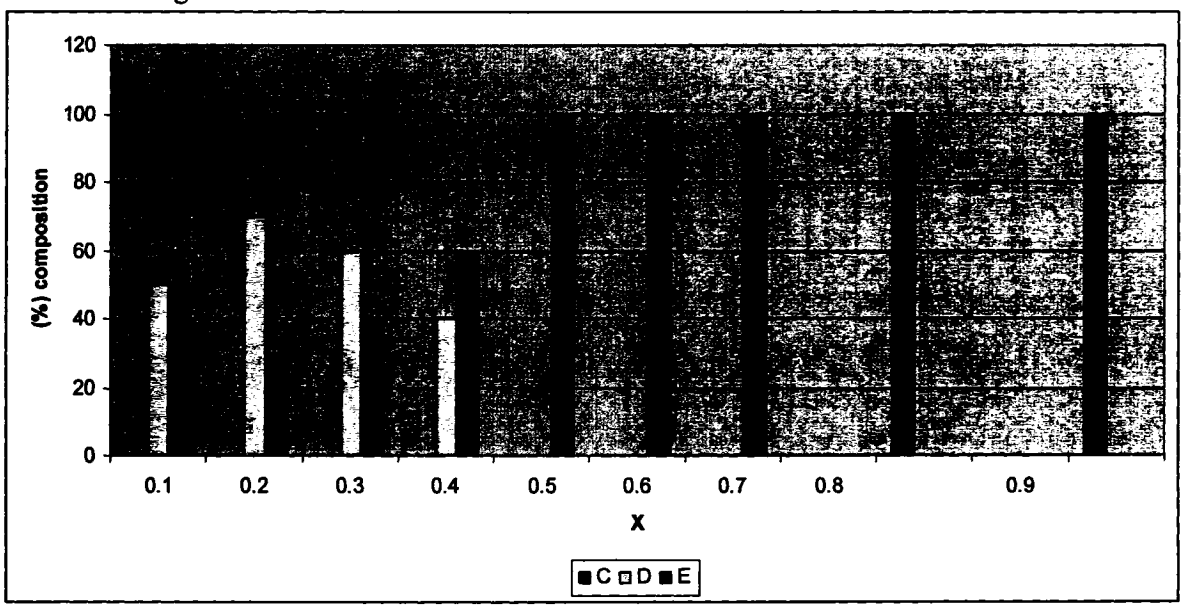

Figure 39 Leaching phases obtained by precipitation reaction (Sn → Ba), reaction allowed stirring for 24 hours after the addition of 100 mL of water at the end of the addition of the reactant, leaching time was 24 hours

Where:

A = $BaSn_2Cl_2F_4$; B = $BaSnClF_3.0.8H_2O$; C = $Ba_{1-x}Sn_xCl_{1+y}F_{1-y}$; D = $BaSn_2F_6$; E = $BaSnF_4$

The actual recovery (%) of $BaSnF_4$ via the aqueous route vary from ca. 26 to 72% (Table 5). Two possible mechanisms could be proposed to explain the mass loss upon stirring in water: (i) the presence of soluble phases which could be dissolved during stirring, leading to a lower yield and disappearance of these phases from the X-ray diagram, and (ii) the precipitated barium tin chloride fluorides product may be unstable in water, and therefore some species are leached out, leaving a product of different composition, namely pure $BaSnF_4$ or a mixture of $BaSnF_4$ and $BaSn_2F_6$. This would also result in a lower yield. Process (i), i.e. the full dissolution of soluble products, is unlikely since the material is precipitated from aqueous medium, and therefore the soluble species would not have precipitated in the first place, although they might be more soluble in pure water than in the solution obtained after precipitation. In addition, if just the initial barium tin(II) chloride fluoride dissolved on stirring, the residue, i.e. $BaSnF_4$ and/or $BaSn_2F_6$ would be already present in the precipitated solid. However, each crystalline phase has its own set of diffraction lines, and therefore large amounts of $BaSnF_4$ and/or $BaSn_2F_6$ would be observed in the precipitates. Since when $BaSnF_4$ is present in the precipitates, it is in a minor amount, and many precipitates contain no $BaSnF_4$, process (ii) is the only possible mechanism, i.e. the initial precipitate of barium tin(II) chloride fluoride undergoes a rearrangement in water, whereby all the chlorine is leached out of the solid and go in solution, resulting in a residue of $BaSn_2F_6$ or $BaSnF_4$, according to reactions below:

$$2BaSnClF_3 \cdot 0.8H_2O(s) \xrightarrow{(in\ H_2O)} BaSnF_4(s) + Ba^{2+}(aq) + Sn^{2+}(aq) + 2Cl^-(aq) + 2F^-(aq) + 0.8H_2O\ (l)$$

Equation 12

$$2BaSnClF_3 \cdot 0.8H_2O(s) \xrightarrow{(in\ H_2O)} BaSn_2F_6(s) + Ba^{2+}(aq) + 2Cl^-(aq) + 0.8H_2O(l)$$

Equation 13

$$2\ BaSn_2Cl_2F_4 \xrightarrow{(in\ H_2O)} BaSn_2F_6 + Ba^{2+}\ (aq) + 4\ Cl^-(aq) + 2F^-\ (aq) + 2Sn^{2+}$$

Equation 14

The theoretical yield for reaction 12 is calculated to be 46% for the fluoride residue being $BaSnF_4$, starting from $BaSnClF_3.0.8H_2O$. When a change of metal stoichiometry takes place (minor reactions), like in equation 13, leaching of metal ions contributes to the mass loss. In addition, even if the metal ratio does not change upon leaching, the replacement of chlorine by fluorine requires breaking up some of the precipitated chloride fluoride, and therefore releasing some metal ions to the aqueous solution.

It should also be noted that the highest yield of $BaSnF_4$ (60.1-72.4%) was obtained when (i) in the precipitation reaction, the precipitate was stirred after the end of addition of barium chloride (t(product) > 0) and water was added ($V(H_2O) > 0$), and (ii) for the shortest leaching times (24 hours). In contrast, a lower yield of $BaSnF_4$ was obtained (26.6-59.5%) when t(product) = 0 and $V(H_2O) = 0$ at precipitation, and for longer leaching times (72-84 hours). It can be suggested that, at precipitation, a longer stirring time with additional water may already leach some material, leaving a minor amount of $BaSnF_4$ and maybe some amorphous material in the precipitate. Some leaching having already taken place at the precipitation stage, less mass loss would occur at the leaching stage, especially for a shorter leaching time.

Table 5 **The recovery of pure $BaSnF_4$ phase when pure $BaSnClF_3.0.8H_2O$ was stirred in water**

Precipitation					Leaching				
Sample ID before leaching	X_{Ba}	$t_{(product)}$ (hours)	$V_{(H2o)}$ (mL)	Order of addition	Sample ID after leaching	Leaching time (hours)	Mass start (g)	Mass recovered (g)	Recovery (%)
JH84	0.50	24	100	Sn → Ba	JH115	24	1.0934	0.2986	60.1
JH85	0.60	24	100	Sn → Ba	JH116	24	1.0934	0.3600	72.4
JH86	0.70	24	100	Sn → Ba	JH117	24	1.0934	0.2985	60.1
JH47	0.75	0	0	Ba → Sn	JH54	84	1.0556	0.1275	26.6
JH48	0.80	0	0	Ba → Sn	JH55	84	1.0188	0.2100	45.4
JH49	0.85	0	0	Ba → Sn	JH56	84	1.0801	0.2505	51.0
JH28	0.75	0	0	Ba → Sn	JH38	72	1.0518	0.2845	59.5
JH29	0.80	0	0	Ba → Sn	JH39	72	1.0278	0.2404	51.5

4.3.3 Unit-cell and crystallite dimension anisotropy of $BaSnF_4$

Figures 40 to 42 show the diffraction pattern of $BaSnF_4$ prepared by the various methods, and the results derived from the patterns are shown in Table 6 and on figures 43 to 49.

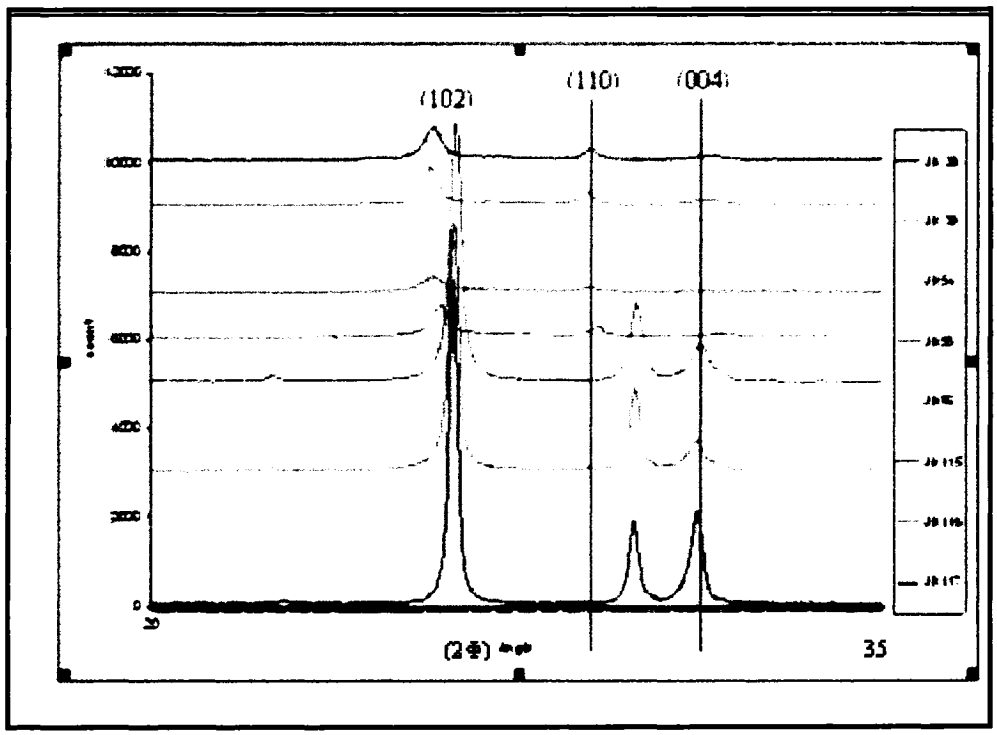

Figure 40 Enlargement (20° – 35°) of the X-ray diffraction pattern of $BaSnF_4$ prepared by leaching reaction

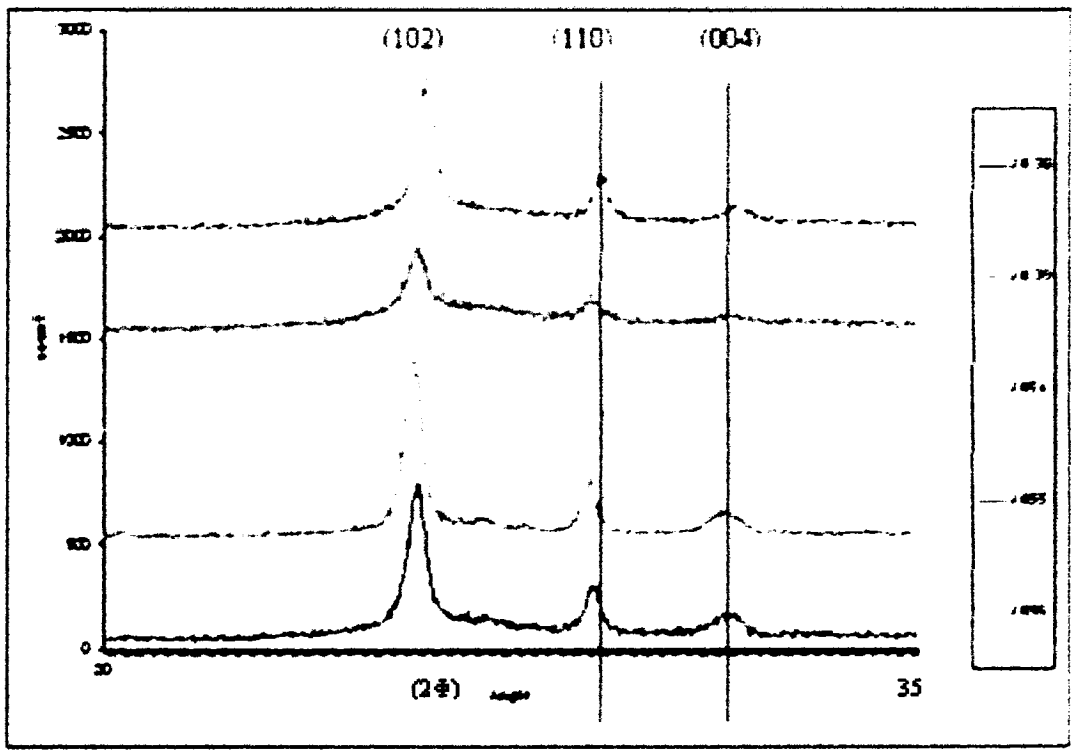

Figure 41 Enlargement (20° – 35°) of the X-ray diffraction pattern of $BaSnF_4$ prepared by leaching reaction (leaching time > 24 hours)

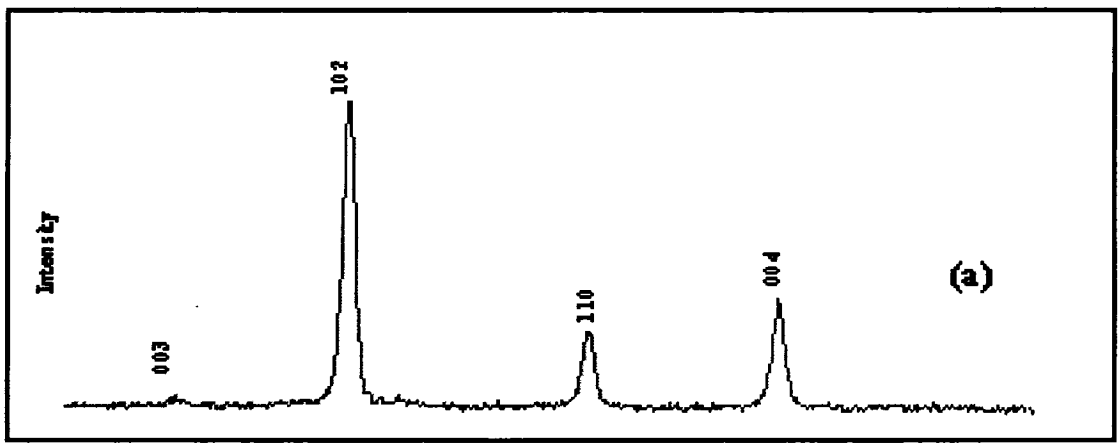

Figure 42 Enlargement (20° – 35°) of the X-ray diffraction pattern of $BaSnF_4$ prepared by direct reaction at 500°C for 4 hours

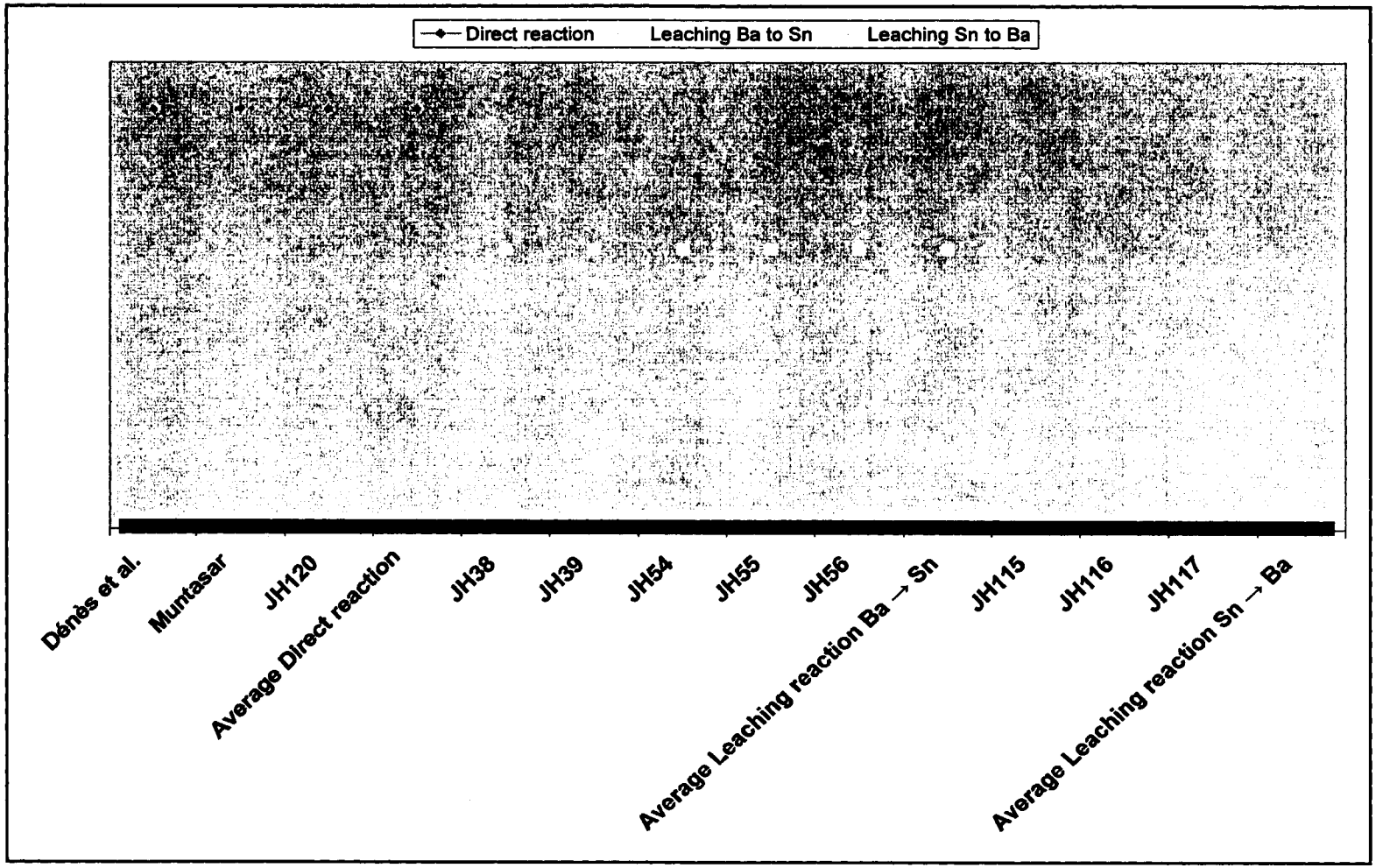

Figure 43 Samples listed in Table 6 versus method of preparation

Table 6 Unit-cell constants and particle dimension anisotropy of $BaSnF_4$ versus the method of preparation

Sample ID	Method of preparation	Stirring period (hours)	a (nm)	c (nm)	V (nm^3)	c/2a	$d_{\parallel}$ (nm)	$d_{\perp}$ (nm)	$d_{\parallel} / d_{\perp}$	Δd (nm) * 10^2
Dénès et al.	Direct reaction	-	0.4356	1.1289	0.214	1.30	-	-	-	2.60
Muntasar	Direct reaction	-	0.4348	1.1344	0.214	1.30	46.50	46.20	1.01	2.38
JH120	Direct reaction	-	0.4339	1.1268	0.214	1.30	34.93	27.07	1.290	2.51
JH38	Leaching reaction Ba → Sn	72	0.4342	1.1360	0.214	1.31	11.32	28.80	0.393	2.30
JH39	Leaching reaction Ba → Sn	72	0.4370	1.1360	0.217	1.30	10.42	26.19	0.398	2.50
JH54	Leaching reaction Ba → Sn	84	0.4342	1.1320	0.213	1.30	6.21	21.49	0.289	2.40
JH55	Leaching reaction Ba → Sn	84	0.4370	1.1360	0.217	1.30	7.47	15.56	0.480	2.50
JH56	Leaching reaction Ba → Sn	84	0.4327	1.1320	0.212	1.31	13.44	28.20	0.477	2.30
JH115	Leaching reaction Sn → Ba	24	0.4214	1.1440	0.203	1.36	22.68	29.49	0.769	1.20
JH116	Leaching reaction Sn → Ba	24	0.4228	1.1440	0.205	1.35	25.83	35.08	0.736	1.39
JH117	Leaching reaction Sn → Ba	24	0.4228	1.1480	0.205	1.36	28.95	38.38	0.754	1.29
Average Direct reaction		-	0.4348	1.1300	0.214	1.30	34.93	27.07	1.150	2.50
Average Leaching reaction Ba → Sn		-	0.4350	1.134	0.215	1.30	9.77	24.05	0.407	2.40
Average Leaching reaction Sn → Ba		-	0.4223	1.145	0.204	1.36	25.82	34.32	0.753	1.29

Table 7 Clarification of the sample ID numbers used in figures 44 to 49

Sample ID used in figures 44 to 49	Sample ID from table 6	Method of preparation
1	Dénès et al.	Direct reaction
2	Muntasar	Direct reaction
3	JH120	Direct reaction
12	Average Direct reaction	
4	JH38	Leaching reaction Ba → Sn
5	JH39	Leaching reaction Ba → Sn
6	JH54	Leaching reaction Ba → Sn
7	JH55	Leaching reaction Ba → Sn
8	JH56	Leaching reaction Ba → Sn
13	Average Leaching reaction Ba → Sn	
9	JH115	Leaching reaction Sn → Ba
10	JH116	Leaching reaction Sn → Ba
11	JH117	Leaching reaction Sn → Ba
14	Average Leaching reaction Sn → Ba	

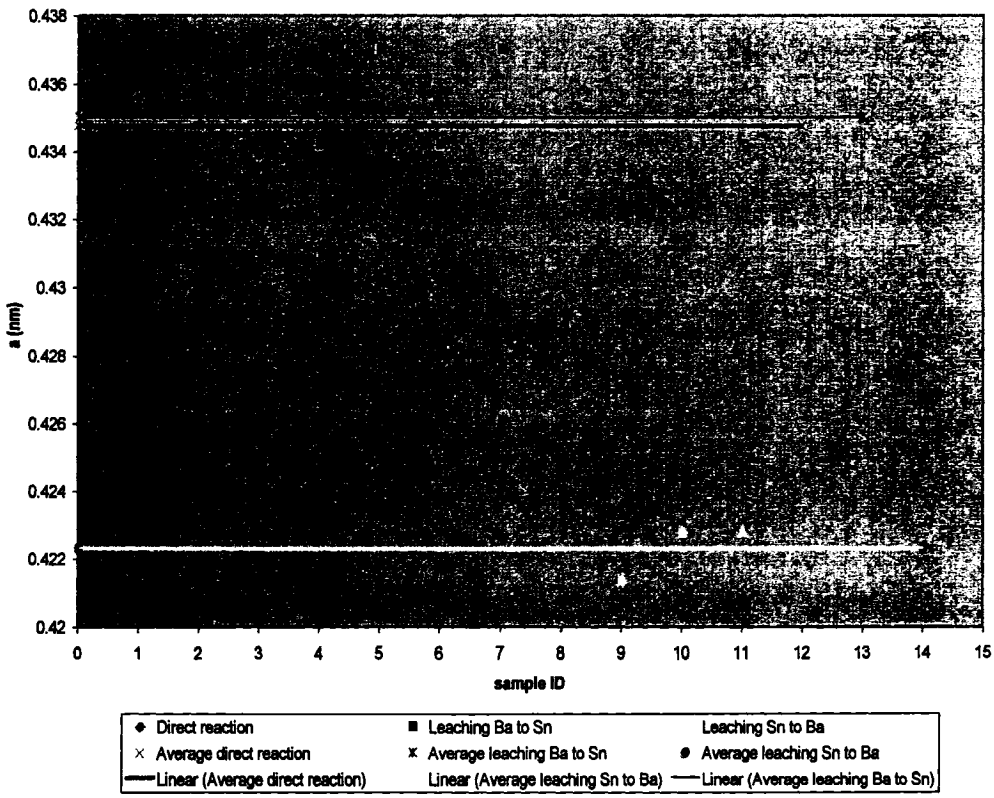

Figure 44 Unit-cell constant (a) of $BaSnF_4$ versus the method of preparation

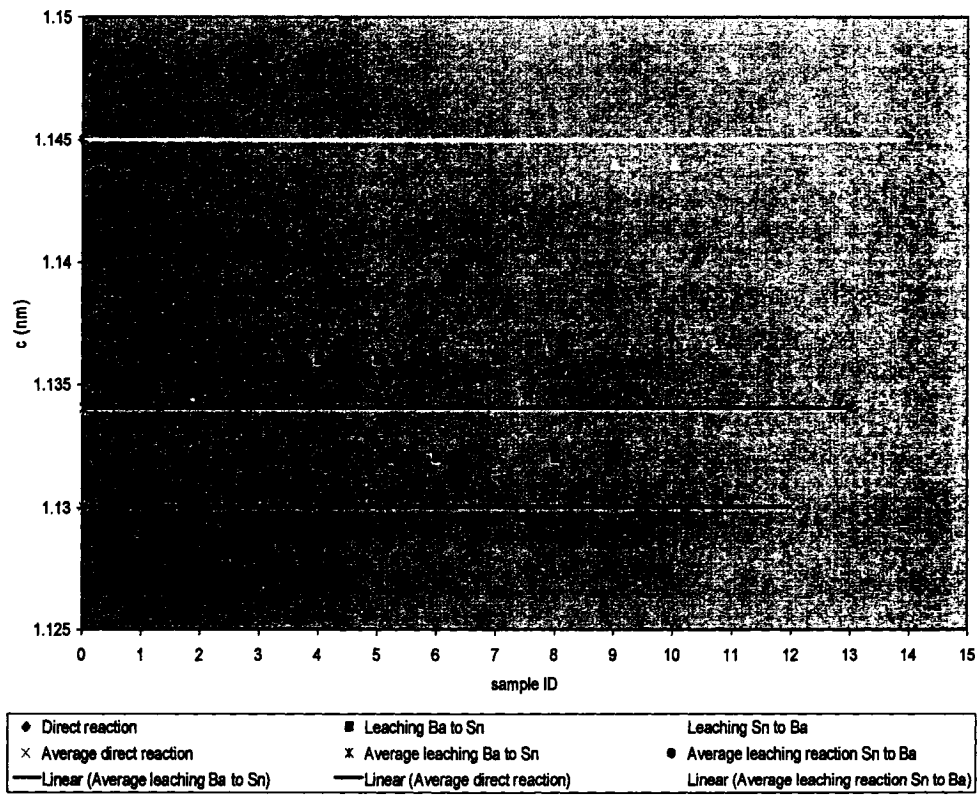

Figure 45 Unit-cell constant (c) of $BaSnF_4$ versus the method of preparation

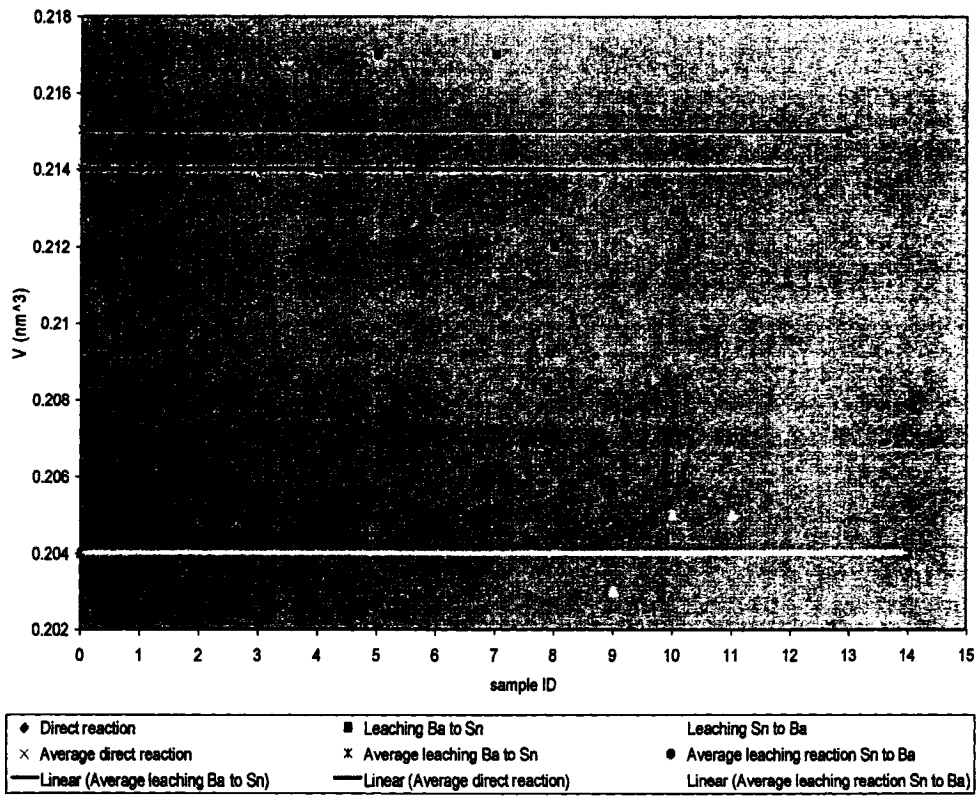

Figure 46 Unit-cell volume (V) of $BaSnF_4$ versus the method of preparation

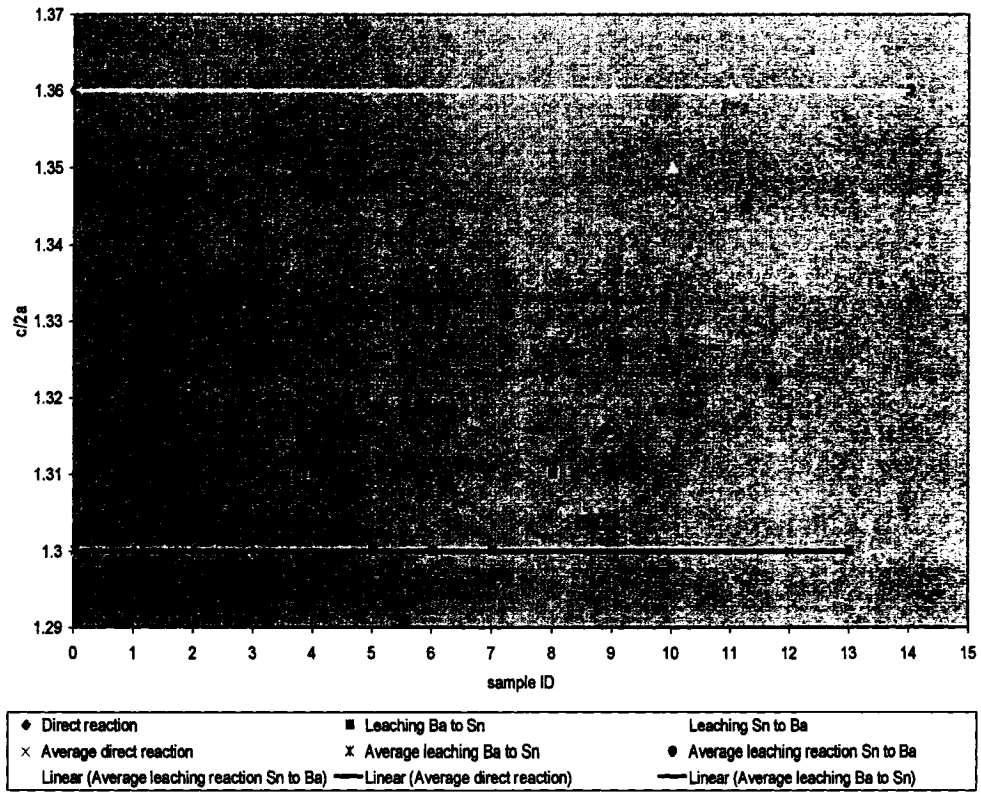

Figure 47 Tetragonal distortion (c/2a) of $BaSnF_4$ versus the method of preparation

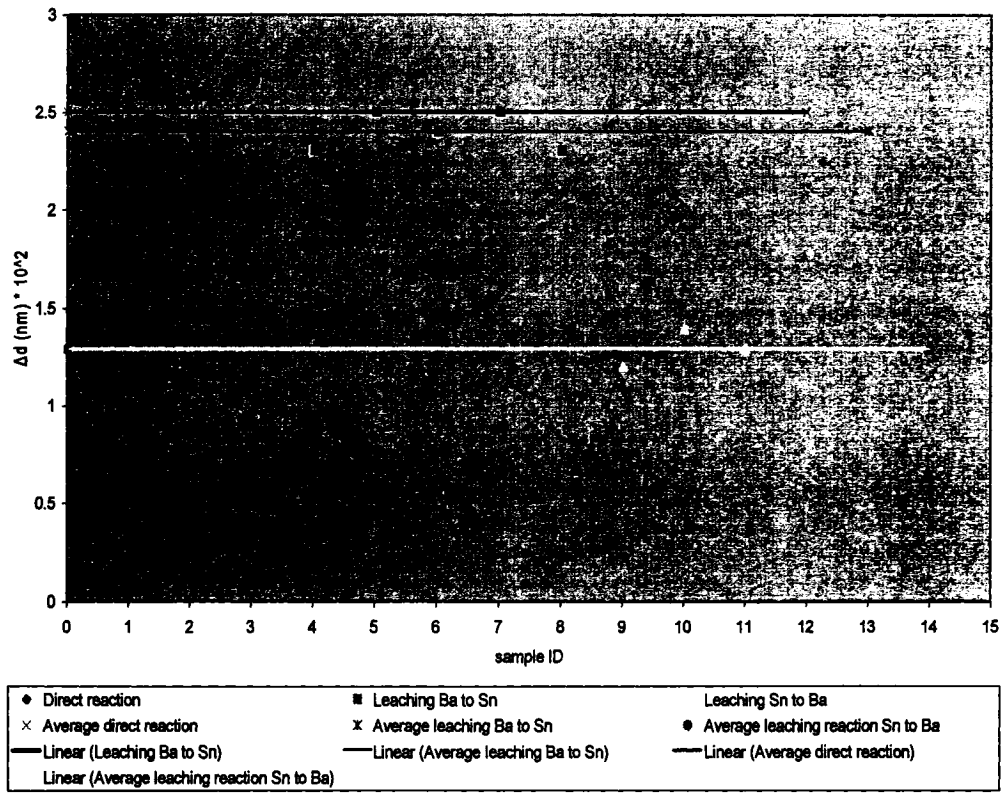

Figure 48 D-spacing difference (Δd) of $BaSnF_4$ between (110) and (004) versus the method of preparation

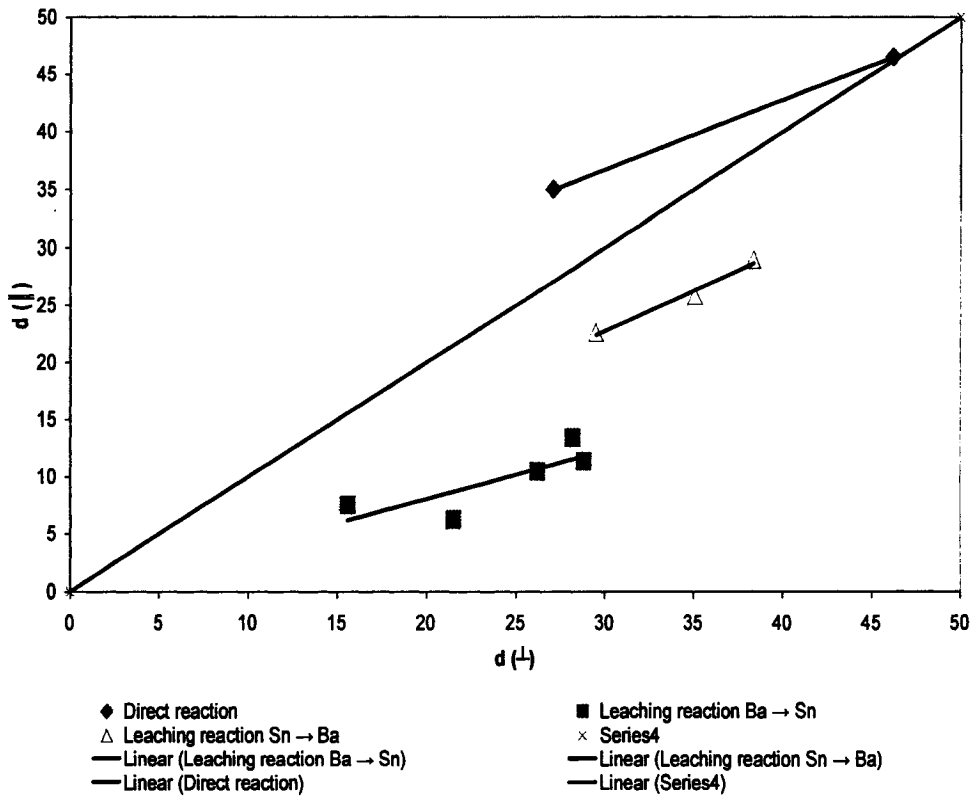

Figure 49 Growth of $BaSnF_4$ crystallites versus direction and versus the method of preparation. The line from (0,0) to (50, 50) has a slope 1, i.e. $d_{\parallel}/d_{\perp} = 1$ and would indicate that growth is isotropic

The diffraction patterns of figures 40 and 41 show significant variations of line position and of line width. The line position is the Bragg angle; it determines the d-spacing through Bragg law, and the d-spacings of all peaks are a function of the unit-cell parameters. In a tetragonal unit-cell, only two parameters are variable, the unit-cell edges a and c, since $b = a$, and the three angles are equal to 90 ° ($\alpha = \beta = \gamma = 90°$).

The d-spacing difference between (110) and (004), $\Delta d = d_{110} - d_{004}$, is directly related to the unit-cell parameters difference $a - c$. Figure 48 shows that the experimental values of Δd are clustered either near 1.3×10^{-2} nm (leaching Sn to Ba) or ca. 2.5×10^{-2} nm (dry preparations, and leaching Ba to Sn). While samples of $BaSnF_4$ obtained by leaching give significantly different values depending on whether $BaSnClF_3.0.8H_2O$ was precipitated using Ba to Sn or Sn to Ba, those prepared by the dry method and those obtained by leaching for Ba to Sn are indistinguishable within experimental error.

The results in table 6 of a and c versus the method of preparation show that the values are clustered around two values: (i) on the one hand, 0.4292 nm average a and 1.138 nm average c for samples prepared by direct reactions, indistinguishable from 0.4350 nm average a and 1.134 nm average c for samples obtained by leaching $BaSnClF_3.0.8H_2O$ that was prepared by using Ba → Sn, (ii) and on the other hand, 0.4223 nm average a and 1.145 nm average c for samples obtained by leaching $BaSnClF_3.0.8H_2O$ that was prepared by using Sn → Ba (figs. 44 & 45).

Figure 40 shows that all peak shifts do not occur in the same direction: when (110) moves to higher angles (lower d-spacings), (004) shifts to lower angles (higher d-spacings). Since d_{110} is a function of the *a* parameters only ($d_{110} = a/\sqrt{2}$) and d_{004} is a function of the *c* parameter ($d_{004} = c/4$), *a* and *c* are inversely related to one another. The results in table 6 of *c* versus *a* shows indeed an inverse relationship: when *a* increases, *c* decreases, and vice-versa. A similar trend is obtained at a larger scale for the three $MSnF_4$ (M = Sr, Pb and Ba), where *a* increases with increasing ionic radius of M^{2+}, while *c* decreases[59, 61, 70, 84]. This can be understood by examination of the crystal structure (fig. 25): the F-F distances in MF_2 and in $MSnF_4$ are determined by the size of the M^{2+} cations, such that the bulkier M^{2+}, the larger the F-F distance. The Sn-F bonding distances are determined by the relative sizes of Sn(II) and F, and they must remain approximately the same in the three $MSnF_4$ structures. In order for the Sn-F distances to remain about the same while large variations of F-F distances take place, the tin atom must move closer to the fluorine plane it is bonded to, when the F-F distance increases, and it moves away from it when the F-F distance decreases. The tin motion must be parallel to the *c* axis of the unit-cell in order to maintain the tetragonal symmetry of the unit-cell and keep the four Sn-F distances equal to one another. This motion changes only the bond angles. It is well known that bond angles vary much more than bond lengths, since the latter are determined by the best orbital overlap and minimal Born repulsion in order to maximize bond strength. The motion of tin parallel to *c* creates an "umbrella effect", i.e. an increase of *c* results in a decrease of *a* (and of *b* since a = b) the same way as partially closing an umbrella increases its length while decreasing its diameter. Although the reason for the different values of unit-cell parameter between the samples obtained by

leaching $BaSnClF_3.0.8H_2O$ prepared using Sn → Ba and the other samples is not known, a similar *umbrella effect* is observed.

The larger *c* parameter (samples from leaching, Sn → Ba) contributes to increasing the unit-cell volume while the simultaneous decrease of *a* contributes to decrease it. Since the increase of *c* (1.09%) is smaller than the decrease of *a* (3.04%), and it applies to one direction only (parallel to $\vec{c}$) while the decrease of *a* applies in two dimensions (($\vec{a},\vec{b}$) plane), the volume is expected to decrease when *a* decreases, even though *c* increases. Indeed, the volume of the unit-cell for samples from leaching/Sn → Ba is smaller by 4.41%, while samples prepared by direct reactions and those by leaching Ba → Sn have the same volume within experimental error (Table 6).

The *c/a* ratio is used to characterize the deviation of tetragonal unit-cells from cubic symmetry (c/a = 1). In the case of the three $MSnF_4$ compounds, the *c/2a* ratio is used instead to account for the doubling of *c* due to the M M Sn Sn order parallel to $\vec{c}$. In addition, since *a* of $MSnF_4$ is equal to half the diagonal of the ($\vec{a},\vec{b}$) face of cubic BaF_2, a cubic $BaSnF_4$ unit-cell, if it existed, would have $c = 2\sqrt{2}a \Rightarrow c/2a = \sqrt{2} = 1.414$. The values of 1.30-1.36 (Table 6) show a significant flattening parallel to $\vec{c}$ relative to a cube. This is due to the absence of a fluoride ion layer between the tin sheets that results in a partial collapse along $\vec{c}$, that is not fully compensated for by the layer of tin lone pairs located at the same place (fig. 25). This can be understood by the following: (i) Sn(II) being smaller than Ba^{2+}, Sn is shifted towards the fluoride ion layer it binds to, (ii) each fluoride ion faces another fluoride ion on each side in the $\vec{c}$ axis direction, resulting in repulsion, while a lone pair faces the middle of the space between four fluoride ions in

the direction opposite to Sn, resulting in less repulsion, thereby allowing a closer approach, and thus a shortening of *c*. The smaller *c/2a* in the samples prepared from leaching/Sn → Ba follows the same trend as the $MSnF_4$ compounds versus the ionic radius of M^{2+}, and again, samples prepared by direct reactions and those from leaching Sn → Ba (Table 6) are identical (fig. 47).

When the unit-cell of a compound is not cubic, properties are expected to be *anisotropic*, i.e. to vary with direction in space. In the tetragonal system, crystal symmetry forces isotropy within the ($\vec{a},\vec{b}$) plane, i.e. identical properties in all directions within the ($\vec{a},\vec{b}$) plane. The $BaSnF_4$ structure is highly layered, since the plane of lone pairs sandwiched between the tin sheets preclude bonding between adjacent [Sn F Ba F Ba F Sn] sheets (fig. 25). Therefore a strong anisotropy is expected between the $\vec{c}$ direction and the ($\vec{a},\vec{b}$) plane. The properties parallel to $\vec{c}$ are called "parallel properties" because they act parallel to the special rotation axis (4-fold axis), while those parallel to ($\vec{a},\vec{b}$) are called "perpendicular properties" since they take place perpendicularly to the 4-fold axis. Table 6 show the average crystallite diameter parallel to $\vec{c}$ ($d_{\parallel}$) and perpendicular ($d_{\perp}$), calculated from the line broadening at half height, and the resulting average crystallite size anisotropy $d_{\parallel}/ d_{\perp}$. It is clear that the three methods of preparation give highly different crystallite size anisotropy. While both aqueous routes give crystallites that have $d_{\parallel}/ d_{\perp} < 1$, i.e. $d_{\parallel} < d_{\perp}$, there is little anisotropy or a reversed anisotropy ($d_{\parallel}/ d_{\perp} > 1$, i.e. $d_{\parallel} > d_{\perp}$) for samples prepared by the dry method. Obviously, the method of preparation has a strong influence on the shape of the crystallites. Flat thin sheets are expected because the layered structure (fig. 25) precludes

efficient growth perpendicularly to the sheets of lone pairs. This happens very efficiently in α-$PbSnF_4$*(aq1)* that is obtained very easily by precipitation with crystallite dimensions parallel to ($\vec{a},\vec{b}$) of ca. 1cm x 1cm and a thickness of 19 nm, i.e. $d_{\parallel}/ d_{\perp} = 1.9 \times 10^{-7}$ [70, 77]. Such an exceptionally small value was not found in the $BaSnF_4$ samples studied here. Since $d_{\parallel}/d_{\perp} < 1$ for $BaSnF_4$ obtained by the wet method in the present study (0.289-0.769), the growth perpendicularly to the sheets of lone pairs is still slower, although much more moderately slower. However, the growth parallel to the ($\vec{a},\vec{b}$) plane ($d_{\perp}$), orders of magnitude higher in α-$PbSnF_4$*(aq1)*, is responsible for the difference, since the growth parallel to $\vec{c}$ ($d_{\parallel}$), is about the same in both compounds: 19 nm in α-$PbSnF_4$*(aq1)*, and 6.21-28.95 nm in $BaSnF_4$ prepared by the wet method. Table 6 and figure 49 show that the $d_{\parallel}/ d_{\perp}$ ratio is nearly twice as large in $BaSnF_4$ prepared using leaching Sn → Ba as compared those from leaching/Ba → Sn. This difference is not understood at the moment. Samples prepared by the dry method have significantly narrower Bragg peaks, and therefore larger crystallite size. The same phenomenon was observed in our laboratory for $PbSnF_4$ [70, 85-88]. This can probably be attributed to the ion motion being favored at high temperature, and to the long heating time that gave the crystallites time to grow, in contrast with the fast particle formation in precipitation reactions that favor nucleation, i.e. the formation of new particles, over the growth of existing crystallites. However, little comment can be made regarding the samples obtained from leaching, since one cannot tell how, at the microscopic level, leaching of $BaSnClF_3.0.8H_2O$ in water gives $BaSnF_4$. It is also not known to date what differentiates $BaSnClF_3.0.8H_2O$ samples prepared at different precipitation conditions.

Figure 49 shows another interesting feature: when $d_{\parallel}$ is plotted versus $d_{\perp}$, the points form three linear groups, one for each method of preparation. Remarkably, the three lines are roughly parallel one another, with a slope of 0.6-0.7. Since the slope is lower than 1, growth is anisotropic, and is favored parallel to the ($\vec{a},\vec{b}$) plane, as expected according to the crystal structure. In addition, since the lines are approximately parallel to one another, crystal growth anisotropy changes at the same rate, regardless of the method of preparation, although the initial anisotropy is not the same. Therefore, it seems that the anisotropy of each crystallite obtained by nucleation determines the anisotropy obtained upon growth, and the anisotropy changes as the crystallites grow, with slower growth parallel to to $\vec{c}$.

A clear evidence of variations of unit-cell parameters and crystallite dimension anisotropy with the method of preparation has been shown. It is unclear how the two wet methods of preparation result in different unit-cell parameters, when the dry method and the wet method for Ba → Sn give very similar values. The differences between the two wet methods can be attributed to reaction conditions. For Ba → Sn, when a drop of solution of $BaCl_2$ enters into contact with the solution of SnF_2, there is a local excess of $BaCl_2$ in a reaction mixture that has a large excess of SnF_2, until enough $BaCl_2$ has been added to counterbalance the 1:1 stoichiometry for X>0.5. For Sn → Ba, it is the other way around. However, all samples of $BaSnClF_3.0.8H_2O$ were characterized by X-ray powder diffraction and did not contain any additional peak that would show the presence of crystalline impurities. Then, why do they behave somewhat differently when stirred in water? Could it be that the $BaSnClF_3.0.8H_2O$ contain variable amounts of an amorphous phase? Answering this question would require an extensive study beyond the scope of

this thesis. Elemental analysis of the barium tin (II) chloride fluorides is a very difficult task[80, 82].

In contrast to $BaSnF_4$, all samples of $BaSn_2F_6$ have narrow lines, thus a large crystallite diameter. Some of the variations observed for $BaSnF_4$ could be due to "hidden" reaction and stirring parameters that have not been identified yet. The reaction that takes place on leaching consists of a large part of the Ba and all the Cl contained in the sample being leached out, and a 40 to 60% mass loss is observed. Breaking up M-Cl bonds (M = Ba and Sn) preferentially to M-F is understood in terms of bond strength, where the M-Cl bonds are weaker.

4.4 Conclusion

It has been shown that both $BaSn_2F_6$ and $BaSnF_4$ can be obtained by leaching of $BaSn_2Cl_2F_4$ and $BaSnClF_3 \cdot 0.8H2O$, respectively, in each case without changing the Ba/Sn ratio. $BaSnClF_3 \cdot 0.8H2O$ is always fully decomposed when stirred in water, leaving $BaSnF_4$ pure phase. Particle size anisotropy is always observed in $BaSnF_4$ obtained by leaching, whereby the particle size is smaller in the direction parallel to the $\vec{c}$ axis than in the perpendicular direction. This is explained by the layered structure of the material, due to the sheets of tin(II) lone pairs perpendicular to $\vec{c}$ that act as perfect cleavage planes.

The unit-cell parameters and cell distortion are a function of the method of preparation, with the dry method and leaching for Ba → Sn giving nearly identical results, while those prepared by leaching for Sn → Ba being clearly different. The crystallite size anisotropy

is much smaller than in α-$PbSnF_4$*(aq)*, and it depends significantly upon the method of preparation, however results are consistent within each method of preparation. Some of the behavior versus the method of preparation have no explanation up to date.

Chapter 5

Future Work

For the first time an attempt to use $BaSnF_4$ as a transducer in a flow cell was reported in this work.

The method of preparation of $BaSnF_4$ sheets thick enough to stand the capillary pressure in the flow cell will need to be optimized further and studied. Although we did not succeed in preparing a $BaSnF_4$ layer thick enough to stand the capillary pressure in a flow cell, one can try different M/Sn/F compounds that would give a thick layer and perform as a transducer in a conductivity flow cell system.

Our study has led to a significant achievement in $BaCl_2/BaF_2/SnF_2$ system, which allows us to contribute to what was already known in literature by adding more data specifically in the $BaCl_2/BaF_2/SnF_2$ system, which is going to increase the knowledge on tin(II) fluoride-containing systems. The unit-cell parameters and cell distortion are a function of the method of preparation, with the dry method and leaching for Ba → Sn giving nearly identical results, while those prepared by leaching for Sn → Ba being clearly different. The crystallite size anisotropy is much smaller than in α-$PbSnF_4$*(aq)*, and it depends significantly upon the method of preparation, however results are consistent within each method of preparation. Some of the behavior versus the method of preparation have no explanation up to date and need to be studied further.

Appendix A - Validation results for chapter 2

Table 8: Linearity – Occasion 1 (rat plasma)

Theoretical concentration (ng/mL)	Back-calculated concentration (ng/mL)	Difference (%)
1.000	0.994	-0.6
1.600	1.562	-2.4
2.000	2.000	0.5
3.000	3.020	0.8
4.000	4.300	7.3
5.000	5.180	3.5
6.000	6.280	4.6
7.000	6.540	-6.7
8.000	7.740	-3.2
10.000	9.620	-3.9

Coefficient of determination (r^2) = 0.996

Table 9: Linearity – Occasion 2 (rat plasma)

Theoretical concentration (ng/mL)	Back-calculated concentration (ng/mL)	Difference (%)
1.000	0.968	-3.3
1.600	1.676	4.7
2.000	1.972	-1.4
3.000	3.120	3.9
4.000	3.940	-1.3
5.000	5.180	3.5
6.000	6.020	0.4
7.000	6.980	-0.3
8.000	7.960	-0.6
10.000	9.440	-5.5

Coefficient of determination (r^2) = 0.998

Table 10: Linearity – Occasion 3 (rat plasma)

Theoretical concentration (ng/mL)	Back-calculated concentration (ng/mL)	Difference (%)
1.000	1.006	0.6
1.600	1.490	-6.9
2.000	2.120	6.1
3.000	3.220	7.2
4.000	3.700	-7.4
5.000	4.900	-1.8
6.000	6.060	0.9
7.000	7.300	4.3
8.000	8.120	1.4
10.000	9.560	-4.3

Coefficient of determination (r^2) = 0.994

Table 11: Lower Limit of Quantitation (rat plasma)

Theoretical concentration (ng/mL)	Measured concentration (ng/mL)	Relative error (%)	Mean relative error (%)	CV (%)
1.000	0.98	-2.0	-2.3	3.2
	1.004	0.4		
	0.984	-1.6		
	0.982	-1.9		
	0.998	-0.3		
	0.916	-8.4		

Table 12: Intra-assay Precision and Accuracy – Occasion 1 (rat plasma)

Theoretical concentration (ng/mL)	Measured concentration (ng/mL)	Relative error (%)	Mean relative error (%)	CV (%)
1.800	1.614	-10.4	-11.0	3.6
	1.574	-12.6		
	1.558	-13.5		
	1.564	-13.1		
	1.698	-5.7		
	1.394	-22.5[a]		
5.000	5.060	1.0	2.7	3.1
	5.280	5.4		
	5.180	3.8		
	5.280	5.6		
	5.160	3.2		
	4.860	-2.8		
8.000	7.900	-1.2	0.1	5.9
	8.060	0.8		
	8.180	2.3		
	8.780	9.7		
	7.360	-8.1		
	7.760	-3.0		

a = outside acceptance criteria set by the FDA guideline, not used in statistical calculation

Table 13: Intra-assay Precision and Accuracy – Occasion 2 (rat plasma)

Theoretical concentration (ng/mL)	Measured concentration (ng/mL)	Relative error (%)	Mean relative error (%)	CV (%)
1.800	1.930	7.2	9.9	2.2
	1.932	7.3		
	1.984	10.3		
	1.992	10.7		
	2.040	13.7		
	1.990	10.5		
5.000	5.380	7.4	6.0	2.8
	5.060	1.0		
	5.340	7.0		
	5.320	6.4		
	5.480	9.8		
	5.220	4.5		
8.000	8.040	0.5	0.4	4.1
	8.020	0.3		
	8.060	0.6		
	7.440	-7.1		
	8.320	4.1		
	8.340	4.2		

Table 14: Intra-assay Precision and Accuracy – Occasion 3 (rat plasma)

Theoretical concentration (ng/mL)	Measured concentration (ng/mL)	Relative error (%)	Mean relative error (%)	CV (%)
1.800	1.982	10.1	11.3	1.3
	1.986	10.3		
	2.020	12.5		
	1.976	9.7		
	2.040	12.9		
	2.020	12.1		
5.000	4.880	-2.3	5.6	3.7
	5.360	7.0		
	5.420	8.5		
	5.340	6.6		
	5.320	6.4		
	5.360	7.2		
8.000	8.380	4.7	2.9	3.6
	8.440	5.6		
	8.440	5.5		
	7.900	-1.2		
	8.400	5.1		
	7.800	-2.4		

Table 15: Inter-assay Precision and Accuracy (rat plasma)

Theoretical concentration (ng/mL)	Occasion 1 relative error (%)	Occasion 2 relative error (%)	Occasion 3 relative error (%)	Global mean relative error (%)	Global CV (%)
1.800	-10.4	7.2	10.1	4.3	2.5
	-12.6	7.3	10.3		
	-13.5	10.3	12.5		
	-13.1	10.7	9.7		
	-5.7	13.7	12.9		
	-22.5[a]	10.5	12.1		
5.000	1.0	7.4	-2.3	4.8	0.7
	5.4	1.0	7.0		
	3.8	7.0	8.5		
	5.6	6.4	6.6		
	3.2	9.8	6.4		
	-2.8	4.5	7.2		
8.000	-1.2	0.5	4.7	1.1	4.1
	0.8	0.3	5.6		
	2.3	0.6	5.5		
	9.7	-7.1	-1.2		
	-8.1	4.1	5.1		
	-3.0	4.2	-2.4		

a = outside acceptance criteria set by the FDA guideline, not used in statistical calculation

Table 16: Linearity – Occasion 1 (apple homogenate)

Theoretical concentration (ng/mL)	Back-calculated concentration (ng/mL)	Difference (%)
1.000	0.988	-1.2
1.600	1.640	2.5
2.000	2.020	1.1
3.000	2.940	-2.1
4.000	3.800	-5.2
5.000	5.300	6.2
6.000	5.860	-2.4
7.000	7.500	7.1
8.000	7.520	-5.9
10.000	10.120	1.2

Coefficient of determination (r^2) = 0.995

Table 17: Linearity – Occasion 2 (apple homogenate)

Theoretical concentration (ng/mL)	Back-calculated concentration (ng/mL)	Difference (%)
1.000	0.996	-0.4
1.600	1.592	-0.5
2.000	2.020	0.6
3.000	3.060	1.8
4.000	4.000	-0.1
5.000	5.200	2.2
6.000	5.860	-2.4
7.000	7.000	-1.1
8.000	7.900	-1.3
10.000	10.120	1.2

Coefficient of determination (r^2) = 1.00

Table 18: Linearity – Occasion 3 (apple homogenate)

Theoretical concentration (ng/mL)	Back-calculated concentration (ng/mL)	Difference (%)
1.000	0.978	-2.2
1.600	1.642	2.7
2.000	2.020	0.6
3.000	3.160	5.6
4.000	3.820	-4.4
5.000	4.920	-1.5
6.000	5.860	-2.3
7.000	7.000	-0.1
8.000	8.120	1.4
10.000	10.020	0.3

Coefficient of determination (r^2) = 0.998

Table 19: Lower Limit of Quantitation (apple homogenate)

Theoretical concentration (ng/mL)	Measured concentration (ng/mL)	Relative error (%)	Mean relative error (%)	CV (%)
1.000	1.074	7.4	8.4	3.8
	1.026	2.6		
	1.116	11.5		
	1.13	12.9		
	1.046	4.7		
	1.112	11.3		

Table 20: Intra-assay Precision and Accuracy – Occasion 1 (apple homogenate)

Theoretical concentration (ng/mL)	Measured concentration (ng/mL)	Relative error (%)	Mean relative error (%)	CV (%)
1.800	1.784	-0.9	-4.5	3.3
	1.706	-5.3		
	1.726	-4.1		
	1.622	-9.9		
	1.766	-1.9		
	1.708	-5.1		
5.000	5.240	4.8	1.8	1.7
	5.020	0.6		
	5.000	0.0		
	5.060	1.3		
	5.080	1.6		
	5.120	2.4		
8.000	7.800	-2.5	1.0	2.5
	8.240	2.9		
	10.280	28.6[a]		
	8.160	1.9		
	7.960	-0.5		
	8.280	3.5		

a = outside acceptance criteria set by the FDA guideline, not used in statistical calculation

Table 21: Intra-assay Precision and Accuracy – Occasion 2 (apple homogenate)

Theoretical concentration (ng/mL)	Measured concentration (ng/mL)	Relative error (%)	Mean relative error (%)	CV (%)
1.800	1.540	-14.5	-0.7	6.8
	1.840	2.2		
	1.850	2.8		
	1.828	1.53		
	1.818	1.05		
	1.846	2.54		
5.000	4.820	-3.7	-0.3	2.7
	4.860	-2.9		
	5.020	0.4		
	5.200	3.8		
	5.000	0.1		
	5.020	0.3		
8.000	7.960	-0.5	0.6	2.7
	7.920	-0.9		
	8.040	0.5		
	7.880	-1.5		
	8.000	0.0		
	8.480	6.1		

Table 22: Intra-assay Precision and Accuracy – Occasion 3 (apple homogenate)

Theoretical concentration (ng/mL)	Measured concentration (ng/mL)	Relative error (%)	Mean relative error (%)	CV (%)
1.800	2.040	13.8	13.1	0.8
	2.020	11.7		
	2.060	14.3		
	2.040	13.1		
	2.040	13.2		
	2.040	12.9		
5.000	5.240	4.7	5.4	2.4
	5.240	4.8		
	5.120	2.5		
	5.380	7.4		
	5.180	3.5		
	5.460	9.3		
8.000	8.260	3.3	2.6	1.7
	8.160	2.0		
	8.420	5.2		
	8.240	3.1		
	7.980	-0.2		
	8.160	2.0		

Table 23: Inter-assay Precision and Accuracy (apple homogenate)

Theoretical concentration (ng/mL)	Occasion 1 relative error (%)	Occasion 2 relative error (%)	Occasion 3 relative error (%)	Global mean relative error (%)	Global CV (%)
1.800	-0.9	-14.5	13.8	2.6	3.4
	-5.3	2.2	11.7		
	-4.1	2.8	14.3		
	-9.9	1.53	13.1		
	-1.9	1.05	13.2		
	-5.1	2.54	12.9		
5.000	4.8	-3.7	4.7	2.3	1.4
	0.6	-2.9	4.8		
	0.0	0.4	2.5		
	1.3	3.8	7.4		
	1.6	0.1	3.5		
	2.4	0.3	9.3		
8.000	-2.5	-0.5	3.3	1.4	1.7
	2.9	-0.9	2.0		
	28.6[a]	0.5	5.2		
	1.9	-1.5	3.1		
	-0.5	0.0	-0.2		
	3.5	6.1	2.0		

a = outside acceptance criteria set by the FDA guideline, not used in statistical calculation.

Validation Summary

Parameter	Completed, results within acceptance criteria for rat plasma	Completed, results within acceptance criteria for apple homogenate
Selectivity	yes	yes
Linearity	yes	yes
LLOQ assessment	yes	yes
Carry-over	yes	yes
Intra-assay precision and accuracy	yes	yes
Inter-assay precision and accuracy	yes	yes

Appendix B - Validation results for chapter 3

Table 24: Linearity – Occasion 1 (rat plasma)

Theoretical concentration (ng/mL)	Back-calculated concentration (ng/mL)	Difference (%)
1.000	0.994	-0.6
1.600	1.562	-2.4
2.000	2.000	0.5
3.000	3.020	0.8
4.000	4.300	7.3
5.000	5.180	3.5
6.000	6.280	4.6
7.000	6.540	-6.7
8.000	7.740	-3.2
10.000	9.620	-3.9

Coefficient of determination (r^2) = 0.996

Table 25: Linearity – Occasion 2 (rat plasma)

Theoretical concentration (ng/mL)	Back-calculated concentration (ng/mL)	Difference (%)
1.000	0.968	-3.3
1.600	1.676	4.7
2.000	1.972	-1.4
3.000	3.120	3.9
4.000	3.940	-1.3
5.000	5.180	3.5
6.000	6.020	0.4
7.000	6.980	-0.3
8.000	7.960	-0.6
10.000	9.440	-5.5

Coefficient of determination (r^2) = 0.998

Table 26: Linearity – Occasion 3 (rat plasma)

Theoretical concentration (ng/mL)	Back-calculated concentration (ng/mL)	Difference (%)
1.000	1.006	0.6
1.600	1.490	-6.9
2.000	2.120	6.1
3.000	3.220	7.2
4.000	3.700	-7.4
5.000	4.900	-1.8
6.000	6.060	0.9
7.000	7.300	4.3
8.000	8.120	1.4
10.000	9.560	-4.3

Coefficient of determination (r^2) = 0.994

Table 27: Lower Limit of Quantitation (rat plasma)

Theoretical concentration (ng/mL)	Measured concentration (ng/mL)	Relative error (%)	Mean relative error (%)	CV (%)
1.000	0.98	-2.0	-2.3	3.2
	1.004	0.4		
	0.984	-1.6		
	0.982	-1.9		
	0.998	-0.3		
	0.916	-8.4		

Table 28: Intra-assay Precision and Accuracy – Occasion 1 (rat plasma)

Theoretical concentration (ng/mL)	Measured concentration (ng/mL)	Relative error (%)	Mean relative error (%)	CV (%)
1.800	1.614	-10.4	-11.0	3.6
	1.574	-12.6		
	1.558	-13.5		
	1.564	-13.1		
	1.698	-5.7		
	1.394	-22.5[a]		
5.000	5.060	1.0	2.7	3.1
	5.280	5.4		
	5.180	3.8		
	5.280	5.6		
	5.160	3.2		
	4.860	-2.8		
8.000	7.900	-1.2	0.1	5.9
	8.060	0.8		
	8.180	2.3		
	8.780	9.7		
	7.360	-8.1		
	7.760	-3.0		

a = outside acceptance criteria set by the FDA guideline, not used in statistical calculation

Table 29: Intra-assay Precision and Accuracy – Occasion 2 (rat plasma)

Theoretical concentration (ng/mL)	Measured concentration (ng/mL)	Relative error (%)	Mean relative error (%)	CV (%)
1.800	1.930	7.2	9.9	2.2
	1.932	7.3		
	1.984	10.3		
	1.992	10.7		
	2.040	13.7		
	1.990	10.5		
5.000	5.380	7.4	6.0	2.8
	5.060	1.0		
	5.340	7.0		
	5.320	6.4		
	5.480	9.8		
	5.220	4.5		
8.000	8.040	0.5	0.4	4.1
	8.020	0.3		
	8.060	0.6		
	7.440	-7.1		
	8.320	4.1		
	8.340	4.2		

Table 30: Intra-assay Precision and Accuracy – Occasion 3 (rat plasma)

Theoretical concentration (ng/mL)	Measured concentration (ng/mL)	Relative error (%)	Mean relative error (%)	CV (%)
1.800	1.982	10.1	11.3	1.3
	1.986	10.3		
	2.020	12.5		
	1.976	9.7		
	2.040	12.9		
	2.020	12.1		
5.000	4.880	-2.3	5.6	3.7
	5.360	7.0		
	5.420	8.5		
	5.340	6.6		
	5.320	6.4		
	5.360	7.2		
8.000	8.380	4.7	2.9	3.6
	8.440	5.6		
	8.440	5.5		
	7.900	-1.2		
	8.400	5.1		
	7.800	-2.4		

Table 31: Inter-assay Precision and Accuracy (rat plasma)

Theoretical concentration (ng/mL)	Occasion 1 relative error (%)	Occasion 2 relative error (%)	Occasion 3 relative error (%)	Global mean relative error (%)	Global CV (%)
1.800	-10.4	7.2	10.1	4.3	2.5
	-12.6	7.3	10.3		
	-13.5	10.3	12.5		
	-13.1	10.7	9.7		
	-5.7	13.7	12.9		
	-22.5[a]	10.5	12.1		
5.000	1.0	7.4	-2.3	4.8	0.7
	5.4	1.0	7.0		
	3.8	7.0	8.5		
	5.6	6.4	6.6		
	3.2	9.8	6.4		
	-2.8	4.5	7.2		
8.000	-1.2	0.5	4.7	1.1	4.1
	0.8	0.3	5.6		
	2.3	0.6	5.5		
	9.7	-7.1	-1.2		
	-8.1	4.1	5.1		
	-3.0	4.2	-2.4		

a = outside acceptance criteria set by the FDA guideline, not used in statistical calculation

Appendix C - Results for chapter 4

Table 32 The phases obtained from the precipitation reaction

Sample ID	X_{Ba}	Order of addition	Time of stirring allowed after end of addition (hours)	Amount of Water added after the end of addition (mL)	Weight recovered (g)	$BaSn_2Cl_2F_4$	$BaSnClF_3.0.8H_2O$	$Ba_{1-x}Sn_xCl_{1+y}F_{1-y}$	Qualitative relative composition
JH02	0.20	Sn → Ba	0	0	2.3080	√			100
JH03	0.40	Sn → Ba	0	0	2.3003	√	√		40:60
JH04	0.60	Sn → Ba	0	0	1.9316	√	√		20:80
JH05	0.65	Sn → Ba	0	0	4.6697		√		100
JH07	0.75	Sn → Ba	0	0	2.8286		√		100
JH08	0.80	Sn → Ba	0	0	6.9967		√		100
JH09	0.85	Sn → Ba	0	0	3.0087		√	√	80:20
JH10	0.90	Sn → Ba	0	0	3.4537		√	√	40:60
JH11	0.95	Sn → Ba	0	0	4.3895			√	100

Sample ID	X_{Ba}	Order of addition	Time of stirring allowed after end of addition (hours)	Amount of Water added after the end of addition (mL)	Weight recovered (g)	$BaSn_2Cl_2F_4$	$BaSnClF_3.0.8H_2O$	$Ba_{1-x}Sn_xCl_{1+y}F_{1-y}$	Qualitative relative composition / comments
JH59	0.10	Sn → Ba	48	0	0.8405		√		100
JH60	0.20	Sn → Ba	48	0	0.9289	√	√		40:60
JH61	0.30	Sn → Ba	48	0	1.2381		√		100
JH62	0.40	Sn → Ba	48	0	1.6216				amorphous
JH63	0.50	Sn → Ba	48	0	1.5084		√		100
JH64	0.60	Sn → Ba	48	0	1.1823				amorphous
JH65	0.70	Sn → Ba	48	0	0.9444		√		100
JH66	0.80	Sn → Ba	48	0	2.0727			√	100
JH67	0.91	Sn → Ba	48	0	1.5948			√	100

Sample ID	X_{Ba}	Order of addition	Time of stirring allowed after end of addition (hours)	Amount of Water added after the end of addition (mL)	Weight recovered (g)	$BaSn_2Cl_2F_4$	$BaSnClF_3.0.8H_2O$	$Ba_{1-x}Sn_xCl_{1+y}F_{1-y}$	Qualitative relative composition / comments
JH68	0.04	Sn → Ba	74	100	1.6809				$BaSn_2F_6$ (100%)
JH69	0.08	Sn → Ba	74	100	1.8577				$BaSn_2F_6$ (100%)
JH70	0.13	Sn → Ba	74	100	2.4762				$BaSn_2F_6$ (100%)
JH71	0.19	Sn → Ba	74	100	3.2432				$BaSn_2F_6$ (100%)
JH72	0.26	Sn → Ba	74	100	3.0168				$BaSn_2F_6$ (100%)
JH73	0.35	Sn → Ba	74	100	2.3646				amorphous
JH74	0.41	Sn → Ba	74	100	1.8888				amorphous
JH75	0.59	Sn → Ba	74	100	4.1454		√	√	60:40
JH76	0.78	Sn → Ba	74	100	3.1895		√	√	50:50

Sample ID	X_{Ba}	Order of addition	Time of stirring allowed after end of addition (hours)	Amount of Water added after the end of addition (mL)	Weight recovered (g)	$BaSn_2Cl_2F_4$	$BaSnClF_3.0.8H_2O$	$Ba_{1-x}Sn_xCl_{1+y}F_{1-y}$	Qualitative relative composition / comments
JH80	0.10	Sn → Ba	24	100	3.1378	√	√		80:20
JH81	0.20	Sn → Ba	24	100	3.2437	√	√		80:20
JH82	0.30	Sn → Ba	24	100	2.4768	√	√		60:40
JH83	0.40	Sn → Ba	24	100	2.6309	√	√		40:60
JH84	0.50	Sn → Ba	24	100	4.2019		√		100
JH85	0.60	Sn → Ba	24	100	3.4307		√		100
JH86	0.70	Sn → Ba	24	100	2.7734		√		100
JH87	0.80	Sn → Ba	24	100	2.5309			√	100
JH88	0.90	Sn → Ba	24	100	4.0010			√	100

Sample ID	X_{Ba}	Order of addition	Time of stirring allowed after end of addition (hours)	Amount of Water added after the end of addition (mL)	Weight recovered (g)	$BaSn_2Cl_2F_4$	$BaSnClF_3.0.8H_2O$	$Ba_{1-x}Sn_xCl_{1+y}F_{1-y}$	Qualitative relative composition / comments
JH89	0.10	Sn → Ba	24	0	NR	√			100
JH90	0.20	Sn → Ba	24	0	NR	√			100
JH91	0.30	Sn → Ba	24	0	NR		√		100
JH92	0.40	Sn → Ba	24	0	NR		√		100
JH93	0.50	Sn → Ba	24	0	NR		√		100
JH94	0.60	Sn → Ba	24	0	NR		√		100
JH95	0.70	Sn → Ba	24	0	NR		√		100
JH96	0.80	Sn → Ba	24	0	NR			√	100
JH97	0.90	Sn → Ba	24	0	NR			√	100

NR = not recorded

Sample ID	X_{Ba}	Order of addition	Time of stirring allowed after end of addition (hours)	Amount of Water added after the end of addition (mL)	Weight recovered (g)	$BaSn_2Cl_2F_4$	$BaSnClF_3.0.8H_2O$	$Ba_{1-x}Sn_xCl_{1+y}F_{1-y}$	Qualitative relative composition / comments
JH23	0.30	Ba → Sn	0	0	2.8516	√			100
JH24	0.55	Ba → Sn	0	0	0.4364	√	√		40:60
JH25	0.60	Ba → Sn	0	0	2.7734		√		100
JH26	0.65	Ba → Sn	0	0	3.1378		√		100
JH27	0.70	Ba → Sn	0	0	3.3202		√		100
JH28	0.75	Ba → Sn	0	0	2.9101		√		100
JH29	0.80	Ba → Sn	0	0	3.0397		√		100
JH30	0.85	Ba → Sn	0	0	3.2437		√	√	60:40
JH31	0.90	Ba → Sn	0	0	3.4307		√	√	20:80
JH32	0.95	Ba → Sn	0	0	3.2365			√	100
JH46	0.70	Ba → Sn	0	0	2.5722		√		100
JH47	0.75	Ba → Sn	0	0	2.4768		√		100
JH48	0.80	Ba → Sn	0	0	2.8367		√	√	60:40
JH49	0.85	Ba → Sn	0	0	2.6309		√	√	50:50
JH50	0.90	Ba → Sn	0	0	4.2019			√	100
JH51	0.95	Ba → Sn	0	0	5.5441			√	100

Table 33 The phases obtained after leaching phases obtained with the precipitation reaction

Sample ID	X_{Ba}	Order of addition	Sample ID that was leached	Amount leached (g)	Period of time of leaching (hours)	Weight recovered (g)	$BaSn_2F_6$	$BaSnF_4$	Qualitative relative composition / comments
JH12	0.50	Sn → Ba	JH02	1.5264	46	0.8990	√		100
JH13	0.55	Sn → Ba	JH03	1.5731	46	0.7750	√	√	20:80
JH14	0.60	Sn → Ba	JH04	1.1954	46	0.5075	√	√	20:80
JH15	0.65	Sn → Ba	JH05	3.4196	46	0.8081	√	√	20:80
JH16	0.75	Sn → Ba	JH07	1.7107	46	0.5684	√	√	20:80
JH17	0.80	Sn → Ba	JH08	1.5842	46	0.6434	√	√	20:80
JH18	0.85	Sn → Ba	JH09	1.6272	46	0.6038			Traces: major peaks correspond to $Ba_{1-x}Sn_xCl_{1+y}F_{1-y}$
JH19	0.90	Sn → Ba	JH10	1.5191	46	0.6054			Traces: major peaks correspond to $Ba_{1-x}Sn_xCl_{1+y}F_{1-y}$
JH20	0.95	Sn → Ba	JH11	1.7178	46	0.9571			Traces: major peaks correspond to $Ba_{1-x}Sn_xCl_{1+y}F_{1-y}$

Sample ID	X_{Ba}	Order of addition	Sample ID that was leached	Amount leached (g)	Period of time of leaching (hours)	Weight recovered (g)	$BaSn_2F_6$	$BaSnF_4$	Qualitative relative composition / comments
JH33	0.30	Ba → Sn	JH23	1.2157	72	0.4035	√		100
JH35	0.60	Ba → Sn	JH25	1.1413	72	0.3867	√	√	30:70
JH36	0.65	Ba → Sn	JH26	1.0705	72	0.2832	√	√	30:70
JH37	0.70	Ba → Sn	JH27	1.0293	72	0.2127	√	√	20:80
JH38	0.75	Ba → Sn	JH28	1.0518	72	0.2845		√	100
JH39	0.80	Ba → Sn	JH29	1.0278	72	0.2404		√	100
JH40	0.85	Ba → Sn	JH30	1.3217	72	0.2435		√	Major peaks corresponded to $Ba_{1-x}Sn_xCl_{1+y}F_{1-y}$
JH41	0.90	Ba → Sn	JH31	1.0605	72	0.3068		√	Major peaks corresponded to $Ba_{1-x}Sn_xCl_{1+y}F_{1-y}$
JH42	0.95	Ba → Sn	JH32	1.1101	72	0.4330			Only $Ba_{1-x}Sn_xCl_{1+y}F_{1-y}$ phase was recovered

Sample ID	X_{Ba}	Order of addition	Sample ID that was leached	Amount leached (g)	Period of time of leaching (hours)	Weight recovered (g)	$BaSn_2F_6$	$BaSnF_4$	Qualitative relative composition / comments
JH53	0.70	Ba → Sn	JH46	1.0614	84	0.1490			amorphous
JH54	0.75	Ba → Sn	JH47	1.0556	84	0.1275		√	100
JH55	0.80	Ba → Sn	JH48	1.0188	84	0.2100		√	100
JH56	0.85	Ba → Sn	JH49	1.0801	84	0.2505		√	100
JH57	0.90	Ba → Sn	JH50	1.0274	84	0.2498			Only $Ba_{1-x}Sn_xCl_{1+y}F_{1-y}$ phase was recovered
JH58	0.95	Ba → Sn	JH51	1.0934	84	0.2377			Only $Ba_{1-x}Sn_xCl_{1+y}F_{1-y}$ phase was recovered

Sample ID	X_{Ba}	Order of addition	Sample ID that was leached	Amount leached (g)	Period of time of leaching (hours)	Weight recovered (g)	$BaSn_2F_6$	$BaSnF_4$	Qualitative relative composition / comments
JH104	0.04	Sn → Ba	JH68	1.0934	24	0.6500	√		100
JH105	0.08	Sn → Ba	JH69	1.0934	24	0.6500	√		100
JH106	0.13	Sn → Ba	JH70	1.0934	24	0.6500	√		100
JH107	0.19	Sn → Ba	JH71	1.0934	24	0.6500	√		100
JH108	0.26	Sn → Ba	JH72	1.0934	24	0.6500	√		100
JH109	0.59	Sn → Ba	JH75	1.0934	24	0.6500		√	Minor peaks correspond to $Ba_{1-x}Sn_xCl_{1+y}F_{1-y}$
JH110	0.78	Sn → Ba	JH76	1.0934	24	0.6500		√	Major peaks correspond to $Ba_{1-x}Sn_xCl_{1+y}F_{1-y}$

Sample ID	X_{Ba}	Order of addition	Sample ID that was leached	Amount leached (g)	Period of time of leaching (hours)	Weight recovered (g)	$BaSn_2F_6$	$BaSnF_4$	Qualitative relative composition / comments
JH111	0.10	Sn → Ba	JH80	1.0934	24	0.6500	√	√	50:50
JH112	0.20	Sn → Ba	JH81	1.0934	24	0.6500	√	√	70:30
JH113	0.30	Sn → Ba	JH82	1.0934	24	0.6500	√	√	60:40
JH114	0.40	Sn → Ba	JH83	1.0934	24	0.6500	√	√	40:60
JH115	0.50	Sn → Ba	JH84	1.0934	24	0.2986		√	100
JH116	0.60	Sn → Ba	JH85	1.0934	24	0.3600		√	100
JH117	0.70	Sn → Ba	JH86	1.0934	24	0.2985		√	100
JH118	0.80	Sn → Ba	JH87	1.0934	24	0.6500			Only $Ba_{1-x}Sn_xCl_{1+y}F_{1-y}$ phase was recovered
JH119	0.90	Sn → Ba	JH88	1.0934	24	0.6500			Only $Ba_{1-x}Sn_xCl_{1+y}F_{1-y}$ phase was recovered

Bibliography

[1] W. J. Rea, *Pesticides. Journal of Nutritional and Environmental Medicine* **6**, 55 (1996).

[2] U.S. Environmental Protection Agency, Office of Drinking Water. Carbaryl Health Advisory. Draft Report, August 1987.

[3] National Library of Medicine. Hazardous Substances Databank. Carbaryl, February 4, 1992.

[4] R. L. Baron, Carbamate Insecticides. in Handbook of Pesticide Toxicology, Volume 3, Classes of Pesticides. Wayland J. Hayyes, Jr. and Edward R. Lawes, Jr. editors. Academic Press, Inc. NY (1991).

[5] ACGIH, Documentation of grow Threshold Limit Values and Biological Indices. American Conference of Governmental and Industrial Hygienists, Inc., Cincinnati, OH (1991).

[6] D. Siebert and G. Eisenbrand, *Mutat. Res.* **22**, 121 (1974).

[7] R. Elespuru, W. Lijinski and J. K. Setlow, *Nature (London).* **247** , 386 (1974).

[8] "Evaluation of Carcinogenic, Teratogenic, and Mutagenic Activities of Selected Pesticides and Industrial Chemicals," Volume 1: "Carcinogenic Study", National Technical Information Service, Washington, D.C. (1968).

[9] J. D. Regan, R. B. Setlow, A. A. Francis and W. Lijinsky, *Mutat. Res.* **38** ,293 (1976).

[10] C. P. Carpenter. *Agricultural and Food Chemistry* **9** , 30 (1961).

[11] R. D. Wauchope, *J. Environ. Qual.* **7**, 459 (1978).

[12] http://www.inchem.org/documents/pims/chemical/pim147.htm.

[13] J. B. Knaak, J. Marilyn, M. J. Tallant and L. F.Sullivan, *J. Agric. Food Chem.* **13** , 537 (1965).

[14] W. J. Hayes and E. R. Laws, Handbook of pesticide toxicology, vol 3 Classes of pesticides, Acad. Press, San Diego (1991).

[15] Textbook Polym. Sic, F. W. Billmeyer, 3'- Ed., John Wiley & Sons (1984).

[16] P. J. Dowding and B. Vincent, *Colloids and surfaces* **161**, 259 (2000).

[17] Practical Macromolecular Organic Chem., D. Braun, H. Cherdonron and W. Kern, vol. 2, Harwood Academic Publisher (1984).

[18] Textbook Fundamentals of Polymer Science, P.C. Painter and M.M. Coleman, CRC Press (1997).

[19] D. Kriz, O. Ramstrom and K. Mosbach, *Anal. Chem.* **69**, 345A (1997).

[20] D. J. Cram, *Angew. Chem., Int. Ed. Engl.* **27**, 1009 (1988).

[21] J-M. Lehn, *Angew. Chem., Int. Ed. Engl.* **27**, 89 (1988).

[22] C. J. Pedersen, *Angew. Chem., Int. Ed. Engl.* **27**, 1021 (1988).

[23] J. S. Lindsey, *New J. Chem.*, **15**, 153 (1991).

[24] K. Mosbach and O. Ramström, *Bio/Technology*, **14**, 163 (1996).

[25] G. Wulff, *Angew. Chem., Int. Ed. Engl.*, **34**, 1812 (1995).

[26] D. Kriz, C. Berggren Kriz, L. Andersson and K. Mosbach, *Anal. Chem.*, **66**, 2636 (1994).

[27] K. Nilsson, J. Lindell, O. Norrlöw and B. Sellergren, *J. Chromatogr. A*, **680**, 57 (1994).

[28] G. Vlatakis, L. I. Andersson, R. Müller and K. Mosbach, K., *Nature*, **361**, 645 (1993).

[29] M. Muldoon and L. Stanker, *J. Agric. Food Chem.*, **43**, 1424 (1995).

[30] R.L. Baron, in W.H. Hayes, Jr. and E.R. Laws, Jr. (Editors), Handbook of Pesticide Toxicology, *Academic Press*, San Diego, CA, vol. 3,. pp. 1125–1189. (1991).

[31] M. Farage-Elawar and W.D. Blaker. *J. Appl. Toxicol.* **12**, 421 (1992).

[32] G.P. Casale, J.L. Vennerstrom, S. Bavari and T.L. Wang., *Immunopharmacol. Immunotoxicol.*. **15**, 199 (1993).

[33] Library of Medicine, Hazardous Substances Databank, Carbaryl, 4 February 1992.

[34] US Environmental Protection Agency, Office of Drinking Water, Carbaryl Health Advisory, Draft Report, August 1987.

[35] R. D. Wauchope, *J. Environ. Qual.*, **7**, 459 (1978).

[36] R. D. Wauchope and Haque R., *Bull. Environ. Contam. Toxicol.*, **9** , 257 (1978).

[37] N. L. Wolfe, R.G. Zepp, G.L. Baughman, R.C. Fincher and J.A. Gordon, Chemical and photochemical transformation of selected pesticides in aquatic systems, USEPA, Athens, GA.123, EPA 600/3-76-067. (1976).

[38] E. Ballesteros, M. Gallego and M. Valcarcel, *Anal. Chem.*, **65**, 1773 (1993)

[39] R. E. Baynes and J. M. Bowen, *J. AOAC Int.*, **78**, 812 (1995).

[40] V. B. Kandimalla and H. X. Ju, *Anal. Bioanal. Chem.*, **380**, (2004).

[41] D. A. Spivk, *Advanced Drug Delivery Reviews* **57**, 1779 (2005).

[42] V. B. Kandimalla and H. X. Ju, *Anal. Bioanal. Chem.*, **380**, 587 (2004).

[43] L. I. Andrsson, *Bioseperation* **10**, 353 (2001).

[44] A. G. Mayes and Mosback, *Anal. Chem.* **68**, 3769 (1996).

[45] Y. Pico, G. Font, J. C. Molto JC; *J. Chrom.* A, **882**, 153 (2000).

[46] E. Ballesteros, M. Gallego, M. Valcarcel, *Anal. Chem.* 1993, **65**, 1773-1778A.

[47] Guidance for Industry Bioanalytical Method Validation, U.S. Department of health and human services, Food and Drug Administration, May 2001.

[48] Source:
http://www.idshealthcare.com/hospital_management/global/esa_biosciences/electrochemi - cal_ detection/101_0/g_supplier.html.

[49] H. Jing, H. and A. Amirav, *Anal. Chem.* **69**, 1426 (1997).

[50] S. Nunes, P. Skladal, H. Yamanka and D. Barcelo, *Anal. Chim. Acta* **362**, 59 (1998).

[51] A. Mulchandani, W. Chen, P. Mulchandani, J. Wang and K. R. Rogers, *Biosens. Bioelectron.* **16**, 225 (2001).

[52] K. Rekha, M. S. Thakur and N. G., Karanth, *Crit. Rev. Biotechnol.* **20**, 213 (2000).

[53] C. R. Suri, M. Raje and G. C. Varshney, *Crit. Rev. Biotechnol.* **22**, 15 (2002).

[54] M. Trojanowicz, **14**, 1311 (2002).

[55] F. Jungbluth, Crop Protection Policy in Thailand: economic and Political factors influencing pesticide use. Pesticide Policy Project Publication Series No. 5, Uni Druck Hannover, Hannover (1996)

[56] A. Thanpinta and P. F. Hudak, *Environ. Monit. Assess.* **60**, 103 (2000).

[57] T. Matuso, T. Kakiya and Y. Sugie., *Fluorine Chem.*, **101**, 257-261. (2000)

[58] S. Chaudhuri, F. Wang and C. P. Grey. *J.Am. Chem. Soc.*, **124**, 11746 (2002)

[59] G. Dénès, J. Pannetier and J. Lucas. *C.R. Acad. Sc. Paris*. **280** C, 831 (1975).

[60] T. Birchall, G. Dénès, K. Ruebenbauer and J. Pannetier, *Hyper.Inter.* **29**, 1331, (1986).

[61] G. Dénès, Y. H. Yu, T. Tyliszczak and A. P. Hitchcock, J. Solid State Chem. **91**, 1 (1991).

[62] A. Wakagi and J. Kuwano, J. Mater. Chem. **41**, 973 (1994).

[63] A. Wakagi, J. Kuwano, M. Kato and H. Hanamoto, *Solid State Ionics* **70/71**, 601 (1994).

[64] T. Eguchi, J. Kuwano. *J. Mater Res. Bull.*, **30**, 1351 (1995).

[65] J. D. Donaldson and B. J. Senior, *J. Chem. Soc.* (A), 1821 (1967).

[66] G. Dénès, A. Muntasar and Z. Zhu, *Hyperf. Inter.* C **1**, 468 (1996).

[67] M. F. Bell, G. Dénès and Z. Zhu, *Phase Transformations and Systems Driven Far from Equilibrium, Mat. Res. Soc. Symp. Proc.* **481**, 273 (1998).

[68] G. Dénès, M. C. Madamba, A. Muntasar, A. Peroutka, K. Tam, and Z. Zhu, Mössbauer Spectroscopy in Materials Science, ed: M. Miglierini and D. Petridis, NATO Science series, 3. High Technology, vol. 66, Kluwer, Dordretch (Netherlands), 25 (1999).

[69] G. Dénès, M. C. Madamba, A. Muntasar, A. Peroutka, K. Tam, and Z. Zhu, *Solid State Ionics V, Mat. Res. Soc. Symp. Proc.* **548**, 491 (1999).

[70] M. F. Bell, G. Dénès and Z. Zhu, *Solid State Ionics VII, Mat. Res. Soc. Symp. Proc.* **755**, 277 (2003).

[71] J. Flahaut, *J. Solid State Chem.* **9**, 124 (1974).

[72] J. Schoonman, *Solid State Ionics* **1**, 121 (1980).

[73] G. Dénès, *Solid State Ionics IV, Mat. Res. Soc. Symp. Proc.* **369**, 295 (1995).

[74] R. Kano, S, Nakamura, K. Ohno and Y. Kawamoto, *Mat. Res. Bull.* **26**, 1111 (1991).

[75] R. Kanno, K. Ohno, H. Izumi, Y. Kawamoto, T. Kamiyma, H. Asono and F. Izumi, *Solid State Ionics* **70/71**, 253 (1994).

[76] Y. Ito, T. Mukuyama, H. Funatomi, S. Yoshikado and T. Tanaka, *Solid State Ionics* **67**, 301 (1994)

[77] G. Dénès, T. Birchall, M. Sayer and M. F. Bell, *Solid State Ionics*, **13**, 213 (1984).

[78] G. Dénès, and A. Muntasar, *Hyp. Interact.* **13**, 153 (2004).

[79] E. B. Craig and R. G. Compton, *Analyst* **131**, 15 (2006).

[80] A. Muntasar, Preparation, Characterization and Properties of Novel Materials in the $BaCl_2/SnF_2$ System, PhD thesis, Chapters 3-5, Concordia University, Montreal, Quebec, Canada (2002).

[81] G. Dénès, *J. Solid State Chem.* **77**, 54 (1988).

[82] B. E. Warren, X-ray Diffraction, 2nd edition, Dover publications, New York, pp. 251-314 (1990).

[83] G. Dénès, A. Muntasar and T. Retrif, *Solid State Chemistry of Inorganic Materials IV, Mat. Res. Soc. Symp. Proc.* **755**, 247 (2003).

[84] G. Dénès, M. C. Madamba and A. Muntasar, *Solid State Chemistry of Inorganic Materials II, Mat. Res. Soc. Symp. Proc.* **547**, 377 (1999).

[85] T. Birchall, G. Dénès, K. Ruebenbauer and J. Pannetier, J.C.S. Dalton, 2296 (1981).

[86] R. Calandrino, A. Collin, G. Dénès, M. C. Madamba and J. M. Parris, *Solid State Chemistry of Inorganic Materials, Mat. Res. Soc. Symp. Proc.* **453**, 585 (1997).

[87] M. C. S. Madamba, Phase Transitions in Superionic $PbSnF_4$, M.Sc. thesis, Concordia University, Montreal, Quebec, Canada (2002).

[88] A. Collin, G. Dénès, D. Le Roux, M. C. Madamba, J. M. Parris et A. Salaün, Intern. J. Inorg. Mater. **1**, 289 (1999).